1 wp

MULTIPLE IMAGE OVERLAY STORAGE METHODS

Peter F Mueller
Technical Operations, Incorporated
Northwest Industrial Park
Burlington, Massachusetts, 01803

June 1971
Final Technical Report
for period 11 August 1970 - 11 May 1971

Prepared for

NATIONAL AERONAUTICS AND SPACE ADMINISTRATION
Goddard Space Flight Center
Greenbelt, Maryland 20771

FACILITY FORM 602

N71-36376 (ACCESSION NUMBER) — (THRU)
167 (PAGES) — G3 (CODE)
CR-122069 (NASA CR OR TMX OR AD NUMBER) — 34 (CATEGORY)

Reproduced by
NATIONAL TECHNICAL
INFORMATION SERVICE
Springfield, Va 22151

TECHNICAL REPORT STANDARD TITLE PAGE

1 Report No	2 Government Accession No	3 Recipient's Catalog No

4 Title and Subtitle	5 Report Date
MULTIPLE IMAGE OVERLAY STORAGE METHODS	June 1971
	6 Performing Organization Code
7 Author(s)	8. Performing Organization Report No
Peter F. Mueller	TO-B 71-15
9 Performing Organization Name and Address	10 Work Unit No
Technical Operations, Incorporated Northwest Industrial Park Burlington, Massachusetts 01803	11 Contract or Grant No NAS5-21302
	13 Type of Report and Period Covered
12 Sponsoring Agency Name and Address	Final Technical Report 11 Aug. 1970-11 May. 1971
National Aeronautics and Space Administration Goddard Space Flight Center Greenbelt, Maryland 20771	14 Sponsoring Agency Code

15 Supplementary Notes

16 Abstract

The primary objective of this study was to demonstrate the image quality achievable with current optical multiplexing techniques. If acceptable, these techniques will significantly reduce film consumption in the distribution of distortion-free ERTS imagery. The study was conducted over a nine-month period and was restricted to 35 millimeter image formats and up to twelve channel multiplex recordings. The results indicate that seven carrier-modulated images can be overlayed on a single film frame and retrieved substantially free from crosstalk and dimensional distortion. Resolution was maintained at 10 line-pairs per millimeter, and the gray scale was reproduced essentially linear over a 100 to 1 brightness dynamic range. Based on these results, we recommend that the techniques be demonstrated with seven spectral zones of ERTS imagery in spatial registration at full size format.

17 Key Words (Selected by Author(s))	18 Distribution Statement
Photographic Storage Modulated Imagery Spatial Filtering Linear Film Processing Optical Multiplexing	

19 Security Classif (of this report)	20 Security Classif (of this page)	21 No of Pages	22 Price*
Unclassified	Unclassified	107	

*For sale by the Clearinghouse for Federal Scientific and Technical Information, Springfield, Virginia 22151

PREFACE

The primary objective of this study was to demonstrate the image quality achievable with current optical multiplexing techniques. If acceptable, these techniques will significantly reduce film consumption in the distribution of distortion-free ERTS imagery. The study was conducted over a nine-month period and was restricted to 35 millimeter image formats and up to twelve channel multiplex recordings. The results indicate that seven carrier-modulated images can be overlayed on a single film frame and retrieved substantially free from crosstalk and dimensional distortion. Resolution was maintained at 10 line-pairs per millimeter, and the gray scale was reproduced essentially linear over a 100 to 1 brightness dynamic range. Based on these results, we recommend that the techniques be demonstrated with seven spectral zones of ERTS imagery in spatial registration at full size format.

PRECEDING PAGE BLANK NOT FILMED

TABLE OF CONTENTS

TABLE OF CONTENTS (Concluded)

LIST OF ILLUSTRATIONS

LIST OF ILLUSTRATIONS (Continued)

LIST OF ILLUSTRATIONS (Continued)

LIST OF ILLUSTRATIONS (Concluded)

LIST OF TABLES

SECTION 1

INTRODUCTION

SCOPE

The results of a nine-month study to evaluate multiple image overlay methods as applied to ERTS (Earth Resources Technology Satellite) imagery are presented in this technical report. Multiple imagery is a photo-optical process for storing and retrieving many overlapped exposures within a single film frame. Experimental camera and projector setups, photographic processing techniques, retrieved image results and system performance characteristics, as well as the theoretical models utilized for this study are reported. Preliminary design requirements for a full-format multiple image system are also presented.

PURPOSE

The purpose of this study was to determine whether multiple image methods that had been published[1] and patented[2] by the contractor offered a practical, acceptable, and economical solution to the problem of ERTS imagery storage and distribution.

To be practical, the methods must lend themselves to implementation within state-of-the-art copying techniques and materials. Laboratory experiments that can be conducted only by highly trained technicians under elaborately controlled conditions would not be considered practical.

To be acceptable, the multiplexing methods must yield an increase in storage density without degrading imagery. The outstanding degradations to be avoided are loss in resolution, dimensional distortion, brightness distortion, and crosstalk.

To be economical, the methods must exhibit a potential for cost savings as compared to alternate solutions. Reduction in film consumption must not be outweighed by additional equipment requirements.

OBJECTIVES

The primary objective of the program was to demonstrate, by means of experimental results, the image quality that can be obtained with current multiplexing methods.

Using black-and-white 35 mm transparencies as inputs,* we were to investigate a minimum of six and maximum of twelve image channels. System resolution had to be maintained at 10 line-pairs/mm or greater. Since the input targets for this primary objective were various scenes as opposed to spectral zones of the same scene, registration of one channel to another did not apply.

However, a secondary objective was to demonstrate how three different spectral zones of a single scene could be printed out in precise registration onto black-and-white film and subsequently retrieved as a tricolor image with no loss in registration. Here, the assumption was that the spectral zones were stored with temporal registration in an electronic buffer as opposed to being stored as spatially separated transparencies. To achieve this objective in its broadest sense would have required not only spectral imagery signals, but also a scanner-modulator system, neither of which was readily available within the scope of this study. The demonstration was therefore to be conducted by synthetically generating the three zone signals by means of a computer technique and printing these signals out with a step-and-repeat photofacsimile device that simulated a scanner-modulator system.

DISCUSSION OF THE PROBLEM

The ERTS program will ultimately require extremely large amounts of photographic materials to disseminate imagery to various users. For a substantial number of users, the mensurational accuracy of the imagery is of vital concern. Thus, once a master print has been produced by ground processing equipment, no distortions should be introduced by subsequent duplication procedures.

Ideally, if all duplication were performed by means of contact printing on stable photographic glass plates, a minimum of distortion would be introduced. The economics of that approach are clearly prohibitive for mass distribution and probably only feasible for a small number of prints to a limited number of users. In fact, even if one accepted the more practical alternative of a thick Estar base duplicating material, the film budget would still be quite substantial. The question is, Can large amounts of distortionless imagery be disseminated in a more economical way?

*These inputs were used because the contractor already had encoding cameras and decoding projector hardware of that format. Additional cost would have been incurred to increase the image size.

One way to use film more economically is to utilize its full storage capacity. Microfilming is a prime example of efficient and economical data storage. Since we assume that the ERTS master prints will have an upper resolution limit of about 10 line-pairs/mm, and films with resolving power far in excess of 500 line-pairs/mm are common, film consumption could be drastically reduced by duplicating at a 50:1 reduction ratio. Lenses are readily available with the required resolution and format capacity. Unfortunately, only a symmetric lens used to image 1:1 at fixed conjugates can be made to operate substantially free of distortion.

Thus with conventional photographic methods we are apparently unable to reconcile low distortion with high efficiency storage. Faced with this impasse, let us review what we mean by distortion. Since lens distortions (i.e., barrel and pincushion) are stationary, they could, at least in principle, be compensated by an inversely distorted master print. On the other hand, it is difficult to conceive how a large number of various enlarger-printer devices could be adequately corrected. The second type of distortions are those introduced by flexible base photosensitive material, and these are nonstationary and present an even less tractable problem. These distortions are random but not completely isotropic since they generally have a strong dependence on the transport mechanisms used during pre-exposure, exposure, and processing. In addition to limiting straightforward mensurational accuracy, film distortions also upset the correlation techniques that are quite fundamental to photointerpretation.

The approach taken in this study is to avoid optical distortions by recording and retrieving at 1·1. Film distortions cannot be avoided, but at least with this approach they are not amplified by a reduction-enlargement ratio. Furthermore, when spectral zones are exposed by multiple imaging methods, random film distortions present no difficulty in retrieval registration because local film distortions are identical for all channels.

Photo-optical multiplexing has no complete analog in the electrical signal domain, but it can be compared to multichannel telemetry where many subcarriers modulated by the output of various sensors are mixed and transmitted over one high frequency carrier. The subcarriers are separated upon detection either by means of their unique frequency or by their unique phase.

Optically we use spatial carriers of either unique frequency or phase, but unlike the electrical analog we can vary the carrier frequency and phase by a simple rotation or translation in the plane of the carrier. It may also be helpful to think of a photographic transparency as performing some of the functions of the high frequency carrier of multichannel telemetry. Just as one would not use a subcarrier of frequency comparable to the main carrier, so we are constrained to use spatial carriers that are well resolved by an emulsion. The sampling theorem[3,4] and aliasing constraints[5] must also be observed in optical multiplexing if no image information is to be lost or distorted in crosstalk.

SUMMARY OF WORK

Recording, processing, and retrieving are the three major task areas associated with the primary study objective. For recording we constructed a 1:1 multiple exposure copy camera from existing bench hardware and prepared two sets of twelve input targets. One set was intended for subjective evaluation and initially consisted of astronaut and moon landing slides. Later, because of the poor photographic quality of these rather cheap slides, we switched to higher quality travel slides of the Washington, D.C. area. The second set of targets was designed specifically for objective measurements and consisted of high and low contrast resolution targets, step tablets, a mensuration grid, and general scenes. The dynamic range of all the targets was controlled so that it did not exceed a 32:1 brightness ratio, and had an average brightness ratio of about 20:1. A special target was also designed for crosstalk measurements. Nine different multiple image recordings were produced: seven-, nine-, and twelve-channel exposures of the subjective, objective, and crosstalk targets.

Photographic processing depended on film selection. In the course of this study three different films were evaluated Eastman Kodak SO-343, 'Minicard, and Recordak AHU Type 5460. Direct reversal processing for a gamma of -2 was worked out for each film. In addition, a print reversal process was devised for SO-343. Since direct reversal of Type 5460 microfilm proved to be optimum, it was used for all the final multiple image recordings.

Initially, demodulation and image retrieval were performed on a general purpose spatial filtering optical bench. Later a special 1:1 projection system was designed and set up, and it was used to record or measure all retrieval imagery and documentation results.

The secondary objective of this study required the generation of synthetic target signals, printout of the targets, and retrieval of the targets in color. Before the first two tasks could be completed, however, the photofacsimile device had to be reactivated and calibrated. Although these requirements were beyond the scope of the study, they influenced the schedule and final results.

The first step in generating the synthetic target signals was to specify graphically the carrier-modulated density distributions for a six-color bar chart, a seven-step gray scale, and a six-element resolution target. The density distributions were then translated to command language for the photofacsimile device. In turn the commands were reduced by a computer routine to a punched tape. The punched tape was, in effect, our simulation of the three-zone imagery stored with temporal registration in a buffer.

The tapes were then used to control printout of the three targets in the photofacsimile device. The resulting black-and-white transparencies were then reconstructed in color on an optical bench decoder system. The six-bar color chart (red, green, blue, cyan, magenta, yellow) was photographed with Kodacolor and printed. The gray scale and resolution targets, although made up of additive primary components, were retrieved as black-and-white. The resolution of this target was limited to 4 line-pairs/mm by the stepping rate of the photofacsimile device.

The final task of this study was to specify the scanner-modulator requirements for encoding and printing three-channel imagery at high speeds for full-format 10 line-pairs/mm inputs.

SUMMARY OF RESULTS

Initial retrieval results of six- and seven-channel recordings were disappointing because of excessive crosstalk, noise, and limited dynamic range. In retrospect, it

is clear that these problems were due chiefly to our first choice of films, SO-343. We were motivated to use this film because its thick Estar base held a potential for outstanding dimensional stability, and its high resolution emulsion apparently offered sufficient storage capacity. Experimentally, however, the Estar base proved to be a source of optical noise, and its storage capacity for carrier modulated imagery was inferior to that of Type 5460 microfilm.

Seven-channel recordings of the subjective targets on Recordak AHU Type 5460 microfilm exhibited virtually no crosstalk and had very low noise backgrounds. Nine- and twelve-channel recordings had barely detectable crosstalk in two to three retrieved channels. Objective target measurements indicated that the effective storage and retrieval gamma was approximately equal to -2 for all recordings (seven, nine, and twelve channels) and was linear over an input range of 10:1 in brightness, yielding a 100:1 output brightness range. Resolution was maintained in excess of 10 line-pairs/mm, and dimensional distortion was less than the size of the system impulse response (i.e., less than 0.05 mm). Control target recordings indicated that the potential for crosstalk was greatest in those regions of the recording where the composite exposure level fell considerably below the average.

Results of the secondary study objective were very much as expected despite early setbacks and delays in troubleshooting and calibrating the photofacsimile device. The six-bar color chart played back very saturated additive and subtractive primary colors; the step tablet played back neutral with the proper brightness range; and the resolution target played back neutral with an upper frequency of 4 line-pairs/mm, as determined by the 8 line-pairs/mm printing frequency of the photofacsimile device.

SECTION 2

THEORETICAL DISCUSSION AND MODELS

HISTORY

In a broad sense, photo-optical multiplexing began in 1899 with R.W. Wood,[6] when he devised an additive three-color process in which red, green, and blue separation positives of a color scene were copied sequentially through three gratings of different spacing (i.e., spatial frequency) onto the same plate. The gratings served as encoders, retaining the essential identity[7] of the separation positives when mixed on a single plate. In addition, the diffractive properties of the grating modulated images were used to filter back the proper colors in a simple retrieval device. By 1906 the father-son team of Frederic and Herbert E. Ives[8,9] had developed a diffraction color process along the lines of Wood's ideas. Gratings of either different spatial frequency or azimuthal orientations were employed to modulate each of three color separation positives. The interlace scheme of Ives is illustrated in Figure 1. Bichromated gelatin was used to prepare these recordings by a delicate laboratory procedure. The recordings, which were in essence phase transparencies, were viewed by the diffraction chromoscope illustrated in Figure 2. A suitable limiting aperture was placed in

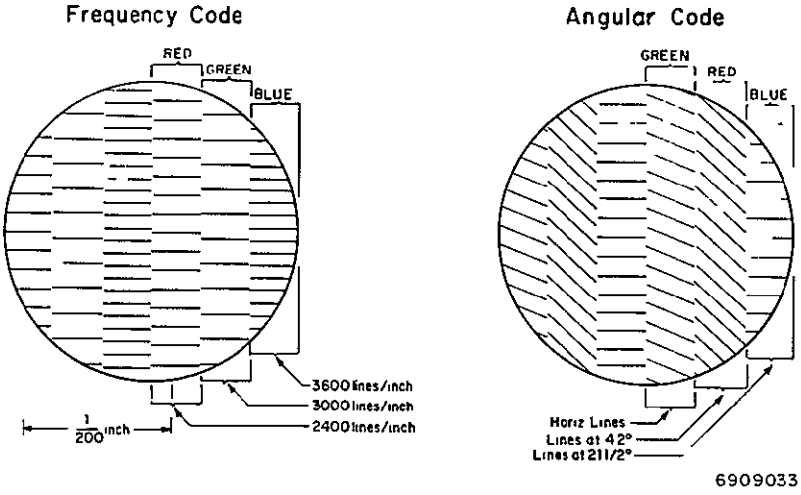

Figure 1. Ives' Diffraction Process of Color Photography (1906)

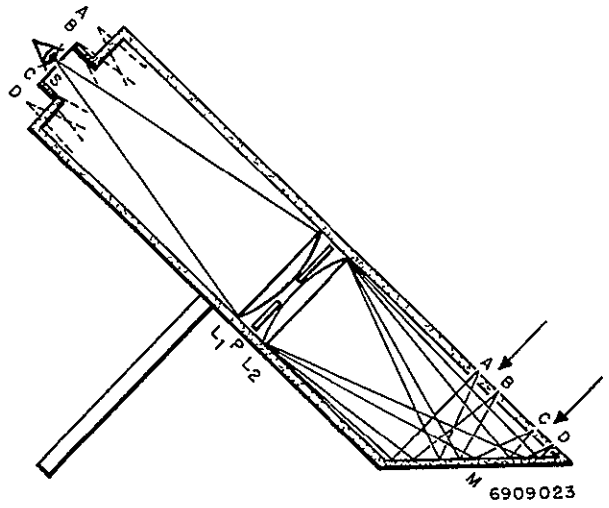

Figure 2. Ives' Diffraction Chromoscope

the chromoscope so that the diffraction pattern of the red image grating was blocked except for its red light component. Similarly, only the green and blue light components of the gratings, modulating the green and blue images respectively, were passed.

Between 1929 and 1939, Carlo Bocca,[10] probably without knowledge of the prior art, developed a diffraction process for projecting color movies. The process never became commercially successful, however, perhaps partly because of some technical difficulties and partly as a result of the success of triple emulsion films. The next emergence of a diffraction process color system appears to be W.E. Glenn[11,12] who applied the principles to the Eidophor[13] system and then to thermoplastic recording in 1959.

The first suggestion of applying optical multiplexing to independent input targets as opposed to the more restricted application to the three separations of a color image was made in 1962 by A. Lohmann.[14,15] Implementing the methods he suggested was relatively impractical, but apparently for the first time the suggestion emerged that a number of independent images could be stored and retrieved from a single film frame. In 1966 R.L. Lamberts and G.C. Higgins[16] demonstrated a more practical photographic method for recording many independent carrier-modulated exposures. However, the exposures with which they dealt were binary in brightness levels and represented digital data recording as opposed to continuous-tone imagery. In 1968 F. Bestenreiner[17] demonstrated the results of a carrier-modulated multiple image process that utilized phase carriers. As with the methods of Lamberts and Higgins, this process was also nonlinear and unsuited for continuous-tone imagery, and it exhibited considerable crosstalk. In 1968 the author introduced the idea of linear multiple image storage[18] and for the first time demonstrated a continuous-tone storage and retrieval process essentially free of crosstalk. It is this process that forms the basis of the current study.

The evolutionary development of photo-optical multiplexing over the past seventy years shows no signs of diminishing, and in fact will probably continue to grow as it receives attention from an increasing number of scientists.[19]

BASIC PRINCIPLES

Spatial carrier encoding, linear photographic processing, and coherent spatial filtering are the basic principles that comprise the multiplexing methods of this study.

Spatial encoding requires that the intensity distribution of an image be periodically modulated prior to exposure. We do this by placing a transmission ruling in contact with the film emulsion and exposing the image through it. The ruling is rotated to a different azimuthal orientation after each exposure so that a unique relationship is established between each image and its carrier. The ruling also samples the image and determines the relative position of each image spectrum in the demodulation process. This implies that the spatial frequency and orientation of the ruling is determined by the number of images to be recorded. Spatial encoding can be accomplished with incoherent illumination in a conventional camera that has been equipped with a rotatable ruling in its focal plane.

Linear photographic processing is vital not only because it is the means by which the unique carrier-image relationship is maintained during storage, but also because it provides the transition mechanism between an incoherent copying procedure and a coherent retrieval procedure.

Spatial filtering to demodulate and retrieve individual images is accomplished by illuminating the multiplex recording with a plane wave, erecting its Fourier spectrum in the filter plane, passing one of the separated spectra through the filter aperture, and retransforming to focus the image. Probably most insight to the multiplexing problem and certainly most of the carrier specifications can be realized by a careful description and analysis of the recording's Fourier spectrum. Thus most of our mathematical treatment dwells on this area.

PHOTOGRAPHIC STORAGE

Since the manner in which we treat the role of photographic storage is perhaps the single most distinctive feature of the current multiplexing method as compared with other proposed schemes, reviewing the fundamentals of film storage will be worthwhile.

Input exposure is conventionally related to output density of a processed film by a characteristic curve referred to as the H and D (Hurter and Driffield) or the D log E (Density versus $\log_{10}$ Exposure) curve. An idealized D log E curve is shown in Figure 3. For exposures restricted to the linear region, density is related to log exposure by the slope or gamma of the curve as

$$D = \gamma \log E \quad . \qquad (1)$$

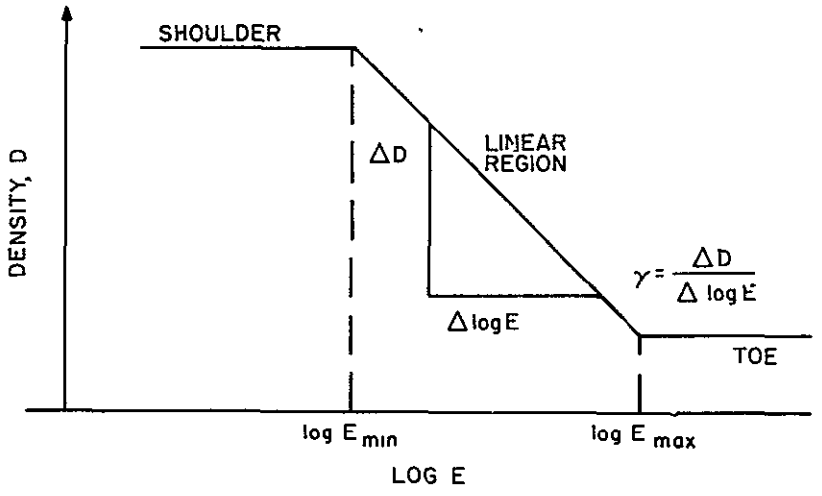

Figure 3. Idealized D log E Curve

Of more interest to us is the relation between exposure and output transmittance. Density is defined in terms of intensity transmittance $\mathcal{T}$ by D = -log ($\mathcal{T}$), and the modulus of the amplitude transmittance T is simply the square root of $\mathcal{T}$. Assuming that any phase components in the emulsion are rendered negligible, amplitude transmittance of a processed film is given by

$$T = E^{-\gamma/2} \quad . \qquad (2)$$

Thus by processing the film so that $\gamma = -2$ we obtain the required linear relation between input exposure (which is accomplished under normal incoherent copying conditions) and output amplitude transmittance (which assumes an essentially coherent plane wave illumination).

Of course exposures must always be restricted to the interval between log E_{min} and log E_{max} which constitutes the available input dynamic range, $DR_{In} = \log (E_{max}/E_{min})$. If the film is to be exposed M times to different images but of the same dynamic range, log (E'_{max}/E'_{min}), where the primes indicate image exposures, then we have the restriction given in Eq. (3) on the brightness range of each exposure:

$$\log \left(\frac{E'_{max}}{E'_{min}} \right) \leq DR_{In} - \log M \quad . \tag{3}$$

For example if a particular $\gamma = -2$ process has a $DR_{In} = 15$ dB and $M = 6$, then log $(E'_{max}/E'_{min}) \leq 7.8$ dB or the brightness range of each exposure should not exceed 6:1, and for $M = 12$ the ratio drops to 2.6:1. Although at first sight the restriction implied in Eq. (3) appears to be quite severe, two experimental conditions tend to soften its impact. First, for a series of random scene exposures, all maxima and minima exposure regions are not likely to be coincident and in that respect Eq. (3) represents a worst possible situation. Second, the $\gamma = -2$ requirement for linear storage (where coherent retrieval is anticipated) implies that the output brightness distribution will have a quadratic distortion. To compensate for this systematic distortion, the original image should be compressed by an intermediate storage at $\gamma' = -1/2$. If this is done, then the actual input brightness ratios for the six and twelve exposure examples become 36:1 and 6.8:1 respectively. The process we are suggesting is summarized by the following equations.

$$\left[E(x, y) \right]^{-\gamma'} = \mathscr{T}(x, y) \tag{4}$$

$$\left[\mathscr{T}(x, y) \right]^{-\gamma/2} = T(x, y) \tag{5}$$

$$I_{Dmod}(x, y) = \left| T_{Dmod}(x, y) \right|^2 = \left| \left\{ \left[E(x, y) \right]^{-\gamma'} \right\}^{-\gamma/2} \right|^2 , \qquad (6)$$

where $E(x, y)$ is one of the original image exposures processed with γ' to an intermediate transparency, $\mathcal{T}(x, y)$, which in turn is exposed and processed with γ to a recording having amplitude transmittance $T(x, y)$. When demodulated, the recording yields an intensity distribution $I_{Dmod}(x, y)$, which since γ is fixed at -2 will be linearly proportional to $E(x, y)$ only when γ' equals -1/2.

Up to this point we have only considered direct reversal processing since that was the type used most successfully in this study. In principle, print reversal processing could also be used to achieve linear storage. Print reversal is represented in Eq. (7).

$$T = \left[(E)^{-\gamma'} \right]^{-\gamma/2} = E^{\gamma'\gamma/2} , \qquad (7)$$

where γ' characterizes the internegative process and γ is the slope of the second or release positive material. The storage requirement is that $\gamma'\gamma$ equal 2 and of course that exposures are restricted to linear regions of the respective D log E curves.

We have kept our treatment of photographic storage elementary and yet have included all the parameters necessary for a basic understanding of its role in this multiplex method. A number of more subtle effects that indicate that gamma is not always the constant we would like it to be can be found in the literature. Higgins[20] has recently shown how the Eberhart effect can render γ a function of spatial frequency; the Clayden and intermittency[21] effects might tend to make γ a function of exposure level when sequential exposures are involved; light latensification[22] could produce nonuniform emulsion sensitivity. Knowing that these potential hazards exist is useful, but they certainly do not prevent us from postulating a simple unified process model.

GENERALIZED OVERLAY MODEL

The most direct method of introducing our functional notation is to describe the retrieval projector as sketched in Figure 4. Optical Fourier transformation[23] is the

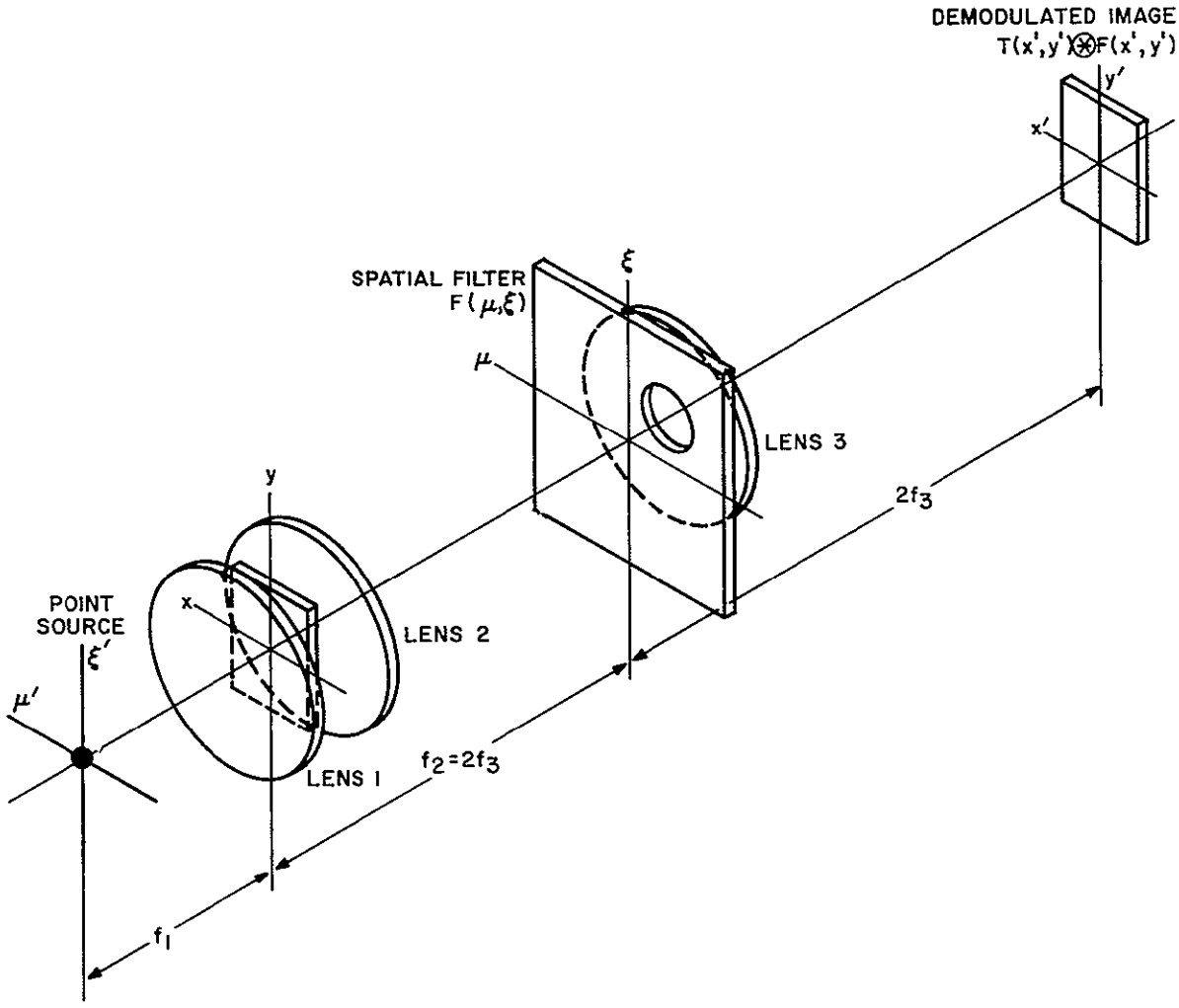

Figure 4. Coherent Spatial Filtering and Retrieval System

fundamental operation performed repeatedly in this projector. Lens L_1 produces the Fourier transform of the amplitude distribution of the $(\mu' \xi')$ plane in the (x, y) plane; lens L_2 transforms the (x, y) functions into the (μ, ξ) plane; lens L_3 likewise transforms the (μ, ξ) distribution into the (x', y') plane. A quasi-monochromatic point source of wavelength λ represented by the delta function $\delta(\mu', \xi')$ produces a plane wave in the (x, y) plane as indicated by Eq. (8).

$$\int_{-\infty}^{\infty} \int_{-\infty}^{\infty} \delta(\mu', \xi')\, e^{\frac{2\pi i}{f_1 \lambda}(x\mu' + y\xi')}\, d\mu'\, d\xi' = 1 \quad . \tag{8}$$

Of course the plane wave is truncated by the size of the collimator lens L_1. The projector film gate is located in the (x, y) plane; therefore when a transparency is inserted, its spectrum is displayed by the field lens L_2 in the filter plane as shown in Eq. (9).

$$\tilde{T}(\mu, \xi) = \int_{-\infty}^{\infty} \int_{-\infty}^{\infty} T(x, y)\ e^{\frac{2\pi i}{f_2 \lambda}(\mu x + \xi y)}\ dx\ dy \quad . \tag{9}$$

A spatial filter represented by the transmittance function $F(\mu, \xi)$ is introduced to modify the spectrum, and the product $T(\mu, \xi)\ F(\mu, \xi)$ is transformed by the projection lens L_3 to form a demodulated image in the (x', y') retrieval plane. This process is described in Eq. (10) where the asterisk symbolizes the convolution integral.

$$\widetilde{\tilde{T}(\mu, \xi)\ F(\mu, \xi)} = \int_{-\infty}^{\infty} \int_{-\infty}^{\infty} \tilde{T}(\mu, \xi)\ F(\mu, \xi)\ e^{\frac{2\pi i}{f_3 \lambda}(x'\mu + y'\xi)}\ d\mu\ d\xi$$

$$= \int_{-\infty}^{\infty} \int_{-\infty}^{\infty} T(\sigma, \eta)\ \tilde{F}(x' - \sigma, y' - \eta)\ d\sigma\ d\eta \tag{10}$$

$$= T(x', y') \circledast \tilde{F}(x', y') \quad .$$

The focal length f_2 of the transform lens L_2 and mean wavelength λ of the illuminant are constants for a given projector, and these parameters determine the spatial frequency scale in the filter plane. As an example we will use Eq. (9) to calculate the size of the spectrum for a transparency with maximum spatial frequency ω_s (i.e., a transparency that is band-limited to $2\ \omega_s$). Since the outer boundary of the spectrum will be determined by the highest frequencies, we need only consider a typical component, $\cos 2\pi\ \omega_s\ (\alpha x + \beta y)$, where $\alpha = \cos\theta$, $\beta = \sin\theta$, and θ designates the orientation

of the frequency component (e.g., $\theta = 0$ for a cosine fringe varying only in the x direction). Rewriting the cosine as $1/2\left[e^{2\pi i\omega_s(\alpha x+\beta y)} + e^{-2\pi i\omega_s(\alpha x+\beta y)}\right]$ and taking the transform, we obtain

$$\frac{1}{2}\int_{-\infty}^{\infty}\int_{-\infty}^{\infty} e^{2\pi i\left[\left(\frac{\mu}{f_2\lambda}+\alpha\omega_s\right)x+\left(\frac{\xi}{f_2\lambda}+\beta\omega_s\right)y\right]}$$

$$+ e^{2\pi i\left[\left(\frac{\mu}{f_2\lambda}-\alpha\omega_s\right)x+\left(\frac{\xi}{f_2\lambda}-\beta\omega_s\right)y\right]} \tag{11}$$

$$= \frac{1}{2}\left[\delta\left(\frac{\mu}{f_2\lambda}+\alpha\omega_s, \frac{\xi}{f_2\lambda}+\beta\omega_s\right)+\delta\left(\frac{\mu}{f_2\lambda}-\alpha\omega_s, \frac{\xi}{f_2\lambda}-\beta\omega_s\right)\right] .$$

The delta functions of Eq. (11) indicate that the greatest radial dimension ρ_s of the spectrum is reached at the coordinate positions $\mu = \alpha\omega_s f_2\lambda$ and $\xi = \beta\omega_s f_2\lambda$, but ρ equals $(\mu^2 + \xi^2)^{1/2}$ so that we obtain the result given in Eq. (12).

$$\rho_s = \left(\alpha^2+\beta^2\right)\omega_s f_2\lambda = \omega_s f_2\lambda \quad . \tag{12}$$

Thus allowing for random orientations of the ω_s components, we know that a circular region of radius ρ_s would be occupied by the frequency spectrum.

Let us now examine what happens if we carrier-modulate this band-limited transparency. As stated previously, our spatial carriers are rulings and any one-dimensional ruling can be described in terms of a Fourier series as in Eq. (13).

$$P(x, y) = \sum_{n=-\infty}^{\infty} a_n\, e^{2\pi i n\omega_o(\alpha x+\beta y)} \quad , \tag{13}$$

where n's are integers including zero, a_n's are the Fourier coefficients, ω_o the fundamental ruling frequency, and α and β have the same meaning as when previously used. Even though the ruling of Eq. (13) extends over a two-dimensional plane, it is one-dimensional in the sense that it is described by a single set of Fourier coefficients:

$$a_n = \omega_o \int_{-\frac{1}{2\omega_o\alpha}}^{\frac{1}{2\omega_o\alpha}} \int_{-\frac{1}{2\omega_o\beta}}^{\frac{1}{2\omega_o\beta}} P(x,y)\, e^{-2\pi i n\omega_o(\alpha x + \beta y)}\, dx\, dy \quad . \tag{14}$$

Other than fundamental frequency, the a_n's specify all the physical properties of the ruling such as maximum and minimum transmittance, duty cycle, and slit shape.

The Fourier spectrum of this ruling as it would be formed in the retrieval projector is given in Eq. (15).

$$\tilde{P}(\mu, \xi) = \sum_{n=-\infty}^{\infty} a_n\, \delta\left(\frac{\mu}{f_2\lambda} - n\alpha\omega_o, \frac{\xi}{f_2\lambda} - n\beta\omega_o\right) \quad . \tag{15}$$

By sandwiching the ruling and the band-limited transparency together in the film gate and describing the filter plane distribution, we can gain some insight to sampling requirements. This convolution process is given in Eq. (16).

$$\widetilde{T(x,y)\, P(x,y)} = \tilde{T}(\mu, \xi) \circledast \tilde{P}(\mu, \xi)$$

$$= \sum_{n=-\infty}^{\infty} a_n\, \tilde{T}(\mu, \xi) \circledast \delta\left(\frac{\mu}{f_2\lambda} - n\alpha\omega_o, \frac{\xi}{f_2\lambda} - n\beta\omega_o\right) . \tag{16}$$

From our previous calculations we know that the diameter of $\tilde{T}(\mu, \xi)$ is $2\omega_s f_2\lambda$ and that the distance between centers for adjacent delta functions is $\omega_o f_2\lambda$. Figure 5 sketches

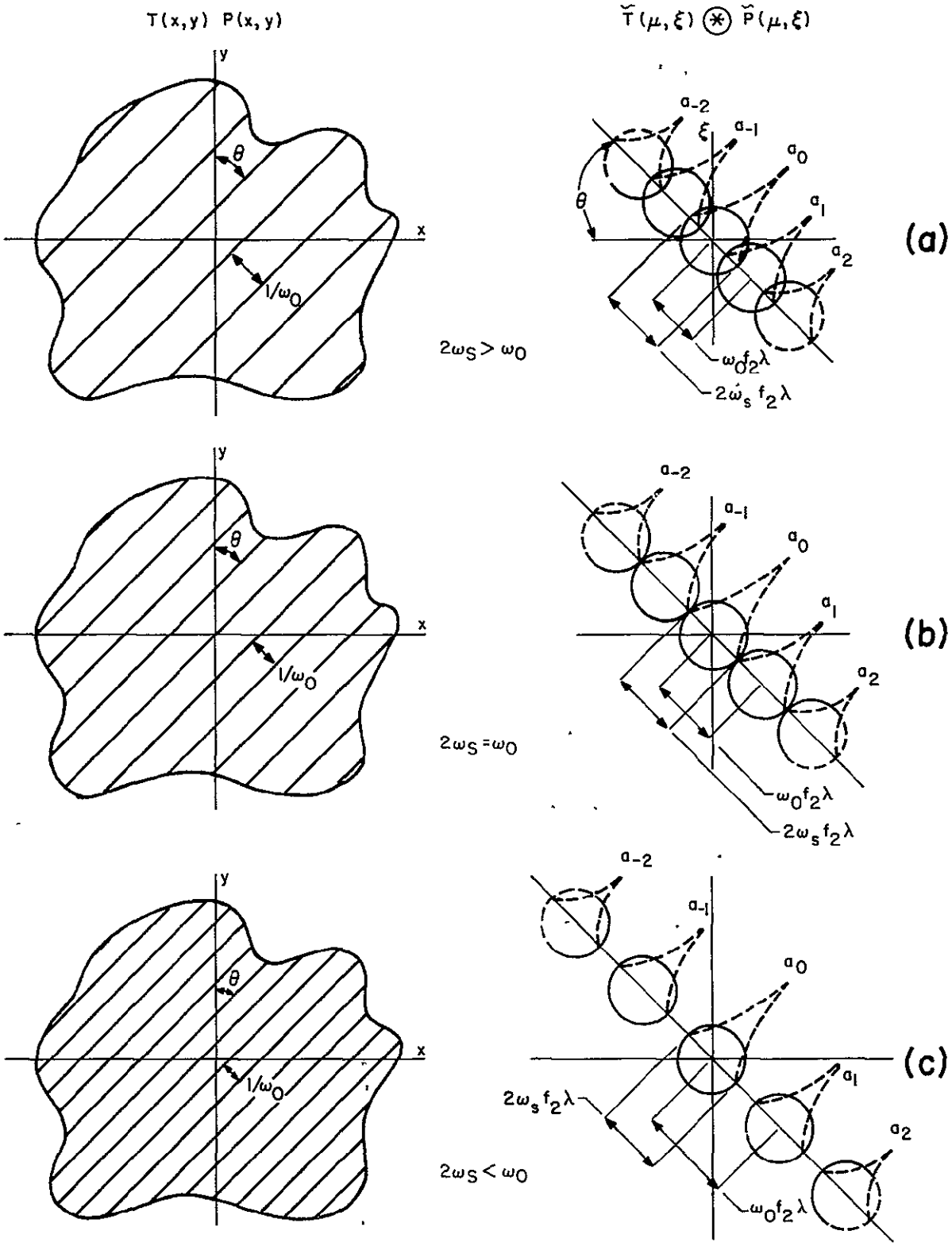

Figure 5. Spectrum of Carrier-Modulated Image for the Cases of Undersampling (a), Adequate Sampling (b), and Oversampling (c)

some of the spectrum characteristics indicated in Eq. (16) for the cases of $2\omega_s > \omega_o$, $2\omega_s = \omega_o$ and $2\omega_s < \omega_o$, which from the graphical representation are quite clearly the cases of undersampling, just adequate, and oversampling respectively. Overlap of the replicated transparency spectra is symptomatic of aliasing in an undersampled signal. Oversampling, on the other hand, simply spreads out the spectra in the filter plane and produces a greater guardband between them.

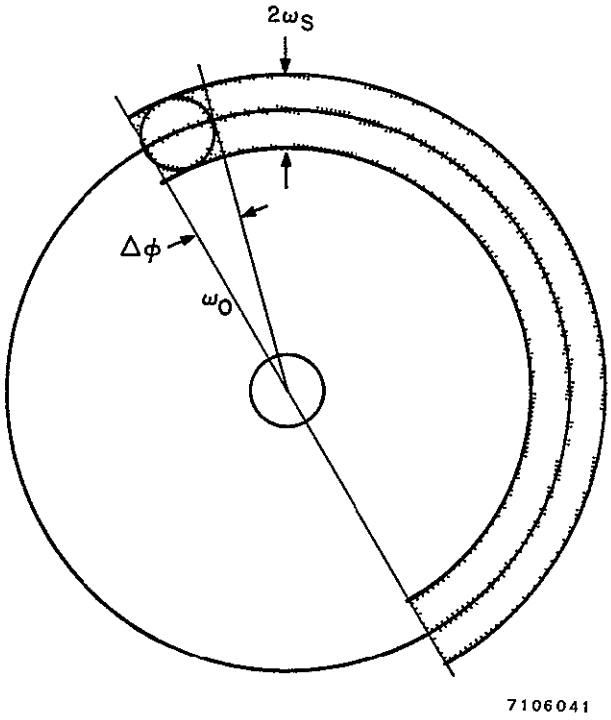

Figure 6. Geometry for an M Channel Spectrum

From the Figure 5 sketch we are in a good position to specify the minimum carrier frequency and angular rotation increments required to accommodate an M channel recording (where M is number of channels) in terms of the bandlimit of the images such that there will be no overlap of the first order spectra. Since the amplitude carriers produced a symmetric replication of spectra, only half the frequency plane is available for coding. The situation is sketched in Figure 6 where the length of the total available bandwidth as indicated by the shaded semi-annulus is $\pi\omega_o$. Assigning equal and contiguous segments of this semi-annulus to each channel leads to the requirement that

$$\Delta\phi = \frac{\pi\omega_o}{M} \quad . \tag{17}$$

When M is greater than 4 or 5, then to a good approximation we can assume that $\Delta\phi\omega_o$ equals $2\omega_s$ and so the carrier frequency requirement is obtained as shown in Eq. (18).

$$\omega_o = \frac{M}{\pi} 2\omega_s \quad . \tag{18}$$

To describe the carrier rotations, we simply introduce the summing index $m = 1, 2, \text{---} M$ into Eq. (13) to obtain Eq. (19):

$$P_m(x, y) = \sum_{n=-\infty}^{\infty} a_n \, e^{2\pi i n \omega_o \left(\alpha_m x + \beta_m y\right)} \quad , \tag{19}$$

where

$$\alpha_m = \cos\left[\theta + (m-1)\frac{\pi}{M}\right] \quad \text{and} \quad \beta_m = \sin\left[\theta + (m-1)\frac{\pi}{M}\right] .$$

The generalized overlay M channel recording is then described by Eq. (20).

$$T(x, y) = \left[\sum_{m=1}^{M} E_m(x, y)\, P_m(x, y)\right]^{-\gamma/2} \quad , \tag{20}$$

where $E_m(x, y)$ is the latent exposure* of the m^{th} image. When linear photographic storage is achieved, the brackets of Eq. (20) are removed along with at least the mathematical possibility of generating crossproducts. In fact, any mechanism in the storage process that would make it unrealistic to describe the recording as in Eq. (21),

$$T(x, y) = K_1 + K_2 \left[\sum_{m=1}^{M} E_m(x, y)\, P_m(x, y)\right] \quad , \tag{21}$$

where K_1 and K_2 could be additive and multiplicative constants, would imply that the unique relationship between image and carrier had been lost and some degree of crosstalk should be expected.

*Considering $E_m(x, y)$ as the latent exposure obviates the questions of spectral sensitivity and exposure duration since this quantity is the result of integrating over time and wavelength.

To demodulate the m^{th} channel we first Fourier transform Eq. (21) (let $K_1 = 0$ and $K_2 = 1$) as shown in Eq. (22).

$$\tilde{T}(\mu, \xi) = \sum_{m=1}^{M} \sum_{n=-\infty}^{\infty} a_n \tilde{E}_m \left(\frac{\mu}{f_2\lambda} - n\alpha_m\omega_o, \frac{\xi}{f_2\lambda} - n\beta_m\omega_o \right) \quad . \tag{22}$$

We must then introduce a spatial filter to pass one of the m^{th} channel's fundamental orders. If we define the transmittance of a clear circular aperture of diameter $2\rho_s$ in an opaque screen as

$$C\left(\mu, \xi \middle| 2\rho_s\right) = \begin{cases} 1 & \left(\mu^2 + \xi^2\right)^{1/2} \leq \rho_s \\ 0 & \left(\mu^2 + \xi^2\right)^{1/2} > \rho_s \end{cases} , \tag{23}$$

then the retrieval filter for the m^{th} image (a_1 order) is given by Eq. (24).

$$F_m(\mu, \xi) = C_m \left(\mu - \alpha_m\omega_o f_2\lambda., \xi - \beta_m\omega_o f_2\lambda \right) \quad . \tag{24}$$

The amplitude distribution transmitted through the filter is

$$\tilde{T}(\mu, \xi)\ F_m(\mu, \xi) = a_1 \tilde{E}_m \left(\mu - \alpha_m\omega_o f_2\lambda\ ,\ \xi - \beta_m\omega_o f_2\lambda \right) \quad , \tag{25}$$

which is then transformed by lens L_3 of the projector to yield

$$T(x', y') \circledast \tilde{F}_m(x', y') = a_1 E_m(x', y')\ e^{2\pi i\omega_o \frac{f_2}{f_3} \left(\alpha_m x' + \beta_m y' \right)} \tag{26}$$

However, only the modulus squared of Eq. (26) is detected as the demodulated image shown in Eq. (27).

$$\left| T(x', y') \circledast \tilde{F}_m(x', y') \right|^2 = \left| a_1 \right|^2 E_m^2(x, y) \quad . \tag{27}$$

The brightness distribution of the retrieved image is quadratically distorted with respect to the input exposure as predicted during our discussion of photographic storage. This distortion is easily compensated, however, by putting the actual image through an intermediate "square root" process before exposure in the multiplexed recording. The overall brightness level of the retrieved image is weighted by $\left| a_1 \right|^2$; methods of optimizing these fundamental Fourier coefficients are treated in the next topic.

In addition to establishing the basic feasibility of a process, an important function of any theoretical model is to aid in specifying the conditions under which the process should be conducted. If the model is too general, then specific physical parameters may be omitted; if the model is too specific, it may become unwieldy and still not furnish enough information about the general process. Our hope is that this treatment has struck a balance between these extremes.

ENCODER OPTIMIZATION

In the previous section we assumed that demodulation would always be accomplished with one of the fundamental orders and thus retrieval brightness would be proportional to $\left| a_1 \right|^2$. To obtain the most favorable signal-to-noise ratio, we wish to maximize $\left| a_1 \right|^2$, which is a measure of modulation efficiency.

The simplest carrier that we can specify is the sinosuid of a single harmonic frequency (i.e., a periodic function where all the a_n's are 0 for n greater than 1) as given in Eq. (28).

$$P(x, y) = a_0 + a_1 e^{2\pi i \omega_o (\alpha x + \beta y)} + a_{-1} e^{-2\pi i \omega_o (\alpha x + \beta y)} \quad . \tag{28}$$

If we choose the origin of P(x,y) so that it is an even function, then $a_1 = a_{-1}$, and Eq. (28) is simply a cosine fringe as shown in Eq. (29).

$$P(x, y) = a_0 + 2a_1 \cos 2\pi\omega_o (\alpha x + \beta y) \quad . \tag{29}$$

The problem is to specify a_0 and a_1 to maximize fringe visibility. The first reaction is to let a_0 go to zero, but this would only lead to a frequency doubling since film is capable of storing only the modulus and not the phase information of the carriers. Thus we have the condition that $a_0 \geq 2a_1$, and so the highest contrast sinusoid carrier is

$$P(x, y) = \frac{1}{2}\left[1 + \cos 2\pi\omega_o (\alpha x + \beta y) \right] \tag{30}$$

where $a_0 = 1/2$ and $a_1 = 1/4$.

If a transparency with uniform modulation as specified in Eq. (30) is placed in a retrieval projector, 25 percent of the film gate energy will go to the zeroth order, 6.25 percent will be diffracted into each of the fundamental orders, and the remaining 62.5 percent will be absorbed by the transparency.

Now let us consider the carrier having the largest number of harmonic components, namely a rectangular ruling as shown in Figure 7, where P_1 and P_0 are the maximum

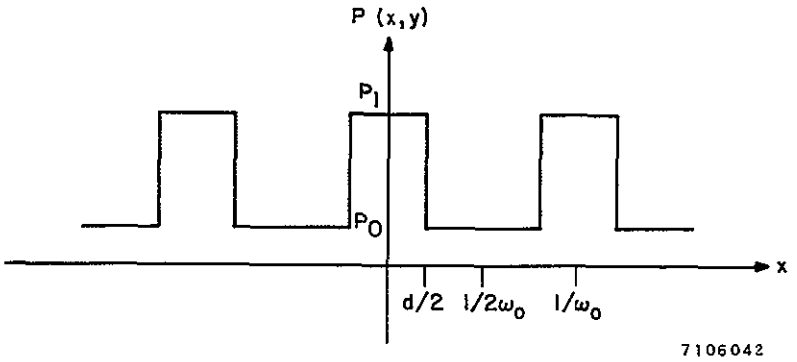

Figure 7. Rectangular Ruling Transmittances ($\alpha = 1$, $\beta = 0$)

and minimum transmittance levels respectively, d is the slit width, and $d\omega_o$ is the duty cycle. Using the half range of Eq. (14), since the function is even, we calculate the Fourier coefficients as shown in Eq. (31).

$$a_n = 2\omega_o \left[P_1 \int_0^{d/2} \cos 2\pi n\omega_o x \, dx + P_0 \int_{d/2}^{1/2\omega_o} \cos 2\pi n\omega_o x \, dx \right] \tag{31}$$

$$= P_0 \operatorname{sinc} n + \left(P_1 - P_0 \right) d\omega_o \operatorname{sinc} nd\omega_o \quad ,$$

where sinc $z = (\sin \pi z / \pi z)$.

From Eq. (31) we see that $a_0 = P_1 d\omega_o$ and $a_1 = (P_1 - P_0)\, d\omega_o \operatorname{sinc} d\omega_o$. First, it is clear that P_0 should go to zero to maximize a_1 for any duty cycle. Second, by rewriting a_1 as

$$a_1 = \frac{\left(P_1 - P_0 \right)}{\pi} \sin \pi d\omega_o \quad , \tag{32}$$

it can be seen by inspection that a_1 will be maximum for a 50 percent duty cycle (i.e., $d\omega_o = 1/2$). Normalizing the peak transmittance level ($P_1 = 1$), making the ruling bars opaque ($P_0 = 0$), and using a 50 percent duty cycle yields a maximum modulation efficiency of $|a_1|^2 = (1/\pi)^2 \approx 10$ percent for a square wave ruling, which makes it about 60 percent more efficient than the highest contrast sinusoid. However, just as with the sinusoid, 25 percent of the film gate energy goes to the zeroth order, but only 50 percent is absorbed by the transparency and the remaining 5 percent is distributed among all the higher order harmonics.

Since within the class of real, non-negative going functions, the only other possible carriers fall somewhere between the two extreme examples we have treated, we conclude that a high contrast square wave ruling provides the optimum encoder.

SQUARE ARRAY INTERLACE MODEL

We develop here the theory behind the secondary study objective and continue as much of the previous functional notation as is practical. Based on the principle of optical subtraction, we had proposed[24] that buffered three-zone spectral imagery could be printed out in a square array geometry so that registration of the three zones was preserved and color information could be retrieved. The printout geometry is shown in Figure 8, where each sample element is composed of four subsamples (A, B, C, D). By defining a high-contrast square wave ruling in the x direction as

$$P(x) = \sum_{n=-\infty}^{\infty} a_n \, e^{2\pi i n \omega_o x} \quad , \tag{33}$$

with

$$a_n = \frac{1}{2} \operatorname{sinc} \frac{n}{2} \quad , \tag{34}$$

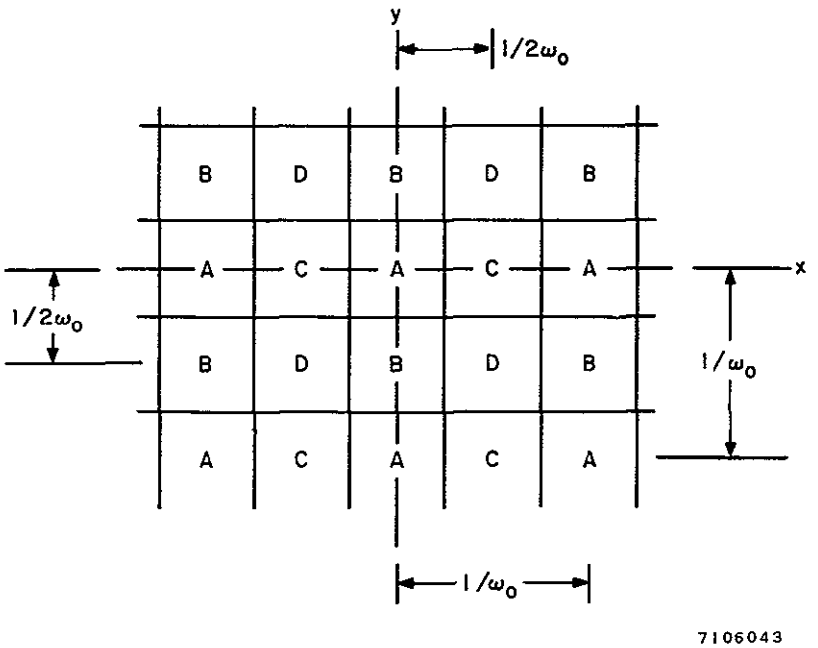

Figure 8. Square Array Geometry

and in the y direction as

$$P(y) = \sum_{\ell=-\infty}^{\infty} a_\ell \, e^{2\pi i \ell \omega_o y} \quad , \tag{35}$$

with

$$a_\ell = \frac{1}{2} \operatorname{sinc} \frac{\ell}{2} \quad , \tag{36}$$

we can describe the square array transmittance by superposition as

$$\begin{aligned} T(x, y) = {} & AP(x)\, P(y) + BP(x)\, P\left(y + \frac{1}{2\omega_o}\right) \\ & + CP\left(x + \frac{1}{2\omega_o}\right) P(y) + DP\left(x + \frac{1}{2\omega_o}\right) P\left(y + \frac{1}{2\omega_o}\right) \quad , \end{aligned} \tag{37}$$

and the Fourier spectrum is

$$\begin{aligned} \tilde{T}(\mu, \xi) = {} & \sum_{n=-\infty}^{\infty} \sum_{\ell=-\infty}^{\infty} a_n a_\ell \, \delta\left(\mu - n\omega_o f_2 \lambda, \; \xi - \ell \omega_o f_2 \lambda\right) \\ & \times \left[A + B\, e^{-\pi i n} + C\, e^{-\pi i \ell} + D\, e^{-\pi i (\ell + n)} \right] \quad . \end{aligned} \tag{38}$$

At various orders as designated by the n, ℓ indices, we obtain the following sums and differences:

$$\tilde{T}(\mu,\xi)\Big|_{\substack{n=0\\ \ell=0}} = a_0^2\,\delta(\mu,\xi)\,[A + B + C + D] \tag{39}$$

$$\tilde{T}(\mu,\xi)\Big|_{\substack{n=\pm1\\ \ell=0}} = a_1 a_0\;\delta\left(\mu \mp \omega_o f_2 \lambda, \xi\right)[A - B + C - D] \tag{40}$$

$$\tilde{T}(\mu,\xi)\Big|_{\substack{n=0\\ \ell=\pm1}} = a_0 a_1\;\delta\left(\mu, \xi \mp \omega_o f_2 \lambda\right)[A + B - C - D] \tag{41}$$

$$\tilde{T}(\mu,\xi)\Big|_{\substack{n=\pm1\\ \ell=\pm1}} = a_1^2\;\delta\left(\mu \mp \omega_o f_2 \lambda,\ \xi \mp \omega_o f_2 \lambda\right)[A - B - C + D] \tag{42}$$

If we make D = A + B + C, then the subsample spectra separate in a very orderly manner as indicated in Eqs. (43) through (46).

$$\tilde{T}(\mu,\xi)\Big|_{\substack{n=0\\ \ell=0}} = 2a_0^2\,\delta(\mu,\xi)\,D \tag{43}$$

$$\tilde{T}(\mu,\xi)\Big|_{\substack{n=\pm1\\ \ell=0}} = -2a_1 a_0\;\delta\left(\mu \mp \omega_o f_2 \lambda, \xi\right) B \tag{44}$$

$$\tilde{T}(\mu,\xi)\Big|_{\substack{n=0\\ \ell=\pm1}} = -2a_0 a_1\;\delta\left(\mu, \xi \mp \omega_o f_2 \lambda\right) C \tag{45}$$

$$\tilde{T}(\mu,\xi)\Big|_{\substack{n=\pm1\\ \ell=\pm1}} = 2a_1^2\;\delta\left(\mu \mp \omega_o f_2 \lambda, \xi \mp \omega_o f_2 \lambda\right) A \quad . \tag{46}$$

This distribution is shown in Figure 9. An identical distribution can be obtained by letting A = B′ + C′, B = C′ + A′, C = B′ + A′, and D = O in Eqs. (39) through (42). The first scheme we refer to as additive because for normal color imagery A, B, and C would be the additive primary separations (red, green, and blue) and D would be the integrated full-color image as recorded on a panchromatic black-and-white film. The second scheme is subtractive since the subsample exposures would be equivalent to cyan (white minus red), magenta (white minus green), and yellow (white minus blue). However, whether the three zones to be recorded are in the visible, ultraviolet, or infrared does not matter. As long as the logic of one of these two schemes is followed, we can store the information in registration and subsequently obtain spatially separated zone spectra. By inserting color filters over the various zone spectra[25] all channels can be projected simultaneously in perfect registration to produce true or false color images.

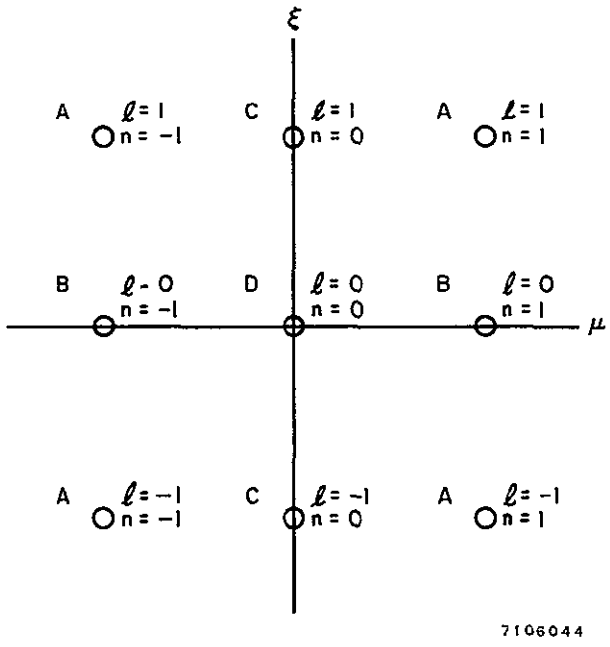

Figure 9. Square Array Fourier Spectrum Geometry

SECTION 3

EXPERIMENTAL APPARATUS, PROCEDURES, AND RESULTS

Only the overlay multiplexing experiments are described in this section; results of the square array interlace experiments involving the photofacsimile device are given in Section 4.

GENERAL

To record twelve channels of 10 line-pairs/mm imagery, Eq. (18) indicates that the encoding ruling must be at least 80 ℓp/mm. Initially we used a carrier of that frequency, but all the final recordings reported in this study were prepared with a 100 ℓp/mm Ronchi ruling, which provided a small guardband even for the twelve-channel experiments. Encoding angular increments of 15, 20 and 24.8 degrees were used for the twelve-, nine- and seven-channel exposures respectively. Six-channel experiments were discontinued early in the study because they did not permit storage of all seven ERTS separations on a single film frame. Twelve- and nine-channel recordings provided a limited means for documenting system parameters as a function of the number of images multiplexed.

COPY CAMERA

Photographs of the copy camera used for all of the overlay recordings are shown in Figure 10. The side view (Figure 10a) shows the major camera components: an Aristo Trans-Luminator, Model T-16, Series 3200 served as an extended uniform incoherent source; a Leitz 2 x 2 in. slide transport was used for holding the 35 mm object transparencies; a Fax-Nikkor f/5.6 (160 mm) was used for the copy lens; and a simple ruling holder-pressure pad fixture provided the film plane. The rear view (Figure 10b) shows this fixture in more detail. The Ronchi ruling is a 2 x 2 in. High Resolution Plate copy of a 100 ℓp/mm metal master, and it is cemented to a brass ring that can be rotated in the square aluminum plate. Studs on the back side of the ring enable rotations to be indexed in total darkness. Pins on the front side of fixture plate are used to locate and hold 35 mm film chips by means of their perforation holes.

A TRANS-ILLUMINATOR

B OBJECT SLIDE HOLDER

C 1:1 COPY LENS

D FILM PLANE

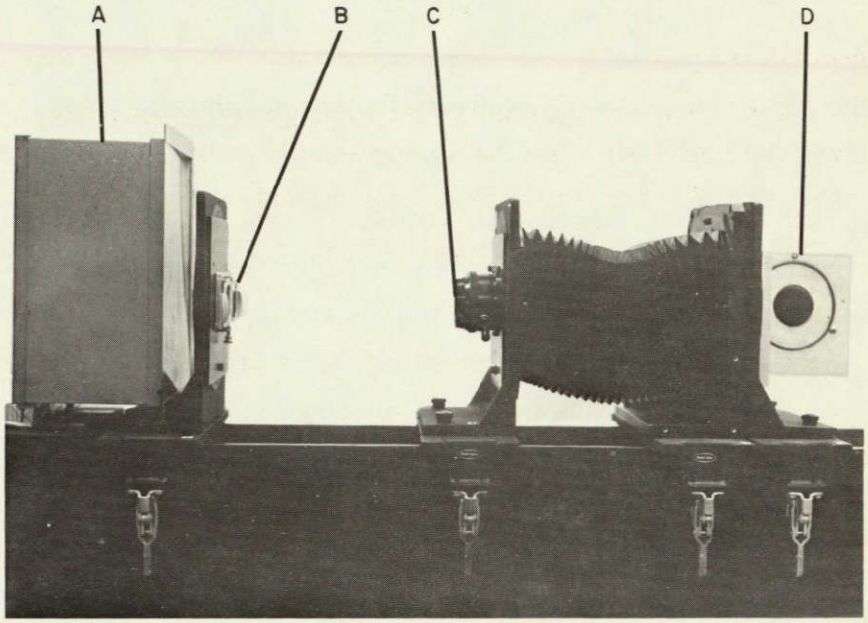

a. Side View

A LOCATING PINS

B ROTATABLE RONCHI RULING

C PRESSURE PAD

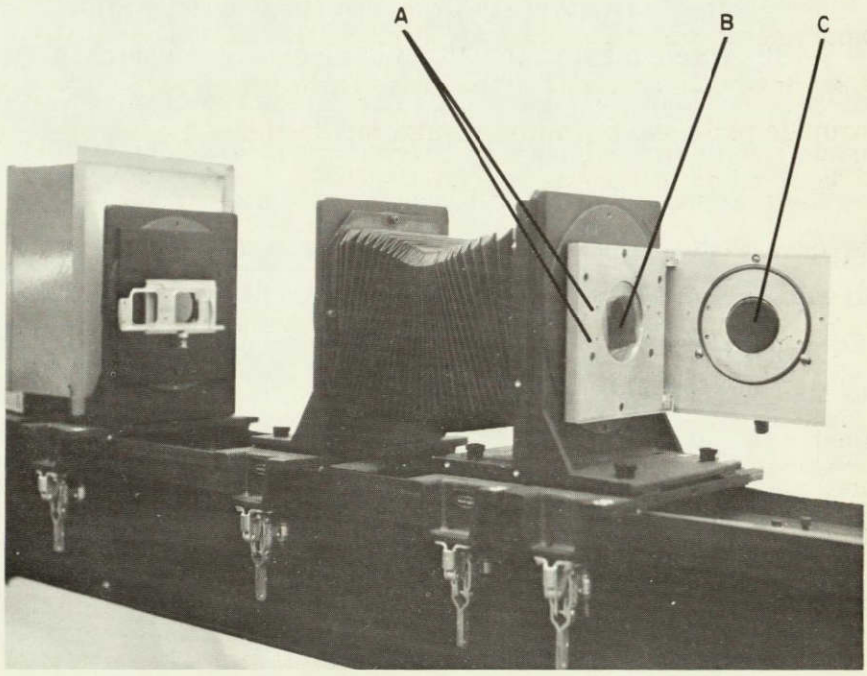

b. Rear View

7106045

Figure 10. Copy Camera

A pressure pad is mounted on a second aluminum plate that is hinged to the first on the right side. During exposure the second plate is closed and locked by means of three thumbscrews, and the spring-loaded pressure pad is actuated.

The distance between the object and image plane is 639.5 mm, and the lens is focused at a location just midway between the two planes. No special alignment procedure was used in setting up this camera. However, since all the machined surfaces of the optical bench carriers and uprights are fairly well squared off, they served as good, but by no means precise, references. For extremely precise alignments the three-point mounting feature of these uprights can be utilized to set two planes parallel by autocollimation, and the lens axis can be made perpendicular to the planes by the Boys point method. It was not necessary to use such techniques for this study.

TARGET PREPARATION

Two sets of targets were prepared for inputs: subjective targets, which in the final recordings consisted of the 35 mm travel slides shown in Figure 11, and objective targets as shown in Figure 12. The subjective targets were black-and-white copies made from color slides with reversal processed Panatomic-X film that was exposed so the maximum density difference would not exceed 1.5 and the average density difference would be about 1.3. These transparencies therefore had a considerably greater brightness range than was indicated desirable by the theoretical model in Eq. (3). However, at the time the targets had to be prepared we decided it was better to risk the possibility of some crosstalk rather than overly restrict the input image contrast. In retrospect it is clear that an extended range reversal process equivalent to $\gamma = -1/2$ storage would have been preferable, but additional photographic investigations would have been required to work out such a process initially.

Only five objective targets were prepared as such, and the additional seven required to make up to twelve exposures were selected from the subjective set. The three resolution targets had the standard spatial frequency progression given in Table 1. The high-contrast positive target had a density difference of $\Delta D = 1.3$, the high-contrast negative a $\Delta D = 1.10$, and the low-contrast positive a $\Delta D = 0.4$.

a

b

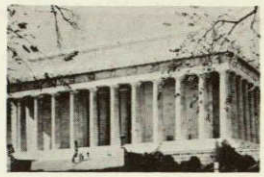

c

d

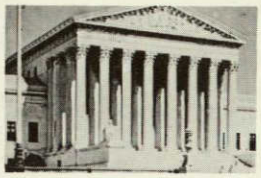

e

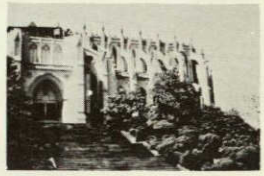

f

g

h

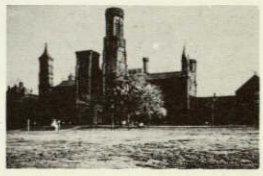

i

j

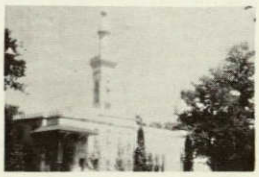

k

l

7105031

Figure 11. Subjective Input Targets
Seven-Channel: a through g
Nine-Channel: a through i
Twelve-Channel: a through l

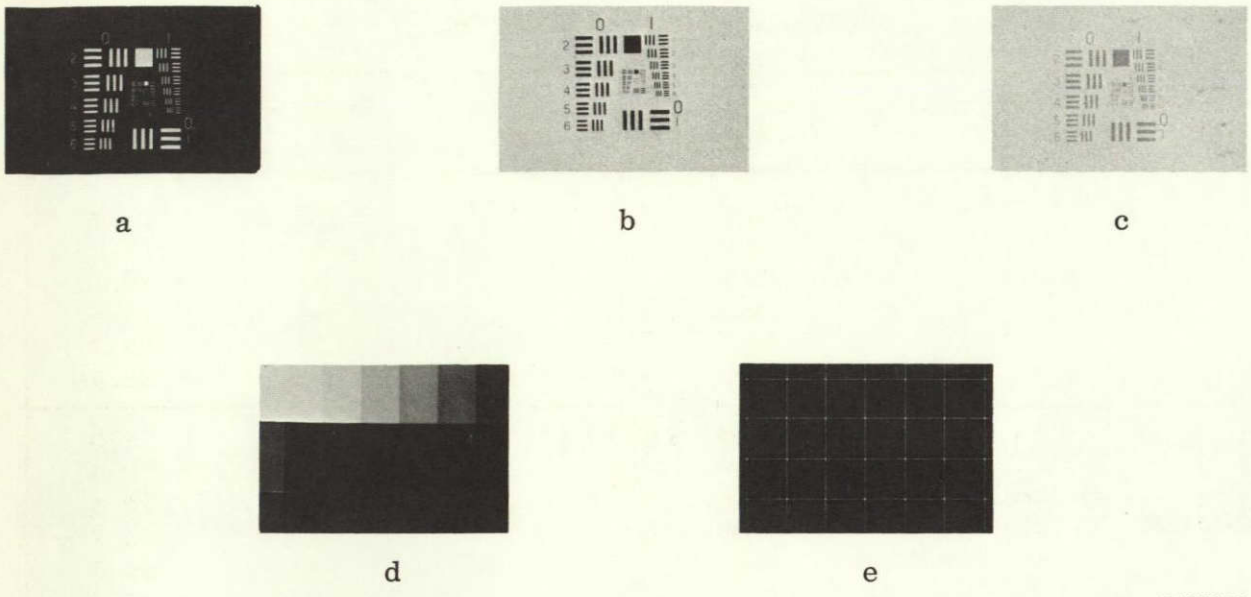

Figure 12. Objective Input Targets
Seven-Channel: these targets plus a and g of Figure 11
Nine-Channel: these targets plus a, g, h, j of Figure 11
Twelve-Channel: these targets plus a, g, h, j, l, e of Figure 11

The step tablet density calibration as measured on a Macbeth Densitometer, Model TD-102 is given in Table 2. This target was made by overlaying the first seven steps of a Kodak step tablet as given in the first row with a strip of uniformly fogged film of 0.08 density to form the second row and a neutral density filter strip of 1.0 to form the third row.

Calibration of the mensuration grid target is given in Table 3 and the line-column designations are shown in Figure 13. This target was calibrated by averaging three measurements for each line and column made on a Scientific Instruments comparator that had a smallest division scale of 0.01 mm.

The final target designed specifically for crosstalk measurements was simply a 0.9 neutral density filter placed over one half the 35 mm field and rotated with each exposure about the optical axis to produce the fan-shaped exposure shown in Figure 14.

Table 1. Resolving Power Target $\sqrt[6]{2}$ Progression
(Values for Individual Targets)

Group No.	Element No.	RP ℓp/mm	Group No.	Element No.	RP ℓp/mm
-2	1	0.250	4	1	16.0
	2	.280		2	17.95
	3	.315		3	20.16
	4	.353		4	22.62
	5	.397		5	25.39
	6	.445		6	28.51
-1	1	0.500	5	1	32.0
	2	.561		2	36.0
	3	.630		3	40.3
	4	.707		4	45.3
	5	.793		5	50.8
	6	.891		6	57.0
0	1	1.000	6	1	64.0
	2	1.12		2	71.8
	3	1.26		3	80.6
	4	1.41		4	90.5
	5	1.59		5	102.
	6	1.78		6	114.
1	1	2.00	7	1	128.
	2	2.24		2	144.
	3	2.52		3	161.
	4	2.83		4	181.
	5	3.17		5	203.
	6	3.56		6	228.
2	1	4.00	8	1	256.
	2	4.49		2	287.4
	3	5.04		3	322.6
	4	5.66		4	362.0
	5	6.35		5	406.4
	6	7.13		6	456.2
3	1	8.00			
	2	8.98			
	3	10.1			
	4	11.3			
	5	12.7			
	6	14.3			

Table 2. Step Tablet Calibration

Step	Density Measurement		
	Row 1	Row 2	Row 3
1	0.06	0.14	1.06
2	.20	.28	1.20
3	.34	.42	1.34
4	.48	.56	1.48
5	.62	.70	1.62
6	.76	.84	1.76
7	.90	.98	1.90

Table 3. Mensuration Grid Calibration

Measurement Average (mm)		
Lines	Columns	
L_1 = 31.26	C_1 = 15.62	C_5 = 15.63
L_2 = 31.27	C_2 = 15.62	C_6 = 15.63
L_3 = 31.27	C_3 = 15.63	C_7 = 15.63
L_4 = 31.26	C_4 = 15.63	C_8 = 15.64
L_5 = 31.26		

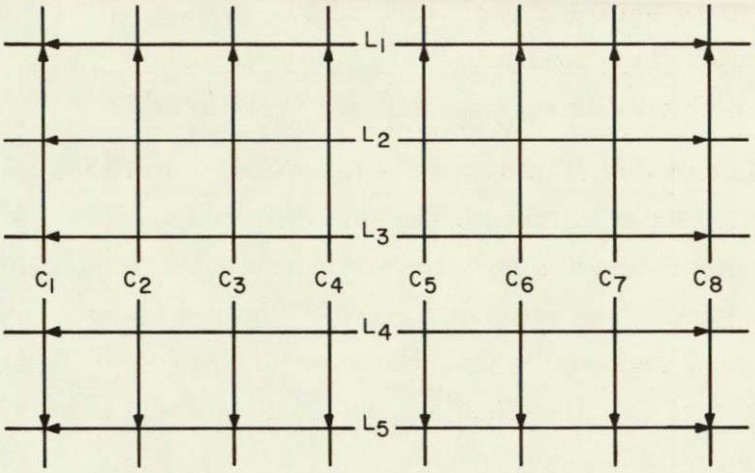

Figure 13. Line-Column Designations for Mensuration Grid

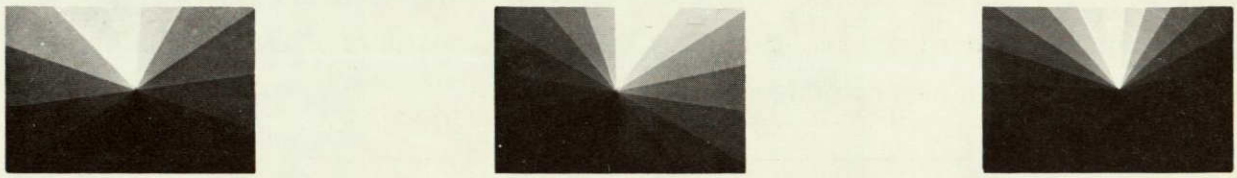

Figure 14. Crosstalk Control Exposure Pattern
a. Seven-Channel
b. Nine-Channel
c. Twelve-Channel

MULTIPLEXED RECORDINGS

The procedure followed in making the multiple image recordings was partially indicated in the copy camera description. Film handling for all the final recordings had to be accomplished in total darkness since AHU 5460 is panchromatic. However, infrared light and a Snooperscope were used to facilitate certain procedures.

One of the first recording defects noticed was Newton rings caused by interference of light reflected in the air cavity between the AHU emulsion and the Ronchi ruling emulsion. The best way to suppress this interference phenomenon is to anti-reflection coat the ruling surface and thereby eliminate the resonant cavity that supports the

rings. Even though high efficiency anti-reflection coatings are simply not practical for application to a gelatin surface, they could be evaporated over or under a metallic ruling copied onto a glass substrate. The lead time required to fabricate such a ruling (8 to 10 weeks) precluded this approach in the present study.

An alternate method of eliminating the reflection is to fill the cavity with a liquid having a refractive index matched to the gelatin. This was the approach we took, and it required the application of a few drops of xylene between the ruling and emulsion before each exposure. The Snooperscope was required to execute this operation. It must be emphasized that this liquid gating procedure was simply an expedient in these experiments and that an anti-reflection coated ruling would have to be used in any practical system.

All exposures were made at a full lens aperture of f/5.6 at an average exposure time of about 1/5 of a second each, although some targets required as little as 1/10 of second and others as much as 1/2 of a second for AHU 5460 film. Photographs of the multiplexed recordings are shown in Figure 15, and details of the modulation patterns are evident in the photomicrographs in Figure 16.

NOT REPRODUCIBLE

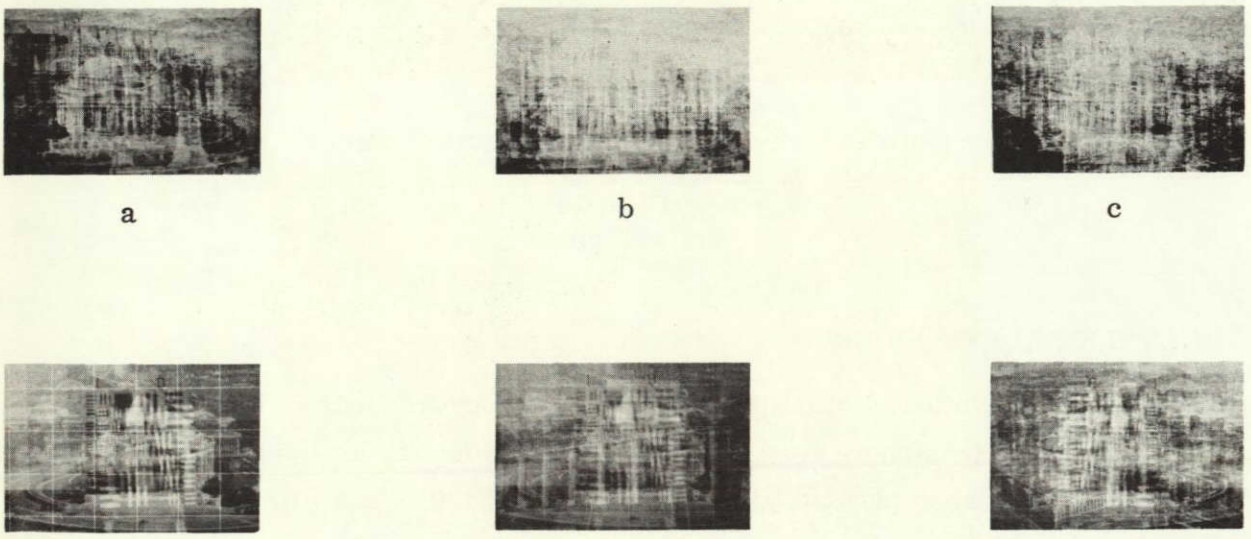

Figure 15. Multiplexed Recordings
a. Seven-Channel Subjective
b. Nine-Channel Subjective
c. Twelve-Channel Subjective
d. Seven-Channel Objective
e. Nine-Channel Objective
f. Twelve-Channel Objective

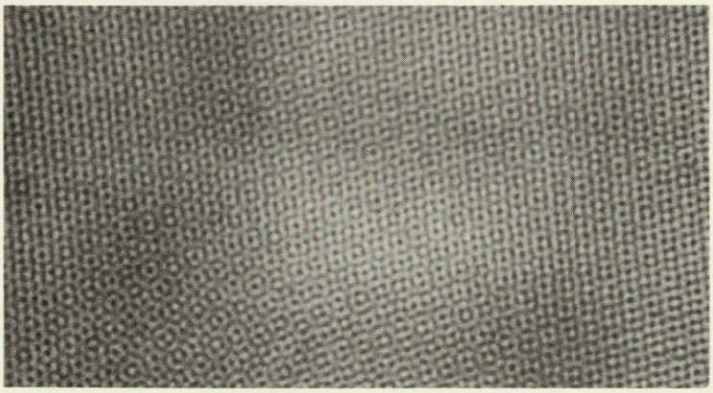

a. Seven-Channel

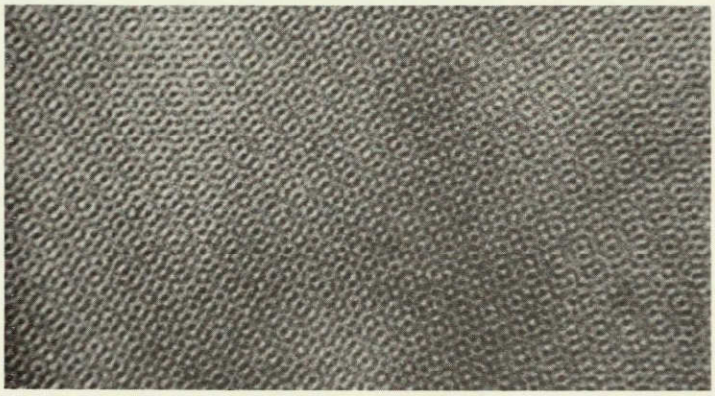

b. Nine-Channel

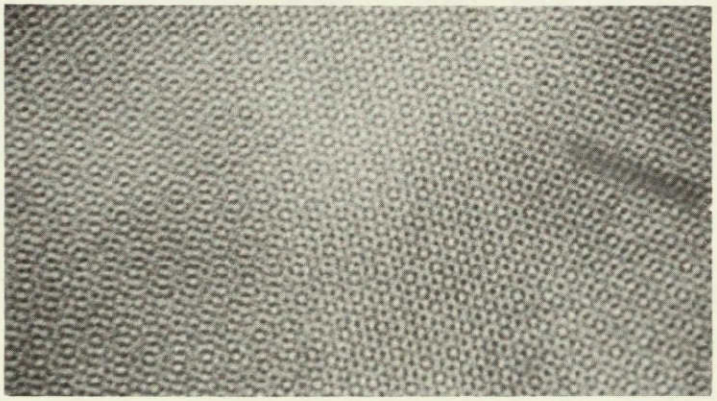

c. Twelve-Channel

7106047

Figure 16. Photomicrographs of Typical Seven-, Nine-, and Twelve-Channel Recordings

NOT REPRODUCIBLE

PROCESSING STUDIES

The first photographic storage was worked out for Eastman Kodak's SO-343. It was a print reversal method in which the negative was processed as indicated in Table 4 to produce the D log E characteristics shown in Figure 17, and the positive

Table 4. Gamma = 1 Process for SO-343
(All solutions at 70°F)

	Step	Duration
1.	Develop (Tech/Ops Extended Range Developer*)	20 min
2.	Wash	30 sec
3.	Fix (E.K. Rapid Fixer)	2 min
4.	Wash	30 sec
5.	Hypo. neutralize (Heico Inc. Perma Wash)	2 min
6.	Wash	2 min
7.	Photo Flo (E.K. 200 solution)	30 sec
8.	Air dry	15-20 min

*Tech/Ops Extended Range Developer formulation

Ingredient	Amount
Distilled water	750 ml
Potassium hydroxide	15 g
Potassium sulfide	100 g
Graphidone (Hunt Chemical Co.)	24 g
E.K. Antifog #1	6 g
Potassium bromide	4 g
Acetic acid to pH 10	
Distilled water to make	1000 ml

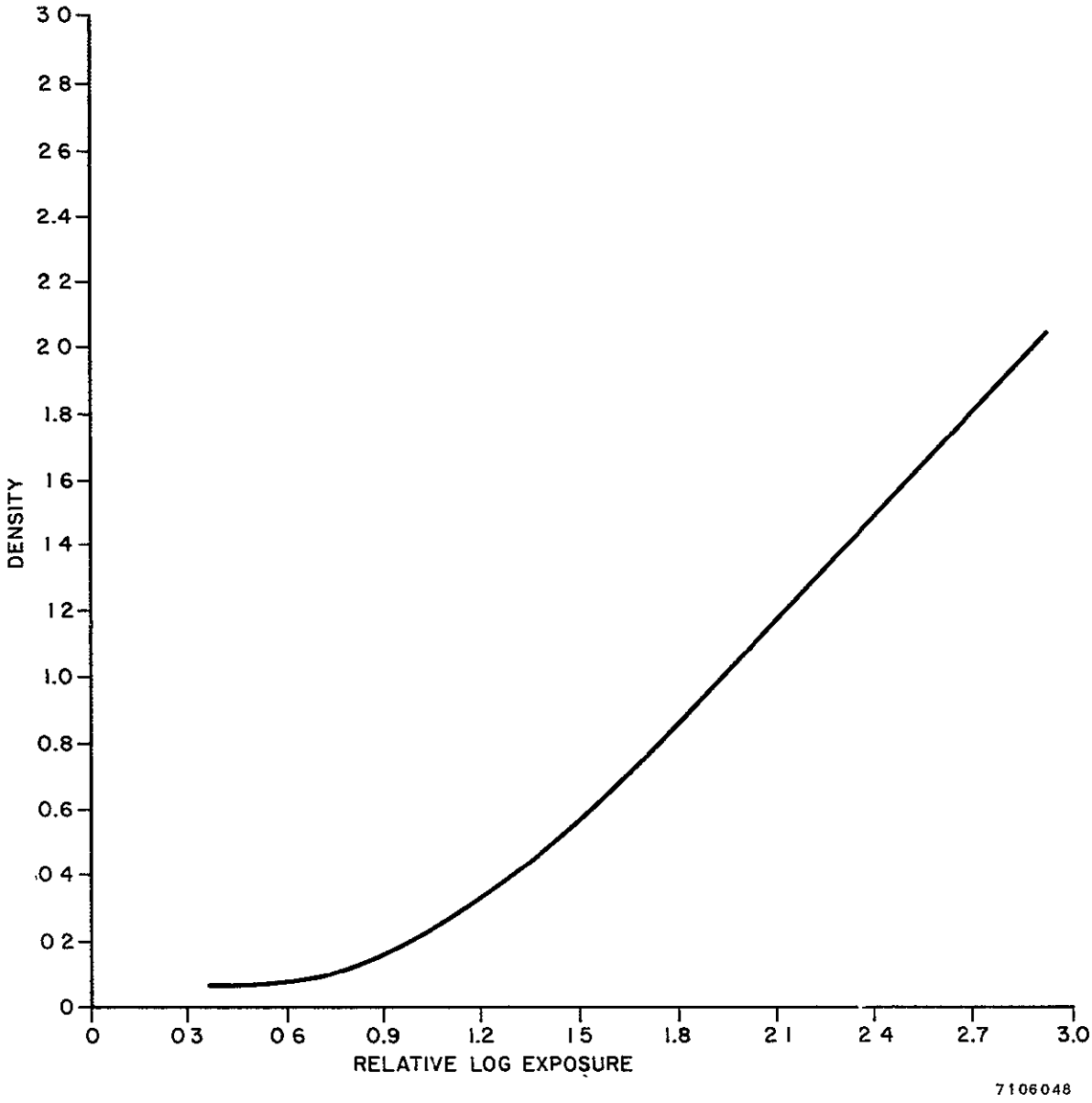

Figure 17. D log E Curve for SO-343 Gamma = 1 Process (Table 4)

print was processed as specified in Table 5 to yield the D log E curve plotted in Figure 18. This combination of gammas satisfied the requirement of Eq. (7) that $\gamma'\gamma/2$ equal 2.

Table 5. Gamma = 2 Process for SO-343
(All solutions at 70°F)

	Step	Duration
1.	Develop (Acufine Inc. Acufine Film Dev.)	5 min
2.	Wash	30 sec
3.	Fix (E.K. Rapid Fixer)	2 min
4.	Wash	30 sec
5.	Hypo. neutralize (Heico Inc. Perma Wash)	2 min
6.	Wash	2 min
7.	Photo Flo (E.K. 200 solution)	30 sec
8.	Air dry	15-20 min

Operationally this process was very awkward because an iterative approach was needed to optimize both the multiple exposures and the contact print exposure. The multiple exposures on the negative could not be optimized independently because the extremely fine detail of the modulation (as shown in Figure 16) is in the range where conventional microdensitometry methods become unreliable. Ultimately, print reversal may be the preferred storage method especially where a large number of positive duplicates are to be made. No doubt this approach could have been worked out successfully once input target exposure limits were fixed, but we abandoned print reversal early in this study primarily because of its relative inflexibility and long turn-around cycle for an experimental program.

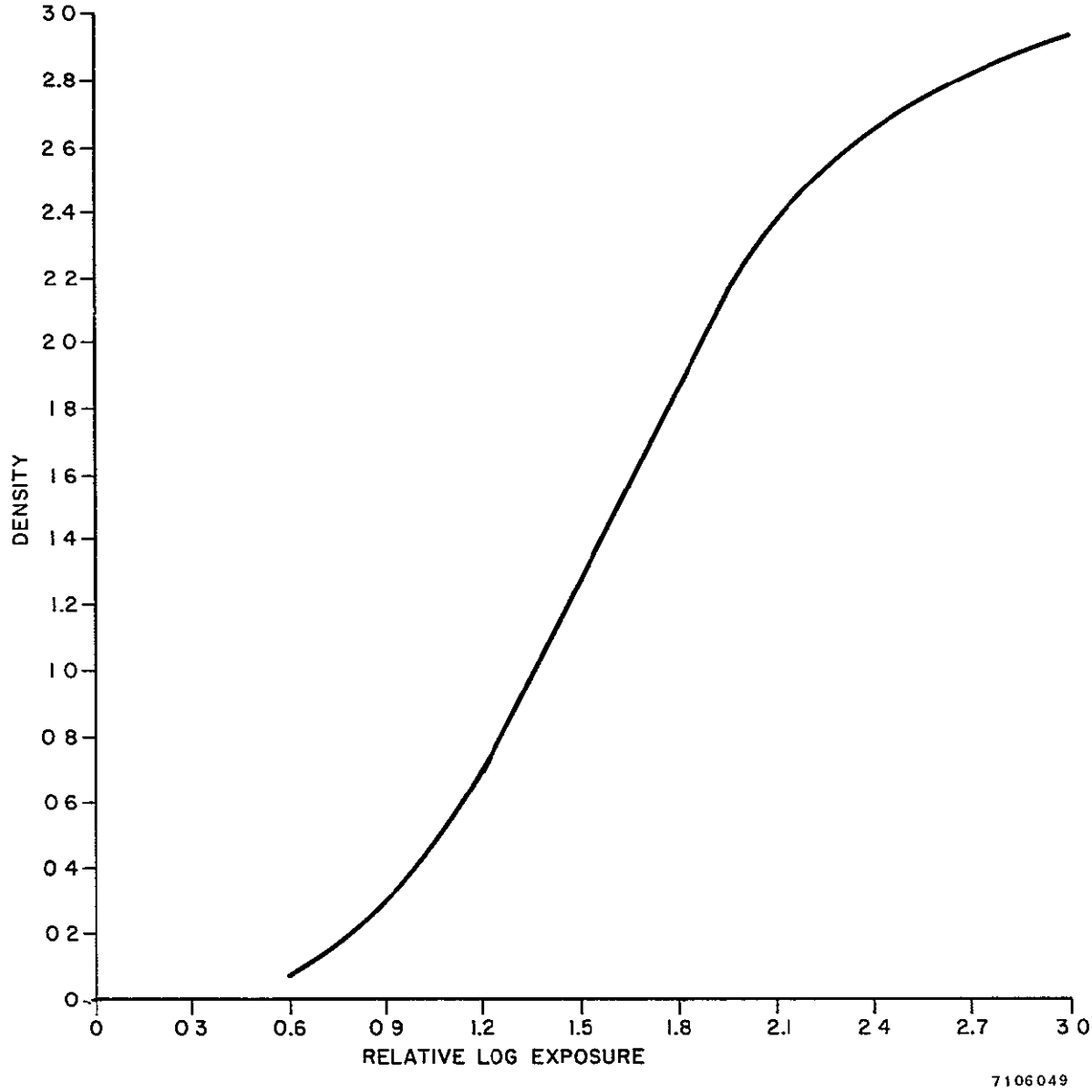

Figure 18. D log E Curve for SO-343 Gamma = 2 Process (Table 5)

To speed up the recording and storage process we next worked out a direct reversal process for SO-343 (as specified in Table 6) that produced the D log E curve shown in Figure 19. Despite the tremendous dynamic range exhibited in this D log E curve, SO-343 did not appear well suited for multiple imagery based on the observation of demodulated images. The reasons appear to be two-fold: the thick Estar base has poor optical quality that is exhibited as random noise in a dark-field viewing system, and resolution seems to be rapidly lost at higher exposure levels

Table 6. Gamma = -2 Process for SO-343
(All solutions at 68°F)

	Step	Duration
1.	Develop (E.K. D-19)	3 min
2.	Wash	30 sec
3.	Bleach (E.K. R-9)	2 min
4.	Wash	30 sec
5.	Clear (E.K. CB-3)	30 sec
6.	Wash	30 sec
7.	Expose to floodlight (500 watts at 30 in.)	30 sec
8.	Develop (E.K. D-95)	1.5 min
9.	Wash	30 sec
10.	Fix (E.K. Rapid Fixer)	2 min
11.	Wash	30 sec
12.	Hypo. neutralize (Heico Inc. Perma Wash)	2 min
13.	Wash	30 sec
14.	Photo Flo (E.K. 200 solution)	30 sec
15.	Air dry	15-20 min

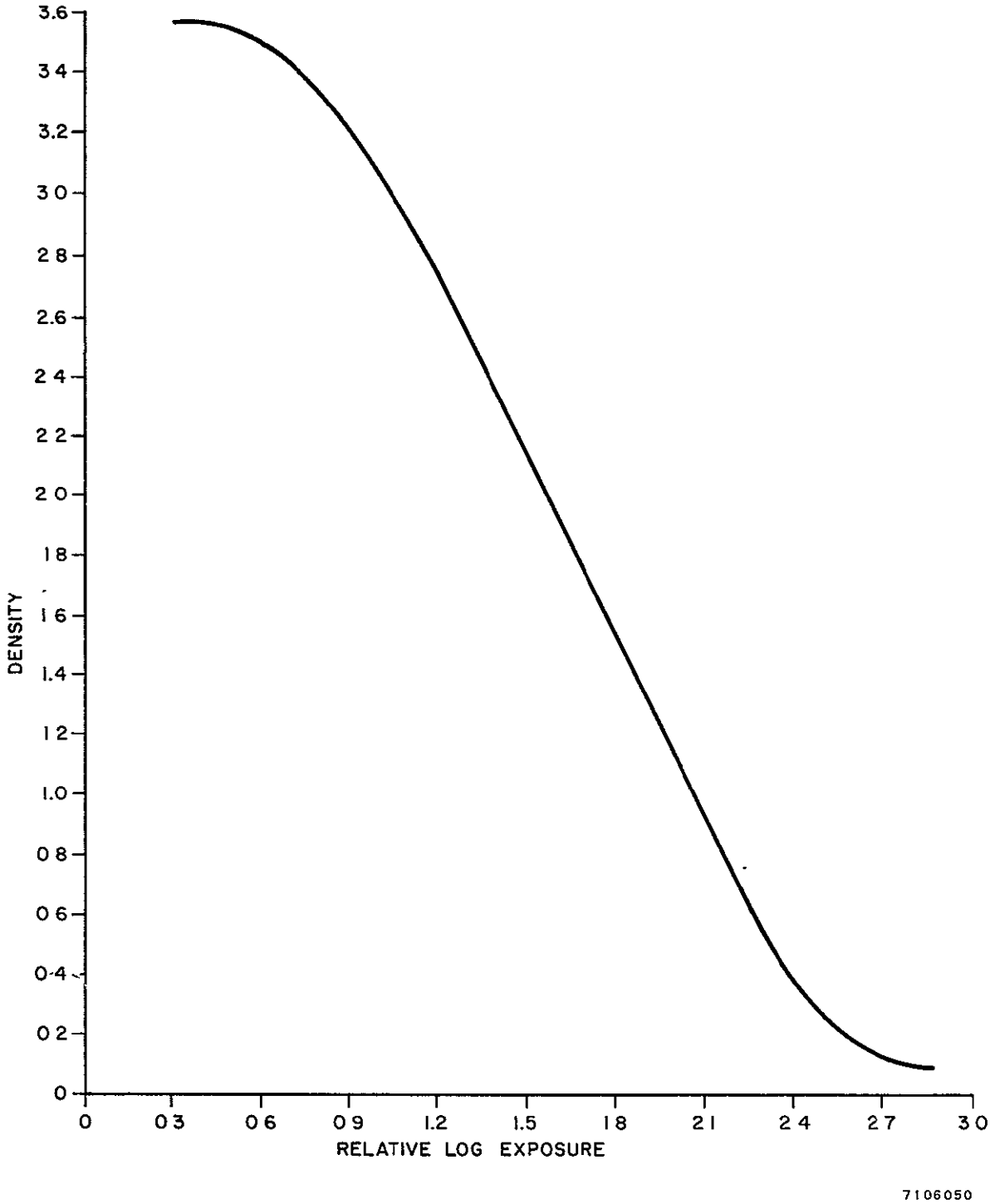

Figure 19. D log E Curve for SO-343 Gamma = -2 Process (Table 6)

perhaps because of its relatively poor antihalation properties. The origin of base noise appears to be particles of different refractive index either embedded in the substrate or in a backing coat. Normally the phase differences produced by these particles would not be detected in diffuse or incoherent illumination, but our retrieval device (since it is a dark-field system, with some properties in common with a schlieren system) enhances the contrast of phase objects.

The third process evaluated during this study was one we had used for several years both for multiple imagery and for the preparation of sequentially exposed tricolor images. The recording material was Recordak AHU, Type 5460, Microfile film. It was direct reversal processed as specified in Table 7 and yielded the D log E characteristics plotted in Figure 20. The D_{max} of this process is relatively low, which

Table 7. Gamma = -2 Process for AHU Type 5460 Microfile
(All solutions at 68°F)

	Step	Duration
1.	Develop (E.K. DK-50, 1 part stock to 2 parts water)	5 min
2.	Wash	1 min
3.	Bleach (E.K R-9)	3 min
4.	Wash	30 sec
5.	Clearing bath (E.K. CB-3)	30 sec
6.	Expose to floodlight (500 watts at 30 in.)	30 sec
7.	Develop (same as Step 1)	5 min
8.	Wash	1 min
9.	Fix (E.K. Rapid Fixer)	2 min
10.	Wash	30 sec
11.	Hypo. neutralize (Heico, Inc. Perma Wash)	2 min
12.	Wash	2 min
13.	Photo Flo (E.K. 200 solution)	30 sec
14.	Air dry	15-20 min

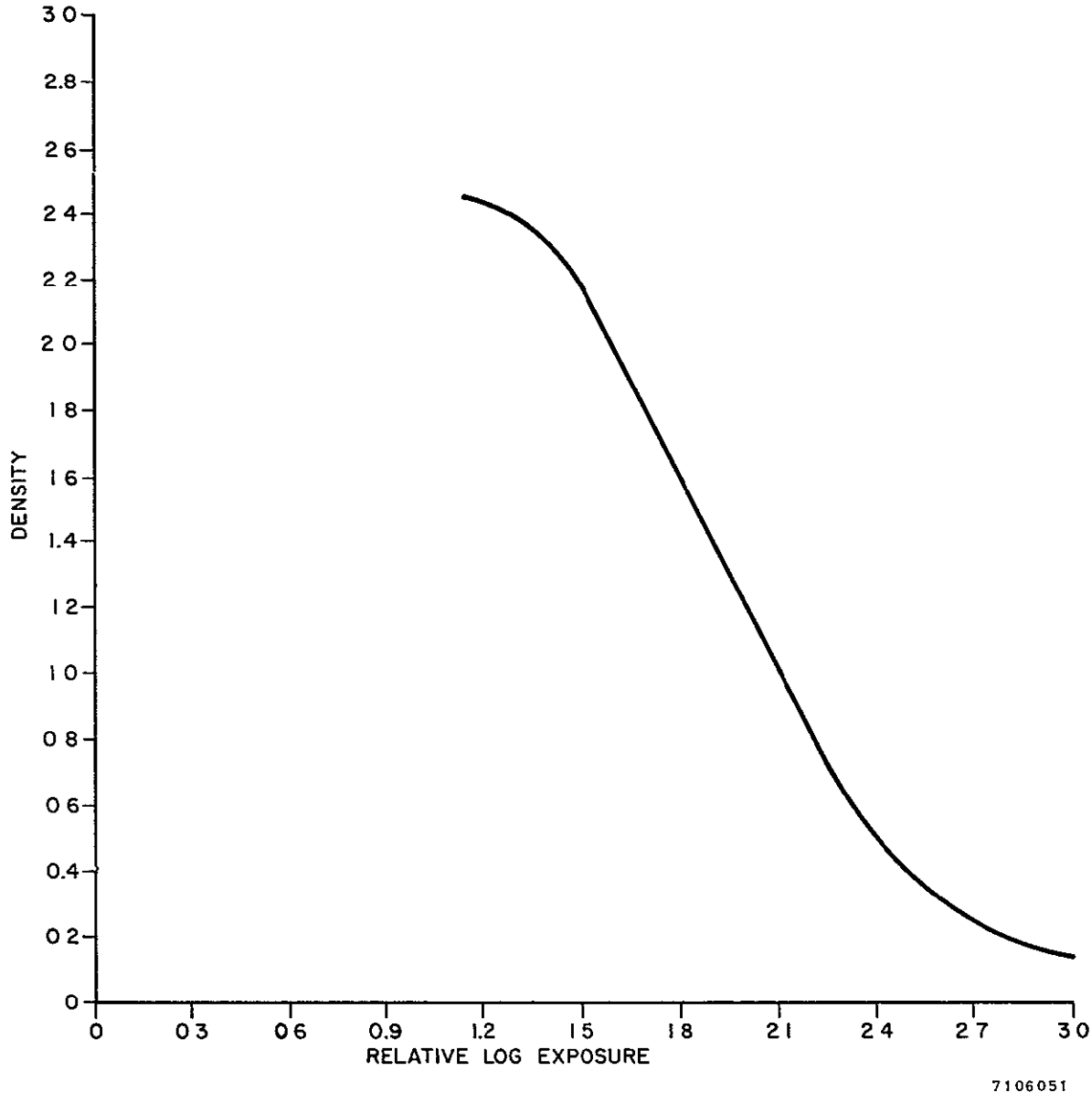

Figure 20. D log E Curve for AHU 5460 Gamma = -2 Process (Table 7)

should adversely influence the dynamic range capability in multiplexed exposures. On the contrary, however, this direct reversal process produced the best retireval, both in terms of minimum crosstalk and maximum retrieval brightness range.

The final process evaluated was one worked out at the Eastman Kodak Research Laboratory several years ago for Minicard film. This process is somewhat unique in that the first step calls for slightly prefixing the film, which tends to differentially dissolve part of the unexposed silver halide more than that which is exposed. The effect is to lower the base density and gamma in a manner similar to a prefogging exposure. Formulation of the process is given in Table 8 and the D log E characteristics in Figure 21. Dynamic range and D_{max} are considerably greater than for Type 5460

Table 8. Gamma = -2 Process for Minicard Film (All solutions at 68°F)

	Step	Duration
1.	Prefix (1 part fixer* to 18 parts water)	2 min
2.	Wash	1 min
3.	Develop (Boller's Developer†)	3.5 min
4.	Wash	1 min
5.	Bleach (E.K. R-9)	3 min
6.	Wash	1 min
7.	Clearing bath (E.K. CB-3)	1 min
8.	Expose to floodlight (500 watts at 30 in.)	30 sec
9.	Develop (E.K. D-95)	2 min
10.	Wash	30 sec
11.	Hypo. neutralizer (Heico, Inc. Perma Wash)	2 min
12.	Wash	2 min
13.	Photo Flo (E.K. 200 solution)	30 sec
14.	Air dry	15-20 min

*Kodak fixing bath F-5.

†Boller's developer formulation:

Sodium sulfite (des.)	60 g	Potassium bromide	10 g
Kodak Elon developing agent	20 g	Water to make	1 liter
Phenidone (Ilford Limited)	10 g	pH = 10.50	
Sodium hydroxide	10 g		

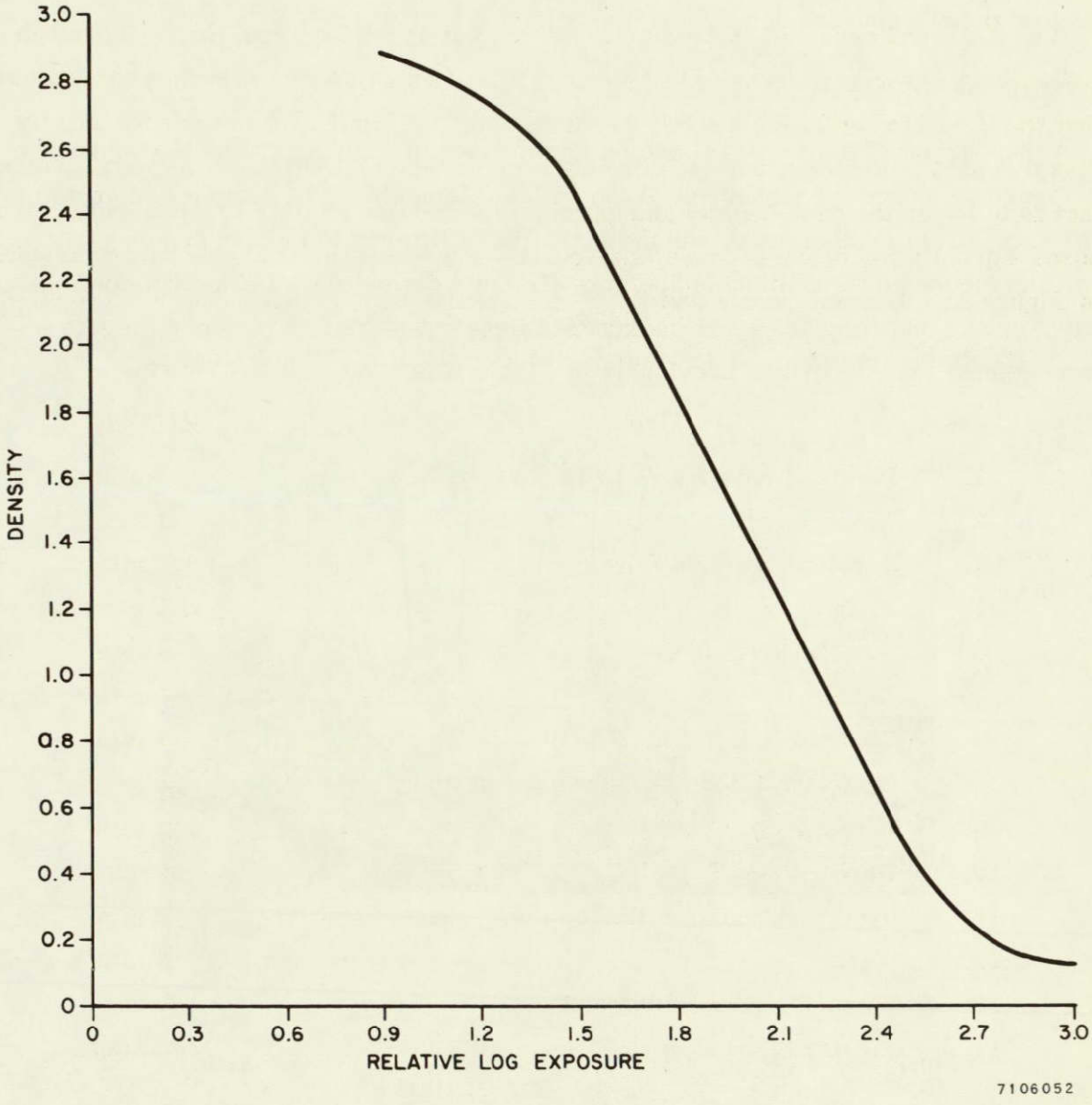

Figure 21. D log E Curve for Minicard Film Gamma = -2 Process (Table 8)

film, and since Minicard film is a higher resolution material, we would expect it to be better suited for multiplexed recording. Experimentally, however, Minicard proved slightly inferior, both in terms of crosstalk levels and its ability to retain shadow or low exposure detail.

RETRIEVAL PROJECTOR

A photograph of the retrieval projector is shown in Figure 22, and the schematic in Figure 23 shows the placement of the optical elements. The lamp house contains a 100 watt Osram mercury arc, which is spectrally filtered to the 546 nanometer green line and focused into the pinhole aperture (1.0 mm diameter). The pinhole defines a source plane and removes stray background light. A slightly different film gate arrangement than described previously in Figure 4 is used, but the Fourier

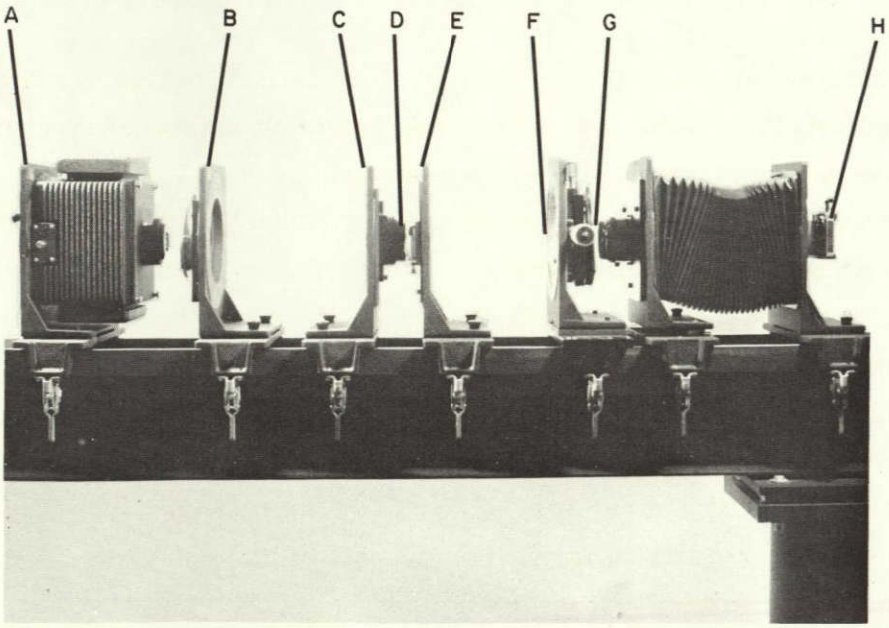

A LAMP HOUSE
B PINHOLE
C CONDENSER
D ROTATABLE PRISM
E MULTIPLEX RECORD
F SPATIAL FILTER APERTURE
G COPY LENS
H RECORDING CAMERA AND RETRIEVED IMAGE

7106053

Figure 22. Photograph of Retrieval Projector

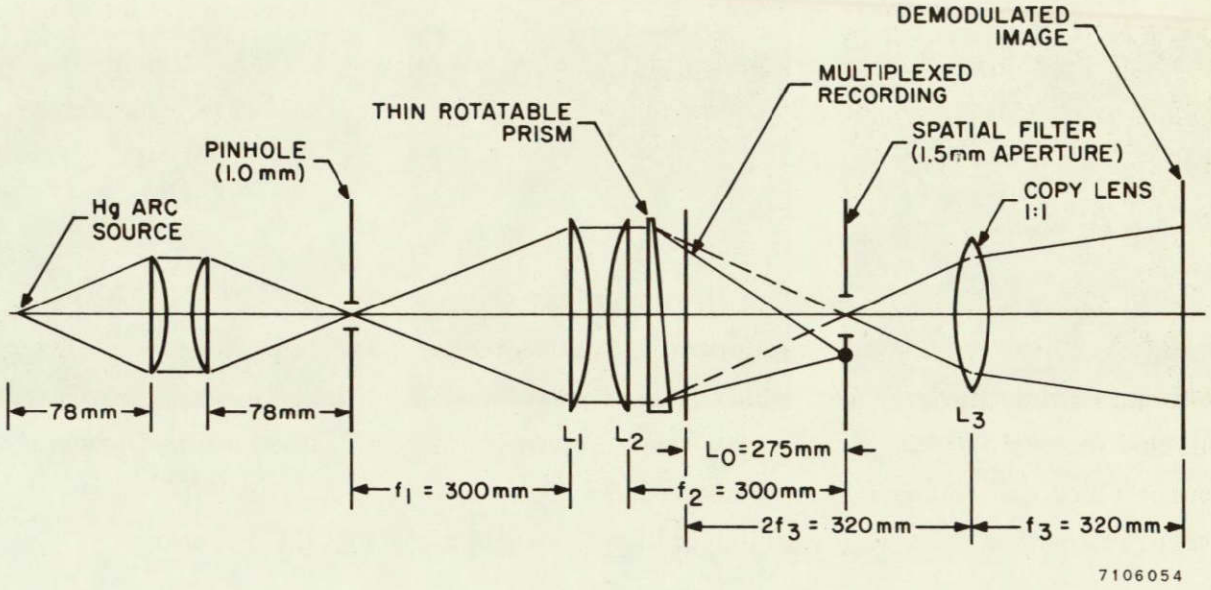

Figure 23. Schematic Diagram of Retrieval Projector

transform operations are identical. First, the film gate is located in a conventional position just beyond the second condenser lens, rather than between condenser elements. Second, a thin prism of diopter number 100 $\omega_o \lambda \approx 5.5$ is inserted between the condenser and film gate. The prism diopter or refraction angle is made just equal to the fundamental diffraction angle of the carrier so that by rotating the prism the various first order spectra are diffracted onto the optical axis. Ideally, to minimize potential copy lens aberrations, the pinhole or Fourier transform array would be imaged into the copy lens iris stop. However, the required aperture stop for spatially filtering the 10 ℓp/mm spectra of the multiplexed recordings is $2\omega_s L_o \lambda \approx 3.0$ mm (see Figure 23) and the Fax-Nikkon could not be stopped down that small. Therefore, we placed a spatial filter screen in front of the lens rather than disassemble the lens to insert the smaller iris stop.

SUBJECTIVE TARGET RETRIEVAL RESULTS

Photographs of the Fourier spectrum arrays as they appeared in the spatial filter plane are shown in Figure 24. One side order at a time was passed through the center of the spatial filter aperture, and the demodulated image was exposed in the 35 mm

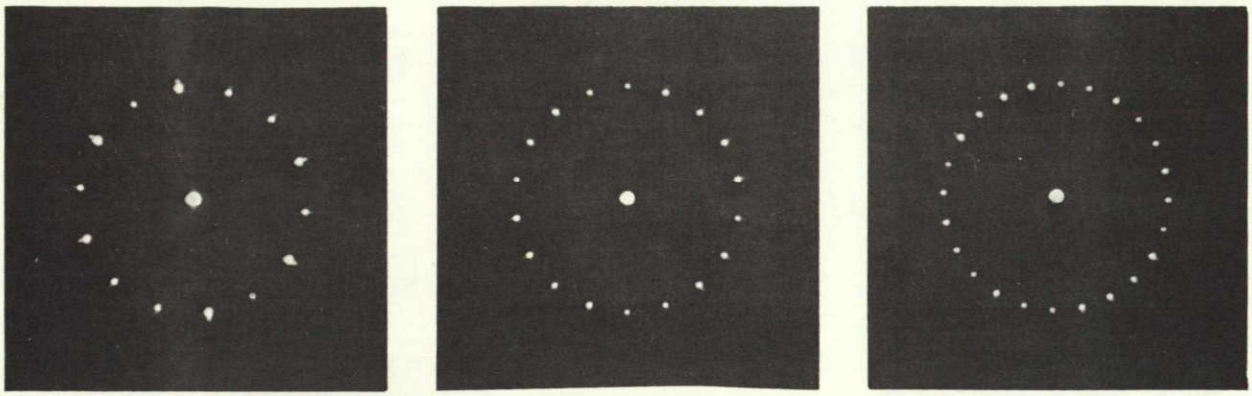

a. Seven-Channel Spectrum

b. Nine-Channel Spectrum

c. Twelve-Channel Spectrum

7106055

Figure 24. Typical Fourier Spectrum Arrays

camera back onto Panatomic-X film. The film was processed to a gamma of 1 and the negatives printed at 1:1; the results are shown in Figures 25, 26, and 27 for the seven-, nine-, and twelve-channel recordings respectively. Overall, the seven-channel retrievals are best, but they are not markedly different from the other two sets. The most noticeable difference is the appearance of low-contrast, low-frequency moiré fringes over several of the demodulated images (e.g., g and h in Figure 26 and e, i, and k in Figure 27). The origin of these fringes is a slight non-linearity in the photographic storage. They can be suppressed, however, by selecting carrier rotation increments that are not submultiples of 60 degrees as in the seven-channel recording. The crossproduct positions for the nine- and seven-channel spectra are compared in Figure 28. If there is the slightest deviation, Δ, from the nominal 20 degree rotation increments of the nine-channel recording, then there will be a very small displacement between the primary order and the crossproduct as indicated in Figure 28a. With Δ in radians this displacement can produce fringes of $\Delta\omega_o$ frequency if both the primary and crossproduct orders are passed through the spatial filter aperture. As Δ gets smaller, the fringe frequency simply becomes lower and perhaps more disturbing, but not lower in contrast. On the other hand, the 25.7 degree rotation increments of the seven-channel recording place any potential crossproducts on an axis just midway between primary orders as shown in Figure 28b,

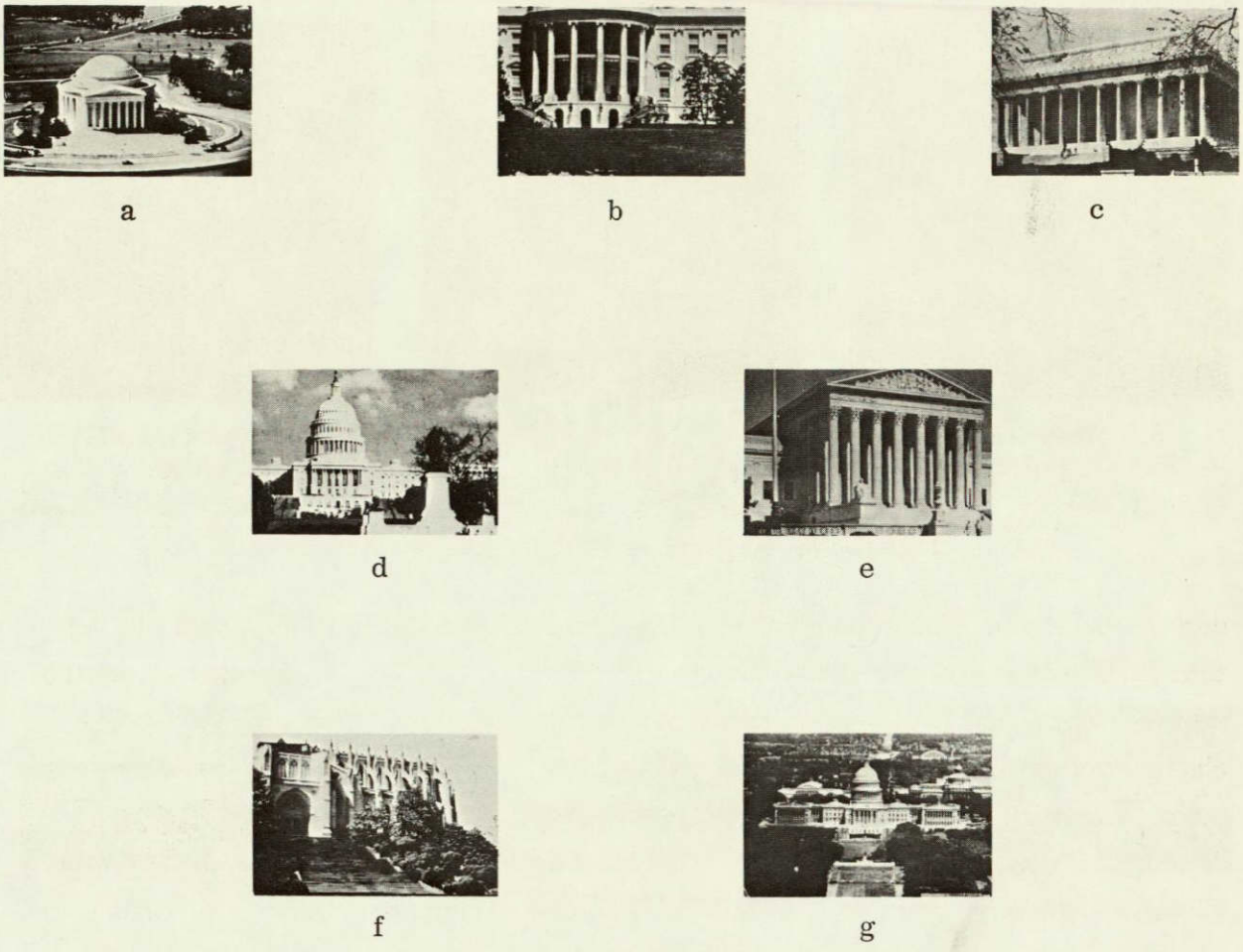

Figure 25. Retrievals of Seven-Channel Subjective Target Recording

and safely out of the $2\omega_s$ = 20 ℓp/mm pass band of the spatial filter. Thus, cross-products can never coherently beat and form moiré fringes in this case. The crossproduct constructions were shown for only one typical combination, but the explanation given can be extended to all other combinations and the same general conclusions will follow. Rotation increments should be chosen to place the potential crossproduct as far from the primary orders as possible and sufficient guardband maintained between these orders to avoid overlap. This last condition may require further oversampling on the part of the carrier.

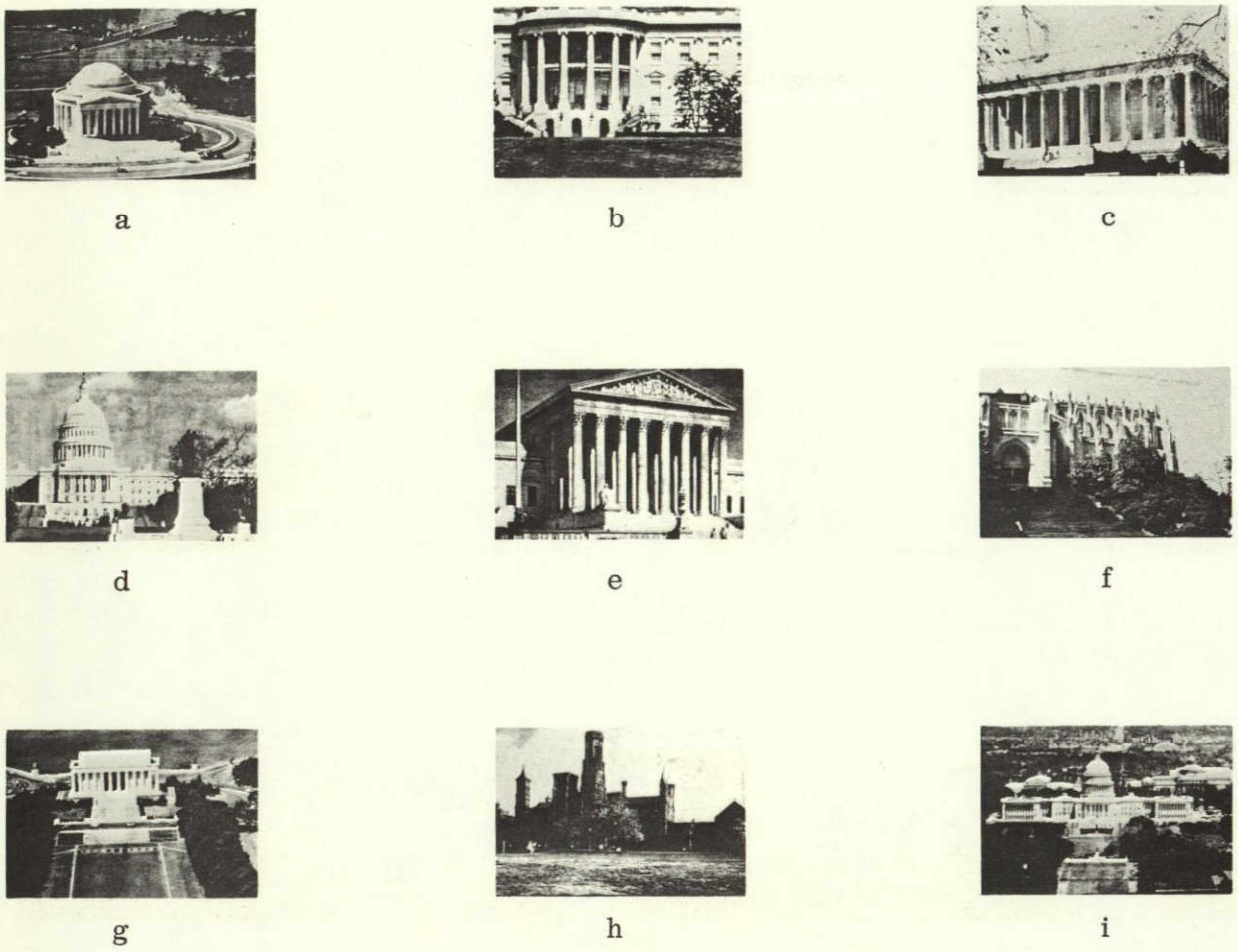

Figure 26. Retrievals of Nine-Channel Subjective Target Recording

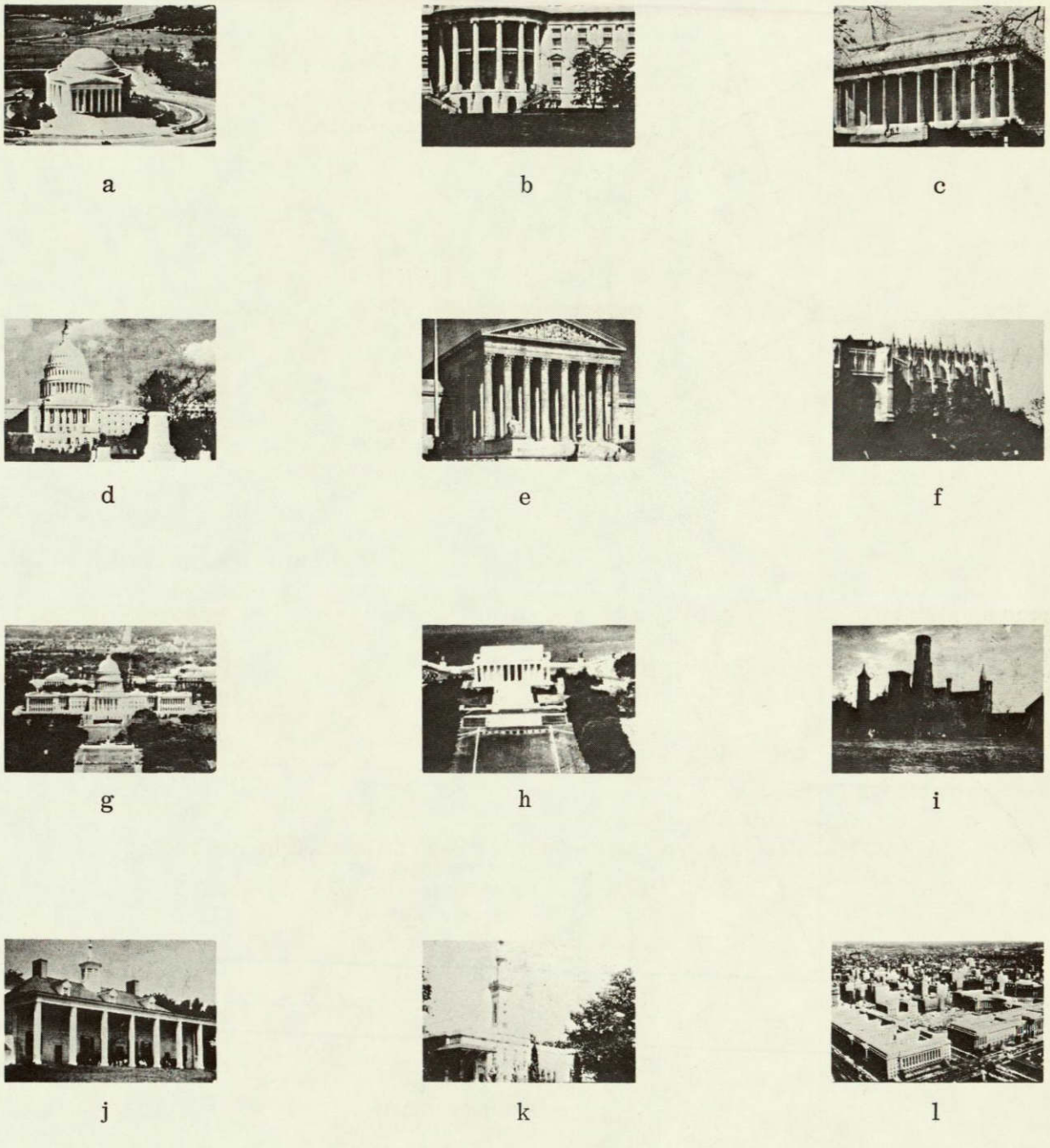

Figure 27. Retrievals of Twelve-Channel Subjective Target Recording

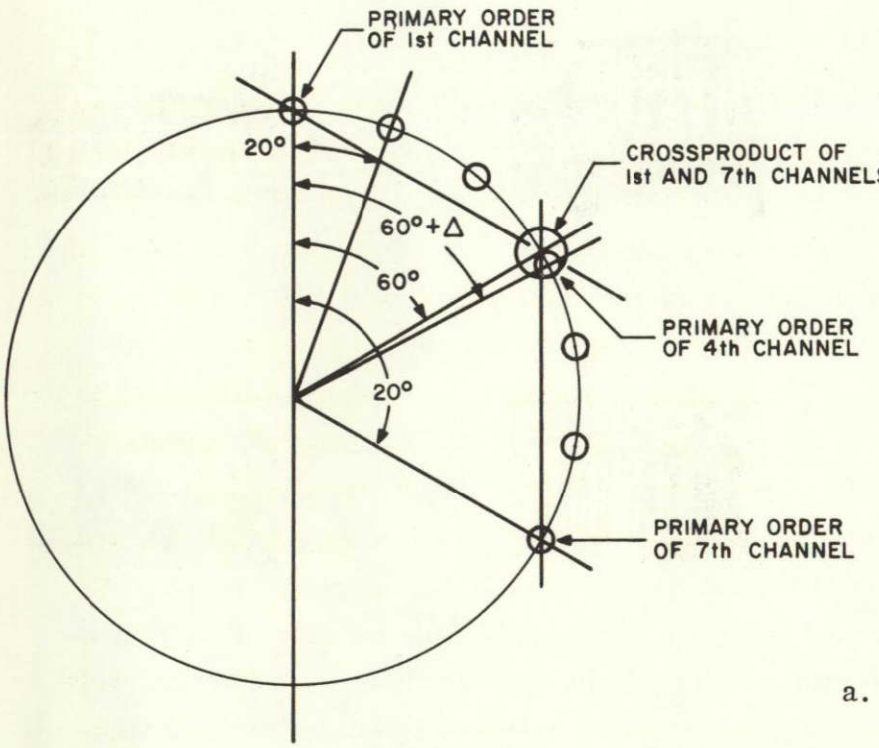

a. Nine-Channel Recording
$\Delta\phi$ = 20 deg

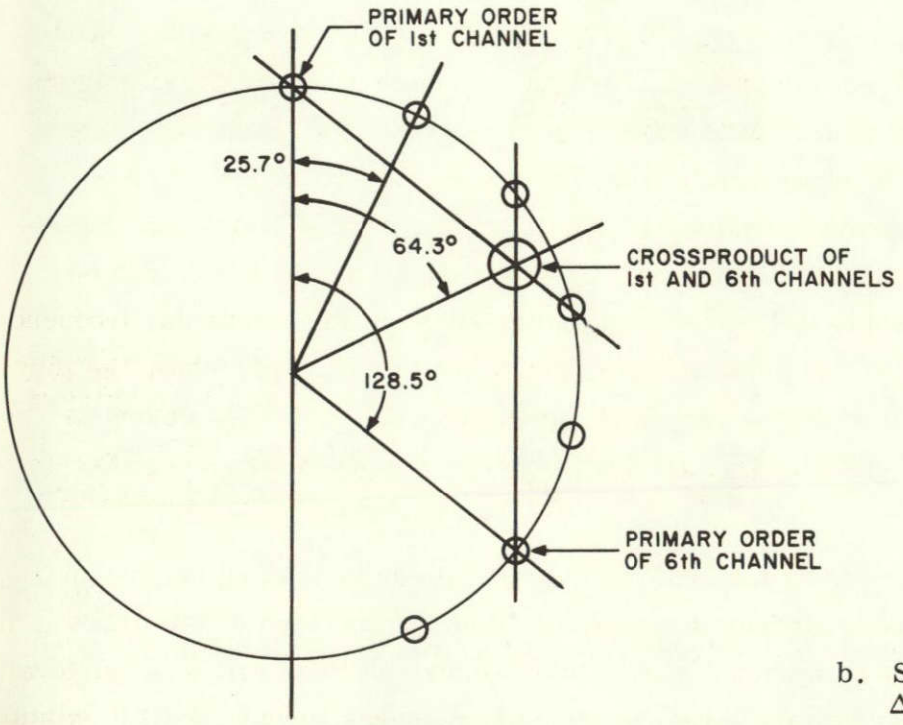

b. Seven-Channel Recording
$\Delta\phi$ = 25.7 deg

7106056

Figure 28. Position of Crossproduct Orders

OBJECTIVE TARGET RETRIEVAL RESULTS

The effective modulation transfer characteristics of this multiplexed system were calculated from the retrieval results of the USAF $\sqrt[6]{2}$ high contrast targets. Initially we had planned to make scanning photometer measurements of the three bar elements in the aerial image plane of the retrieval projector. Since that approach proved impractical and unreliable for the probes we had available, gamma = 1 recordings were made on Panatomic-X film and the film subsequently measured on a Joyce-Loebl scanning microdensitometer. These density readings were then converted back to the maximum (I_{max}) and minimum (I_{min}) intensity levels of the exposure. Modulation was then calculated for each frequency as $V = (I_{max} - I_{min})/(I_{max} + I_{min})$. The results of these measurements and calculations are plotted in Figures 29, 30, and 31 for the seven-, nine-, and twelve-channel recordings respectively. Ideally, if the encoding ruling performed as a point sampler (or as a line sampler in two dimensions) and the retrieval projector were perfectly coherent (i.e., if the source were infinitely small), the transfer function would be unity out to 10 $\ell p/mm$ and then fall abruptly to zero. This would not be a particularly desirable transfer function since it could introduce Gibb's phenomenon of edge ringing. Fortunately, the encoding ruling and film impulse response tend to produce average value sampling, and the finite size of the retrieval source makes the projector only partially coherent. These two conditions lead to an inherent falloff in the MTF curves. The major cause of visibility decay with higher frequencies, however, is not at all due to multiplexing principles, but rather to the MTF of the copy camera lens. Camera lenses can be designed that have reasonably flat transfer characteristics out to a particular frequency and then drop very rapidly. Such lenses were outside the scope of this study, but they are used in the television industry where large apertures are required to gather as much light as possible, but where high spatial frequency components could cause aliasing.

There is no direct reason why the MTF should fall with an increasing number of channels, but it is intuitively obvious that a greater demand is placed on the film's storage capacity, which in turn should lead to lower signal-to-noise ratios in retrieval. We should also expect that with the larger number of exposures, crosstalk (if it exists)

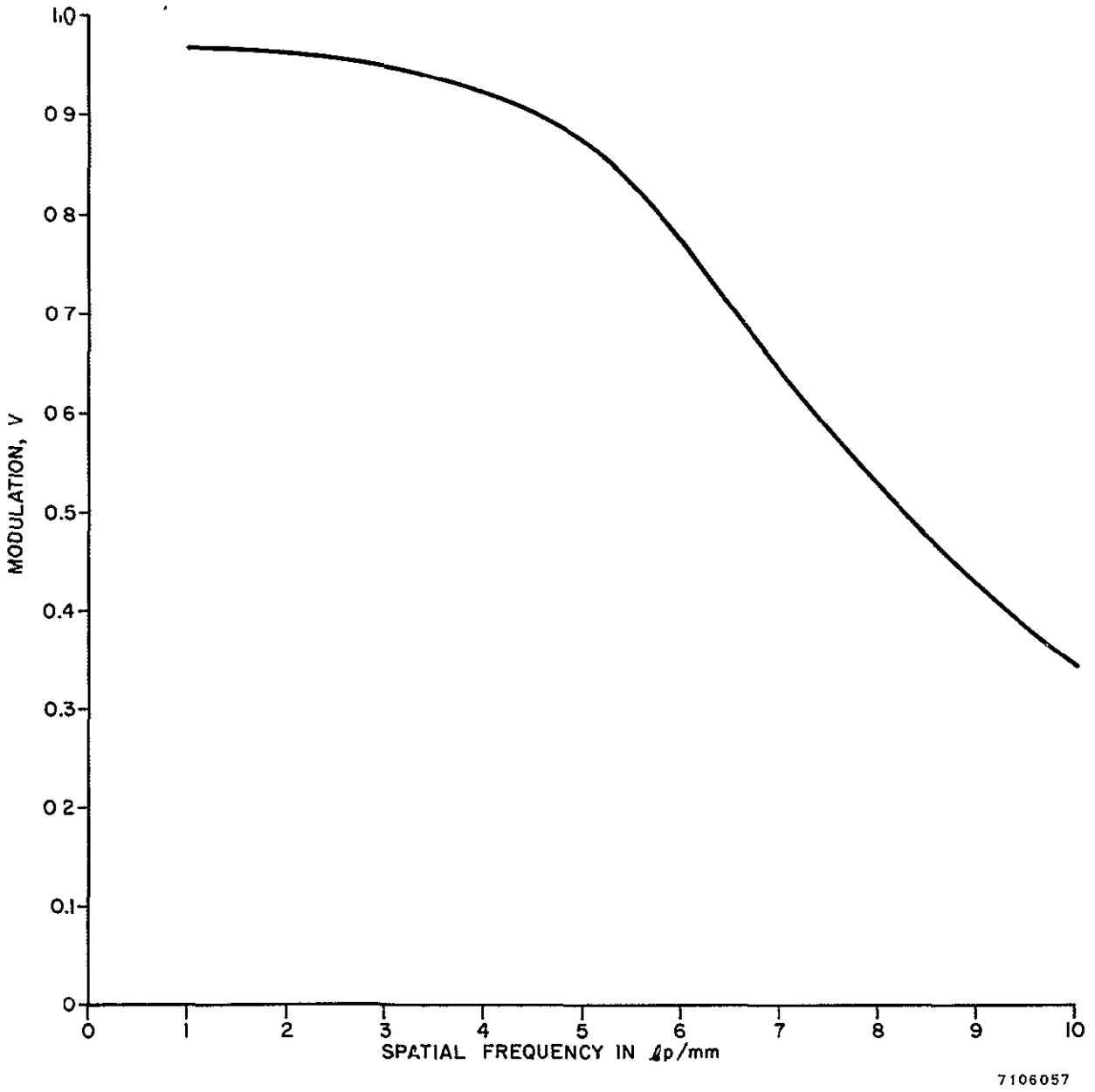

Figure 29. Effective Modulation Transfer Function for Seven-Channel Recording

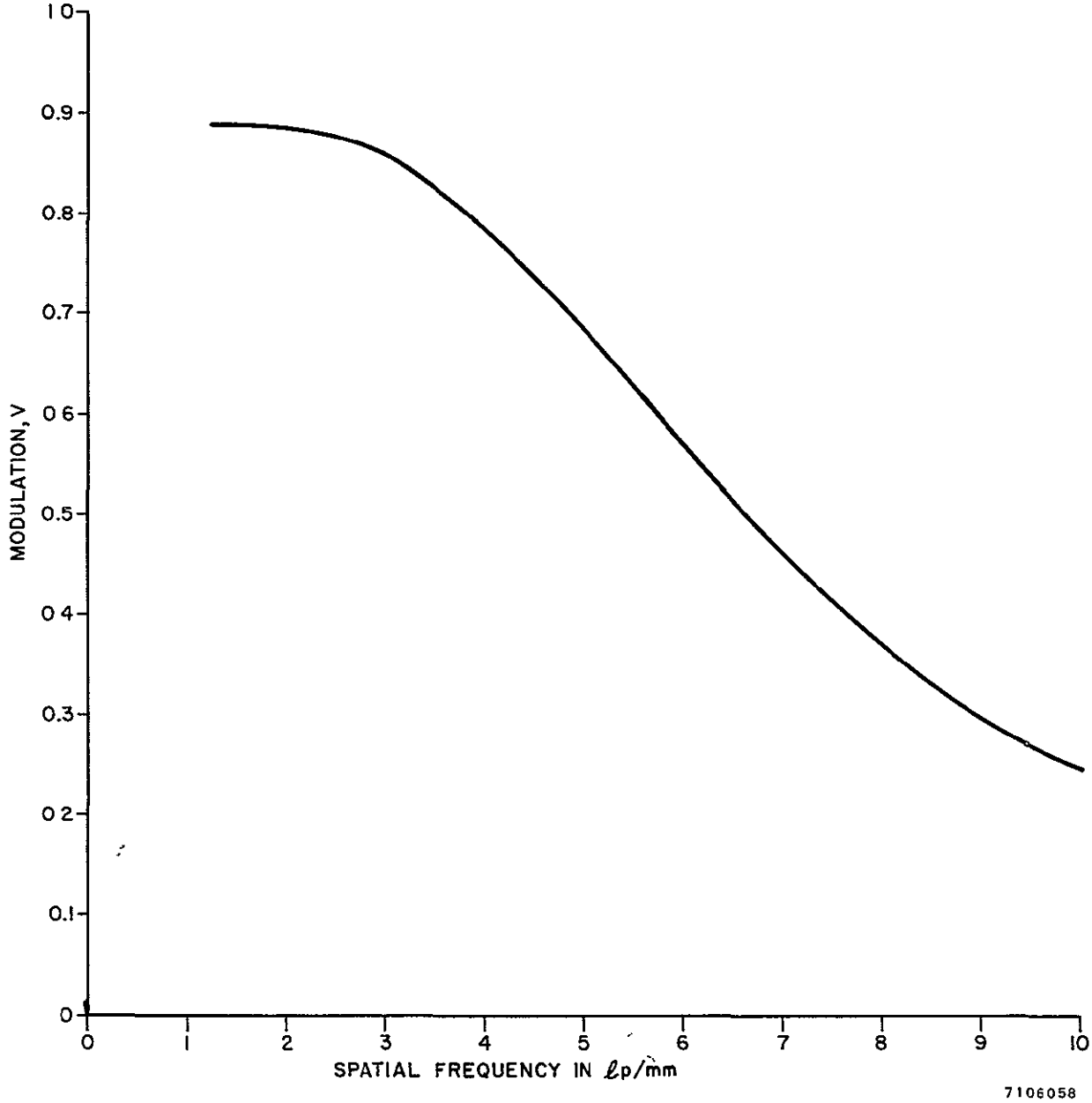

Figure 30. Effective Modulation Transfer Function for Nine-Channel Recording

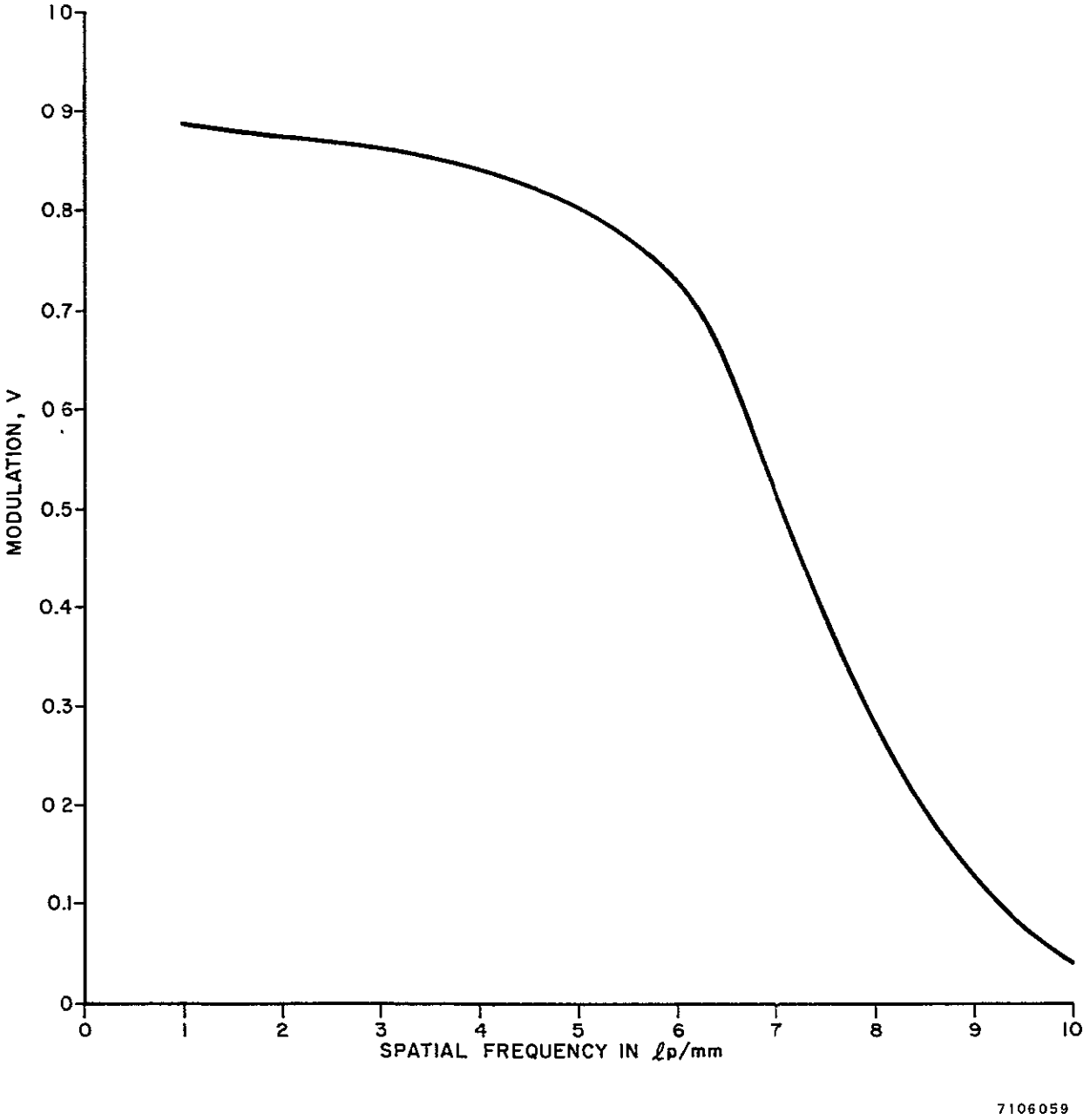

Figure 31. Effective Modulation Transfer Function for Twelve-Channel Recording

will become increasingly homogeneous and eventually become equivalent to a uniform low-level fogging exposure.

If enhancement of the higher spatial frequencies of a demodulated image was desirable in any particular application, the required operation is quite straightforward. Instead of using a clear, uniformly transparent aperture as the spatial filter in the retrieval projector, a shaded or inverse filter can be placed over the clear aperture. This filter is designed to attenuate low frequency components most strongly, intermediate frequencies only slightly, and high frequencies not at all. An example of such a filter that would make the MTF of the seven-channel recording equal to unity out to 10 ℓp/mm is shown in Figure 32.

The effective D log E characteristics were determined by means of the low-contrast step tablet described in Table 2. Retrieval measurements were made by scanning each step with a large aperture photometer probe. The results are shown in Figures 33, 34, and 35 for the seven-, nine-, and twelve-channel recordings respectively. The gammas of all three curves are very nearly equal to -2 as predicted theoretically, but with the seven- and nine-channel recordings just slightly less steep than -2, and the twelve-channel results a little steeper. A small variation in gamma can be expected since the film strips were hand-processed at different times with variously aged chemicals. The processing variations could be further reduced by automatic machine processing with scheduled chemistry replenishment. The important question, however, is not really whether the characteristic curve is precisely equal to -2, but whether the curve is linear. The results achieved and plotted in Figures 33, 34, and 35 are remarkably linear, indicating that no substantial distortion need be introduced by this multiplexing method. Of course, the gamma of -2 storage itself represents a quadratic distortion; as explained previously, however, this distortion can be anticipated and completely compensated by compressing the input exposures through an intermediate square root (i.e., $\gamma = 1/2$) storage. Exercising this precaution, we can store and reproduce tonal values of 100:1 dynamic range (i.e., 20 decibels) with no brightness distortions. It is interesting to note that unlike conventional sensitometry, we cannot generate toe and shoulder regions in the characteristic curves because these would require exposures that themselves would violate one of the linear storage requirements (i.e., exposures must be within E_{max} and E_{min}).

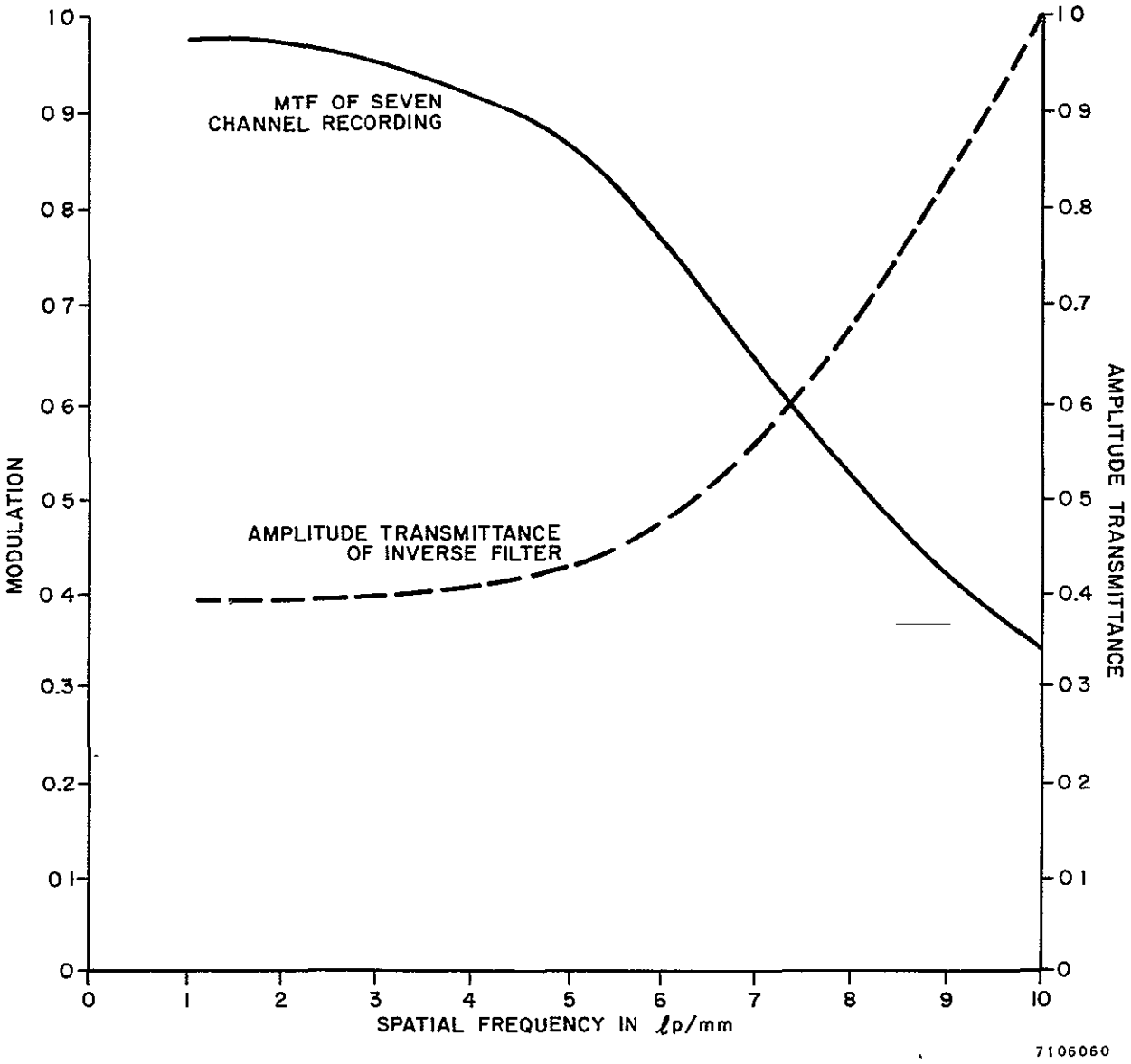

Figure 32. Amplitude Transmittance of An Inverse Filter That Would Normalize the Seven-Channel MTF Out to 10 Line-pairs/mm

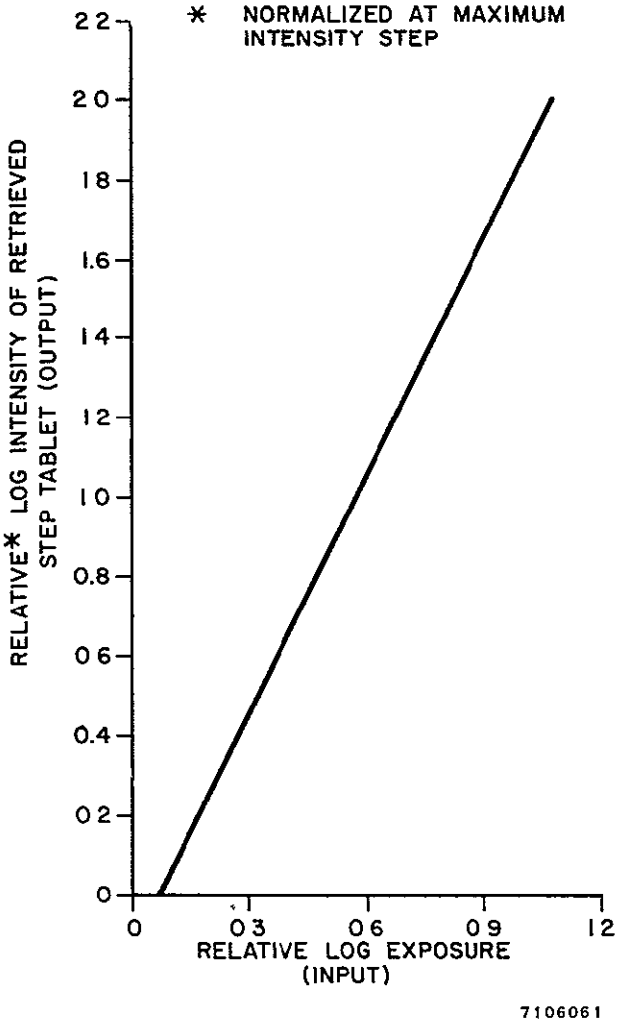

Figure 33. Effective D log E Curve for Seven-Channel Objective Target Recording (gamma ≈ -2)

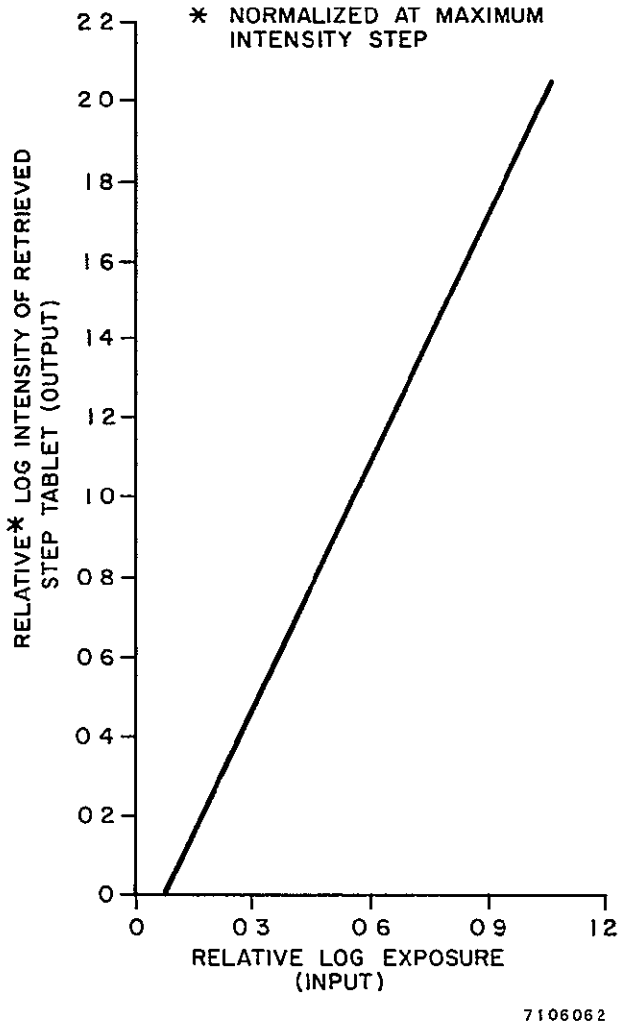

Figure 34. Effective D log E Curve for Nine-Channel Objective Target Recording (gamma ≈ -2)

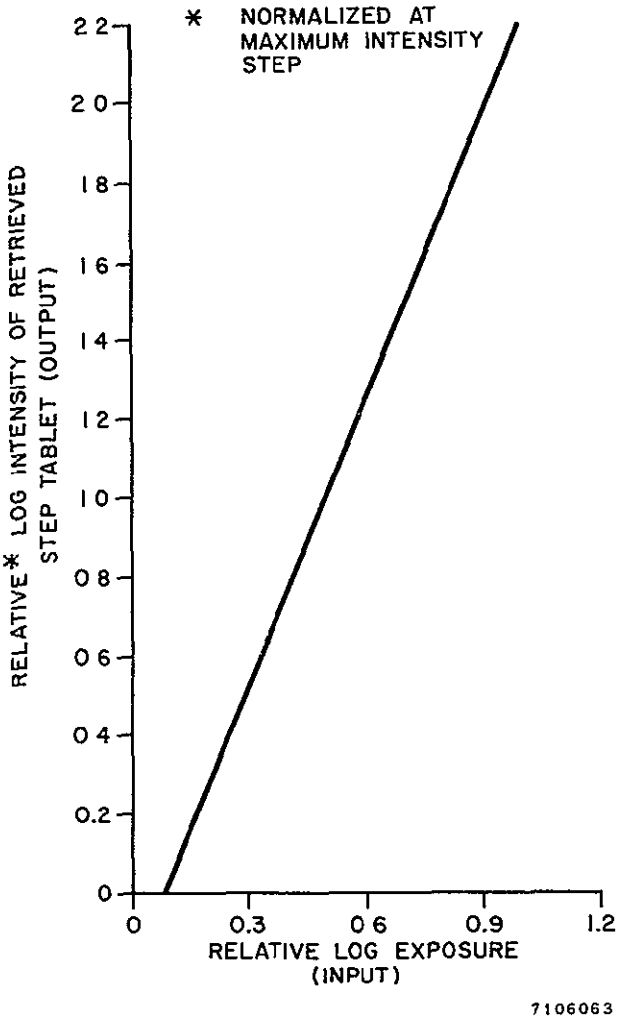

Figure 35. Effective D log E Curve for Twelve-Channel Objective Target Recording (gamma ≈ -2)

Dimensional distortions were documented by means of the coarse grid target calibrated as specified in Table 3. Theoretically, positional accuracy is limited only by the sampling period in this multiplexing method, and even that factor is no limitation if the image exposure has been properly band-limited. For example, the 100 ℓp/mm carrier has a period of 10 microns and so points cannot be located more accurately than ±5 microns simply because the carrier was introduced. On the other hand, one should not expect that points can be located with accuracy exceeding the

system's spread function; since we are dealing with 10 ℓp/mm imagery, the spread function introduces a nominal uncertainty of ±0.05 mm. Retrieval results of the mensuration grids are summarized in Table 9. This table was prepared by first measuring the raw line and column dimensions by the same comparator procedure used to calibrate the grid. The magnification factors shown on the top line of data were calculated as the average deviation between input and output grids. In other words, between the copy lens and projector lens there was actually a very slight magnification of

Table 9. Line and Column Dimensions (in mm) of Mensuration Grid Targets

Line or Column	Original Input Target	Seven-Channel Retrieval	Nine-Channel Retrieval	Twelve-Channel Retrieval
	Magnification Correction			
	1.0000	0.9846	0.9814	0.9807
L_1	31.26	31.27	31.25	31.25
L_2	31.27	31.28	31.27	31.26
L_3	31.27	31.28	31.29	31.27
L_4	31.26	31.29	31.30	31.27
L_5	31.26	31.29	31.28	31.25
C_1	15.62	15.64	15.60	15.65
C_2	15.62	15.65	15.62	15.62
C_3	15.63	15.64	15.63	15.61
C_4	15.63	15.63	15.60	15.63
C_5	15.63	15.63	15.62	15.62
C_6	15.63	15.62	15.62	15.61
C_7	15.63	15.62	15.64	15.64
C_8	15.64	15.63	15.65	15.64

about 1:1.012 in going from input targets to retrievals. The magnification correction factors were used as constant multipliers to the raw data, and the resulting products were tabulated as shown. Table 9 indicates that in the overall multiplexing system there was no pincushion, barrel, or any other dimensional distortion. The greatest deviation was 0.04 mm, which is still less than the spread function uncertainty. It is not surprising on the basis of the optics used that distortion was immeasurable in these experiments. The lenses were symmetric and designed for distortionless 1·1 imaging. In addition, only a small portion of the potential lens format was utilized in the paraxial region where distortions would be minimum even for nonsymmetric lenses. What is surprising initially is that random film shrinkage was not detected. However, when we recall that in this process only film chips and hand processing were used, it becomes reasonable to expect that stretching and subsequent shrinking would not be as severe as in a normal film transport device in which the film is pulled by the sprocket holes in one predominant direction. Since the variations exhibited in Table 9 are, for the most part, within measurement or judgment error, we conclude that in this study there was no detectable dimensional distortion.

Measurements of objective crosstalk are not as straightforward to make as those for resolution, gray scale, or distortion. The experimental plan was based on the simple proposition that, in the complete absence of crosstalk, fields of uniform exposure would be retrieved as fields of uniform intensity Variations from uniform intensity are a measure of crosstalk levels. The least complicated control target we could devise was a clear field divided by a 0.9 ND filter that produced an 8·1 exposure difference. The choice of a 0.9 ND filter was somewhat arbitrary, but it represented a realistic maximum Δ log E. By rotating the filter along with the encoding ruling, the fan-shaped exposure patterns previously shown in Figure 13 were formed.

Taking the seven-channel recording as an example, we can see that the brightest wedge segment running in an almost vertical direction received the maximum composite exposure, namely 7 overlapped bright-field exposures. The segments on either side received 6; the next two 5, then 4, 3, 2, and 1, and finally one segment on the bottom received no bright-field exposure. This situation is sketched in Figure 36. Notice that only channels 1 and 7 have wedges varying from 1 to 7 bright-field

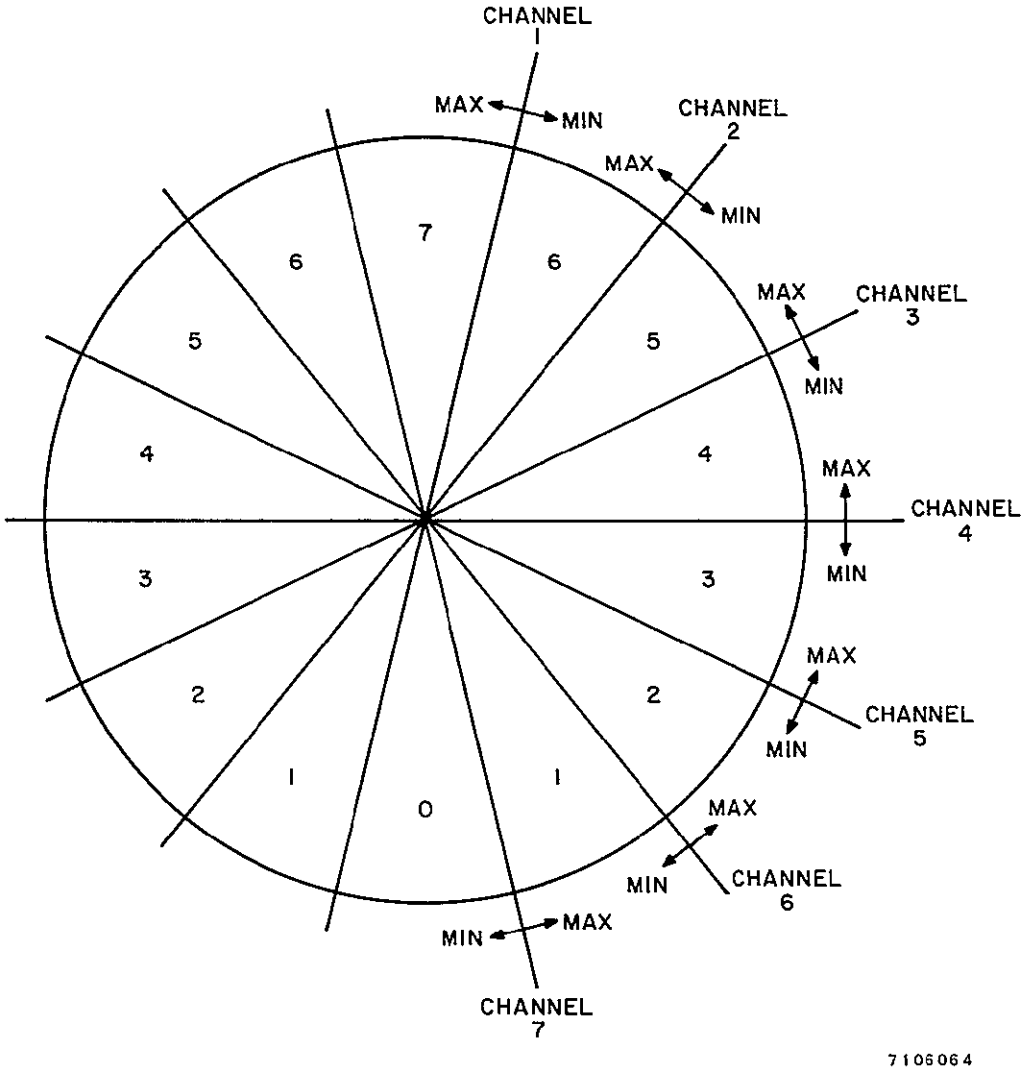

Figure 36. Exposure Geometry of Seven-Channel Crosstalk Target (numbers inside the wedges indicate the number of overlapped bright-field exposures)

exposures, whereas channel 4 has the least spread in exposure extremes varying only between 4 and 7 bright-field exposures. Similar exposure geometries are shown in Figures 37 and 38 for the nine- and twelve-channel recordings respectively.

All channels of each target were demodulated and photographed on Panatomic-X film (processed to a $\gamma = 1$). Densities of each wedge segment were then measured,

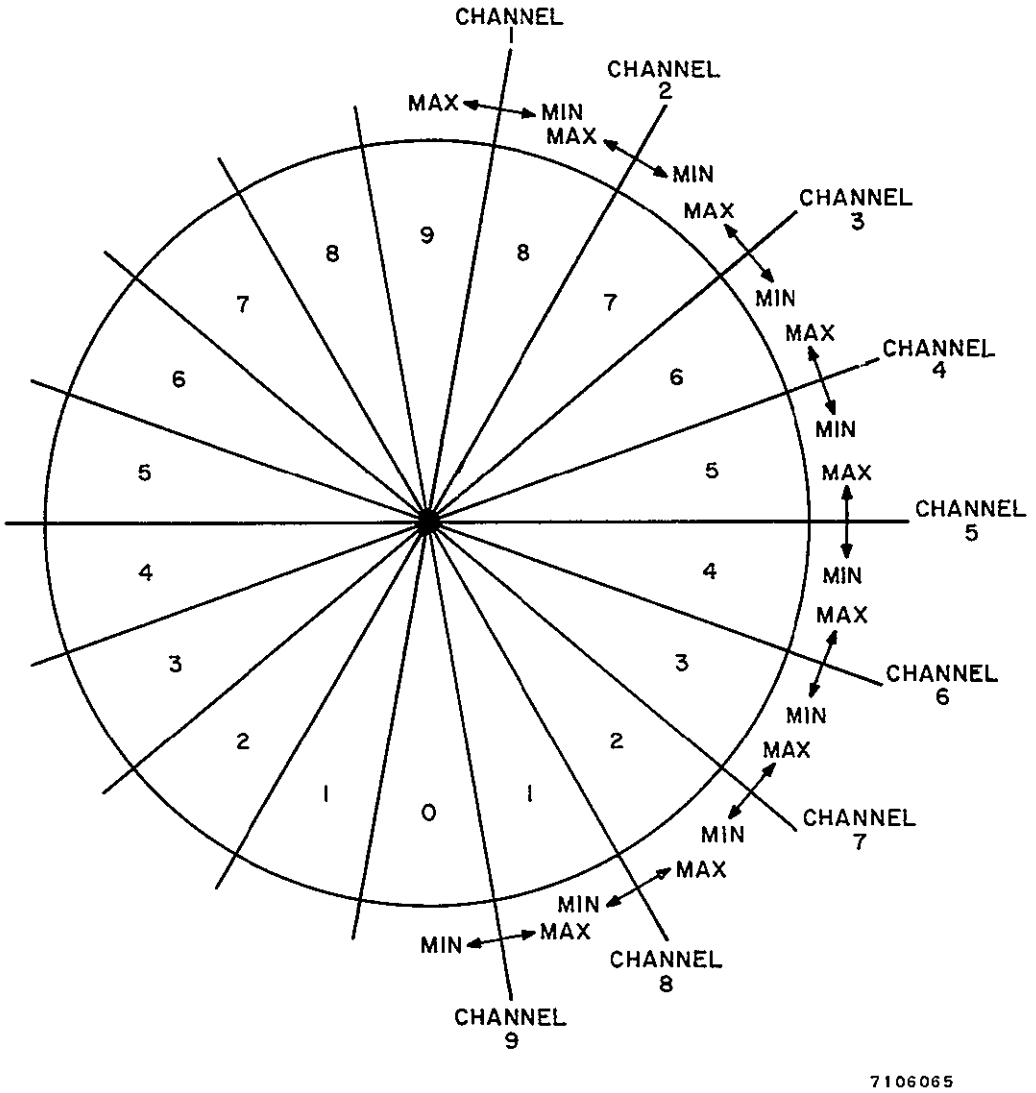

Figure 37. Exposure Geometry of Nine-Channel Crosstalk Target (numbers inside the wedges indicate the number of overlapped bright-field exposures)

but only for the bright-field half of each retrieval target. Densities were converted to relative log brightness and the average log brightness calculated for all segments having the same number of overlapped bright-field exposures for each of the three crosstalk recordings. The results of these calculations are summarized in the curves of Figure 39. Interpreting these curves requires some explanation because the physical quantities involved are somewhat unconventional. Figure 39a indicates that

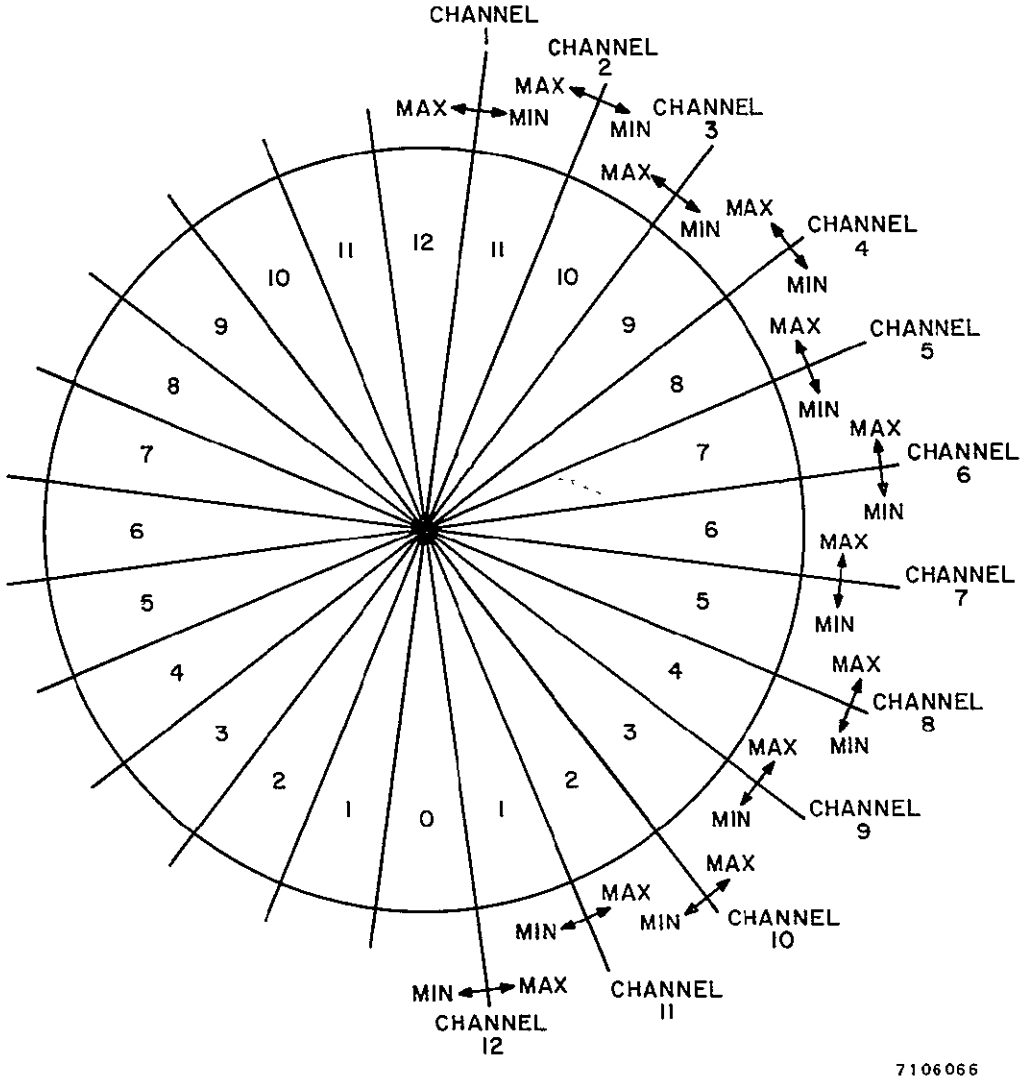

Figure 38. Exposure Geometry of Twelve-Channel Crosstalk Target (numbers inside the wedges indicate the number of overlapped bright-field exposures)

channels having between 4 and 7 overlapped exposures will play back with relatively uniform intensity over the bright half field. In other words (referring to Figure 36), channel 4 was retrieved with most field uniformity and therefore least crosstalk. Channels 5 and 3 where next best, followed by channels 6 and 2. Channels 7 and 1, however, exhibited considerable falloff in brightness for those segments of the field that had only one bright-field exposure. Similarly, curve 39b indicates that crosstalk

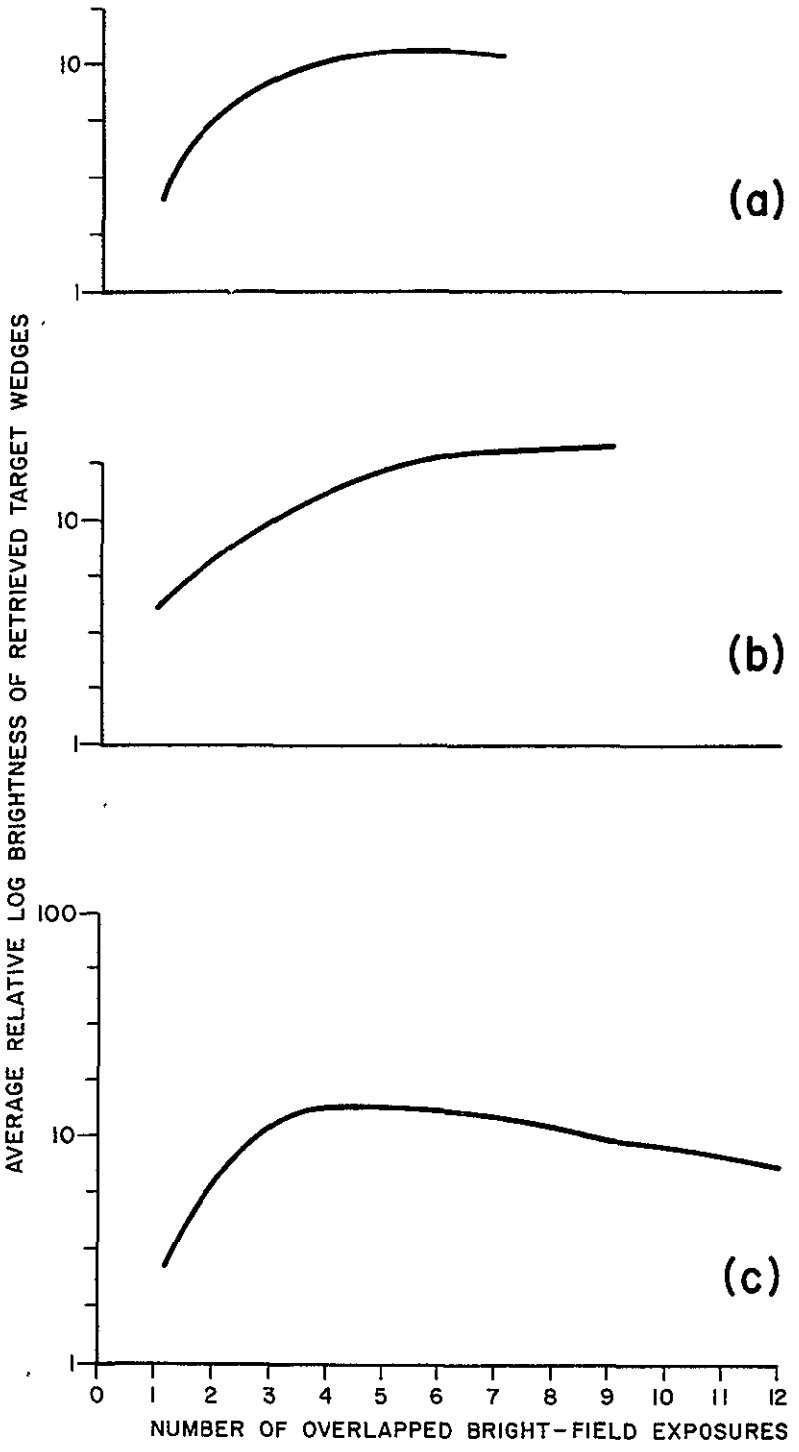

Figure 39. Summary of Crosstalk Measurements for Seven (a), Nine (b), and Twelve (c) Channel Recordings

was minimum for those channels that had between 4 and 9 overlapped exposures. Thus channels 4, 5, and 6 exhibited the least amount of crosstalk in the nine-channel recording. Finally, the curve in Figure 39c is fairly flat between 3 and 10 overlapped exposures, which from Figure 38 indicates that the eight channels from 3 to 10 showed reasonably uniform half field retrievals with very little crosstalk. It must be pointed out that the channel number designation corresponding to relatively low and high crosstalk levels is peculiar only to the crosstalk control targets and in no way is to be carried over to either the subjective or objective target exposure series.

Two very significant results emerge from these crosstalk data. The most glaring deviation is the falloff in retrieval brightness for those regions of the multiplexed recording that have received a relatively low composite exposure level; that is, in terms of the Figure 39 data, those regions receiving less than 3 or 4 bright-field exposures. Nothing in the theoretical multiplexing model suggests this phenomenon, but our model relied heavily on the assumption that a photographic emulsion was nearly an ideal storage device. Unfortunately, a number of well-known emulsion effects will tend to upset our linearity conditions, especially when exposures are made sequentially.

One effect that may come into play is light latensification. The sensitivity or speed of an emulsion can be increased if it is subjected to a short-duration high-intensity fogging exposure. Of course when only two or three exposures have been overlapped, this type of latensification is less likely to occur than when more exposures superimpose. The Clayden and intermittency effects are also likely to introduce nonlinearities where few exposures are overlapped. Probably certain emulsion effects that are difficult to control account for the crosstalk or falloff displayed on the left-hand side of the Figure 39 curves. The falloff evident on the right side of the Figure 39c curve is probably a straightforward saturation effect. The average exposure level was slightly high for a twelve-channel recording and thus the film's storage capacity was somewhat overtaxed beyond nine exposures.

The second result of these measurements is that crosstalk becomes less detectable as the ensemble exposure becomes more uniform. Thus the more channels recorded, the more likely is the ensemble exposure to approach a constant over macroscopic

regions (i.e., the multiplexed recording will tend to appear more like a uniformly fogged film as the number of overlayed exposures is increased).

Resolution, gray scale, and dimensional distortion data can be assimilated practically at a glance from the objective target results. A little more effort may be required to understand the implications of the crosstalk data since there are no standard or traditionally familiar methods of presenting these data in the two-dimensional optical domain.

SECTION 4

GENERATION OF THREE ZONE TARGETS (INTERLACE EXPOSURES)

GENERAL

The previous multiplexing method involved the use of overlapped carriers that resulted in a complex pattern of exposure elements extending randomly over the emulsion format (e.g., as shown in the photomicrographs of Figure 16). The method described in this section (the theory of which was developed previously) produces a geometry that is very well ordered with respect to the arrangement of sample elements. Each sample element that is part of a precise periodic array consists of four subsamples having either additive or substractive interlace geometry. Because this multiplexing method is exactly periodic in two dimensions, the square array approach is well suited for printout by a modulated rotating mirror scanner, CRT, or flying spot scanner.

The basic feasibility of the square array method had been demonstrated previously by means of dichroic encoding filters consisting of red, green, blue and, white (clear) subsample elements. The encoding filter was held in contact with a panchromatic film and a color scene exposed through the filter. Subtractive logic filters consisting of cyan, magenta, yellow, and black (opaque) subsample elements have also been fabricated and balanced for tricolor photography. In this study, however, encoding was accomplished for the first time by simulating the scanner printout geometry equivalent to exposure through a subtractive square array filter.

GRAPHICAL REPRESENTATION OF TARGETS

The first task was to represent graphically the amplitude transmittances of a color bar chart (red, green, blue, cyan, yellow, and magenta patches), a gray scale, and a resolution target. Actually the density levels of all the subsample elements had to be specified. This was accomplished directly by visualizing the equivalent encoding filter geometry as shown in Figure 40 and writing down the resulting densities as in Figure 41. By letting a black subsample patch fall in the upper left-hand corner of the blue patch (i.e., a patch exposed only by blue light) it becomes evident that a

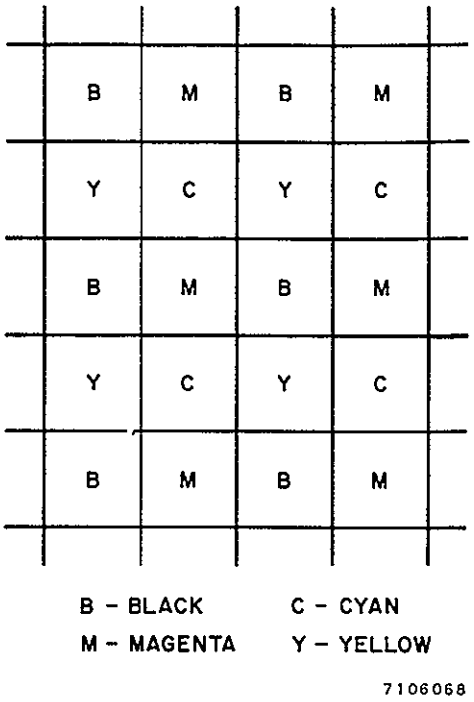

Figure 40. Equivalent Encoding Filter Geometry

vertical ruling pattern must be formed since the black and yellow subsamples permit no exposure and the cyan and magenta subsamples transmit blue light that produces moderate density levels. Similarly, the red light patch consists of a checkerboard pattern since only the yellow and magenta subsamples produce moderate densities. Since the yellow and cyan subsamples are transparent in green light, the green patch consists of a horizontal ruling pattern. Finally the subtractive colors such as yellow have one subsample element of minimum density because they transmit two of the three primary color components; that is, the yellow subsample produces the highest exposure level in yellow light. Only three density levels were required to specify the color bar chart: maximum density, which was set at 3.08 because higher exposure levels would have caused severe distortion (blooming) of the square subsample; moderate density of 0.62 corresponding to about 50 percent amplitude transmittance; and low density of 0.0 corresponding to 100 percent amplitude transmittance.

Specification of the gray scale densities as shown in Figure 42 follows the same approach except that in this case only neutral exposures of varying intensity increments (quarter stops) were simulated. This target required seven different density levels.

Finally the resolution target densities shown in Figure 43 were determined on the basis of a high-contrast black-and-white exposure with the highest frequency (4 ℓp/mm) equal to one-half of the square array frequency (8 ℓp/mm). Only maximum and minimum densities were required for this target.

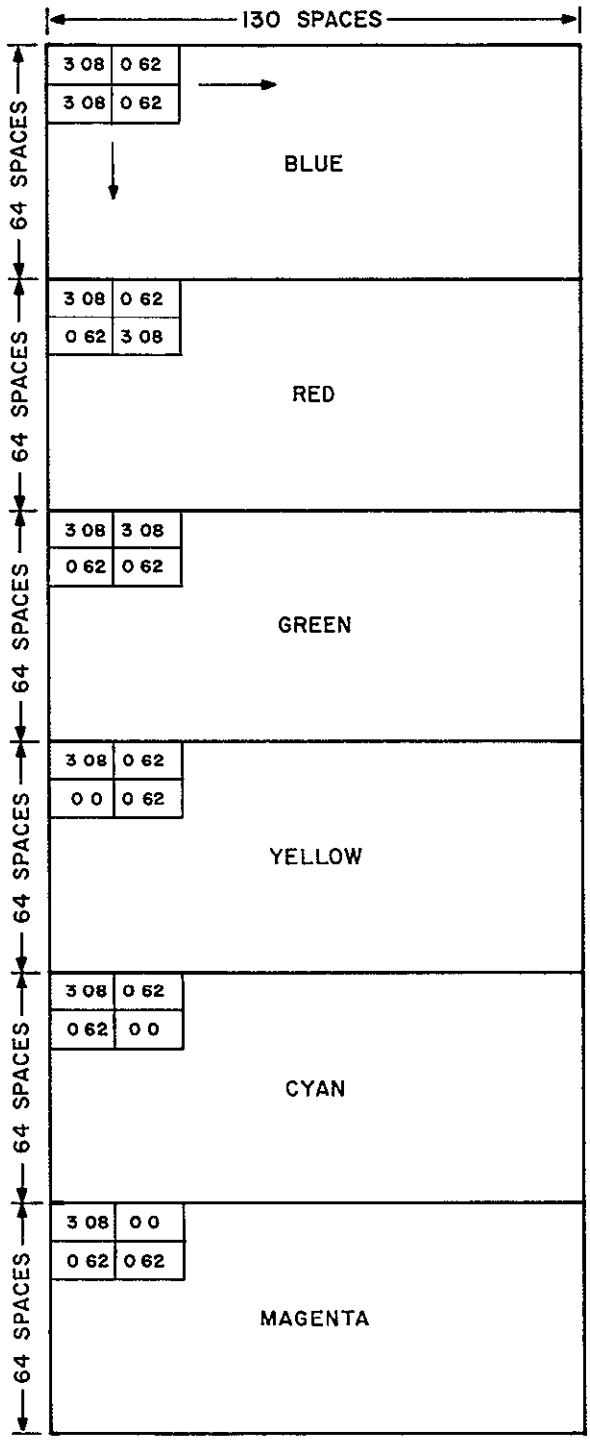

Figure 41. Color Bar Chart Densities

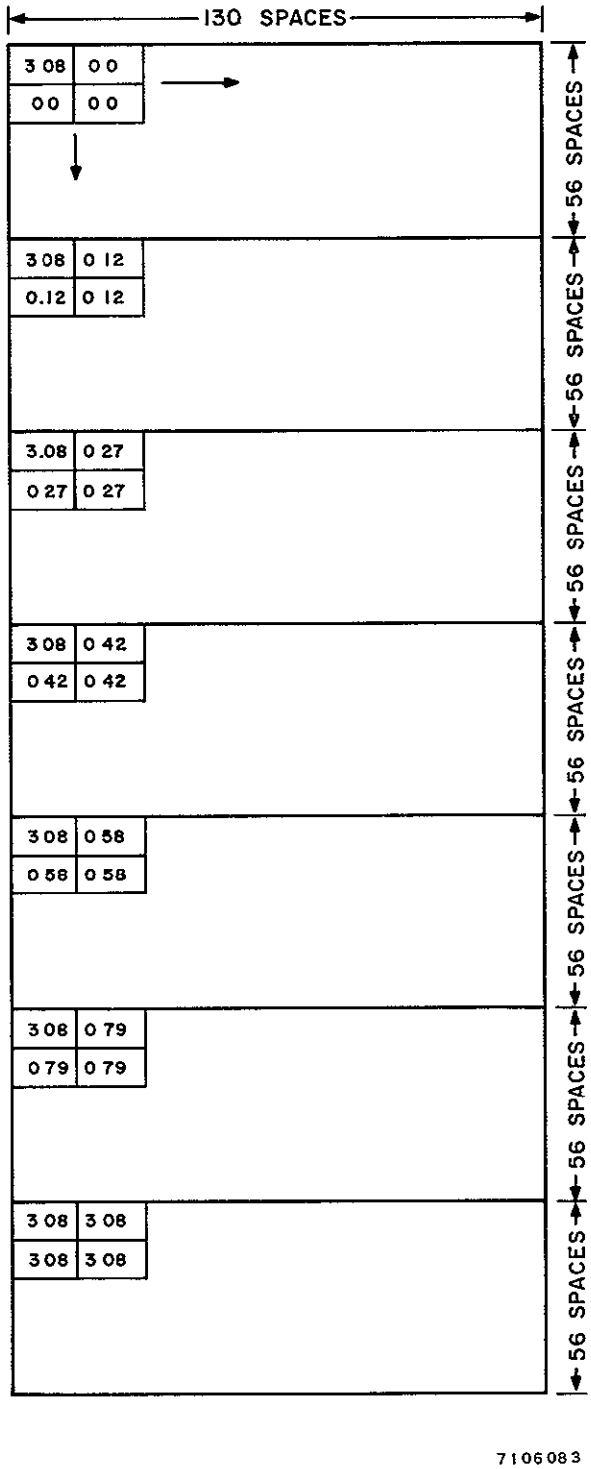

Figure 42. Gray Scale Densities

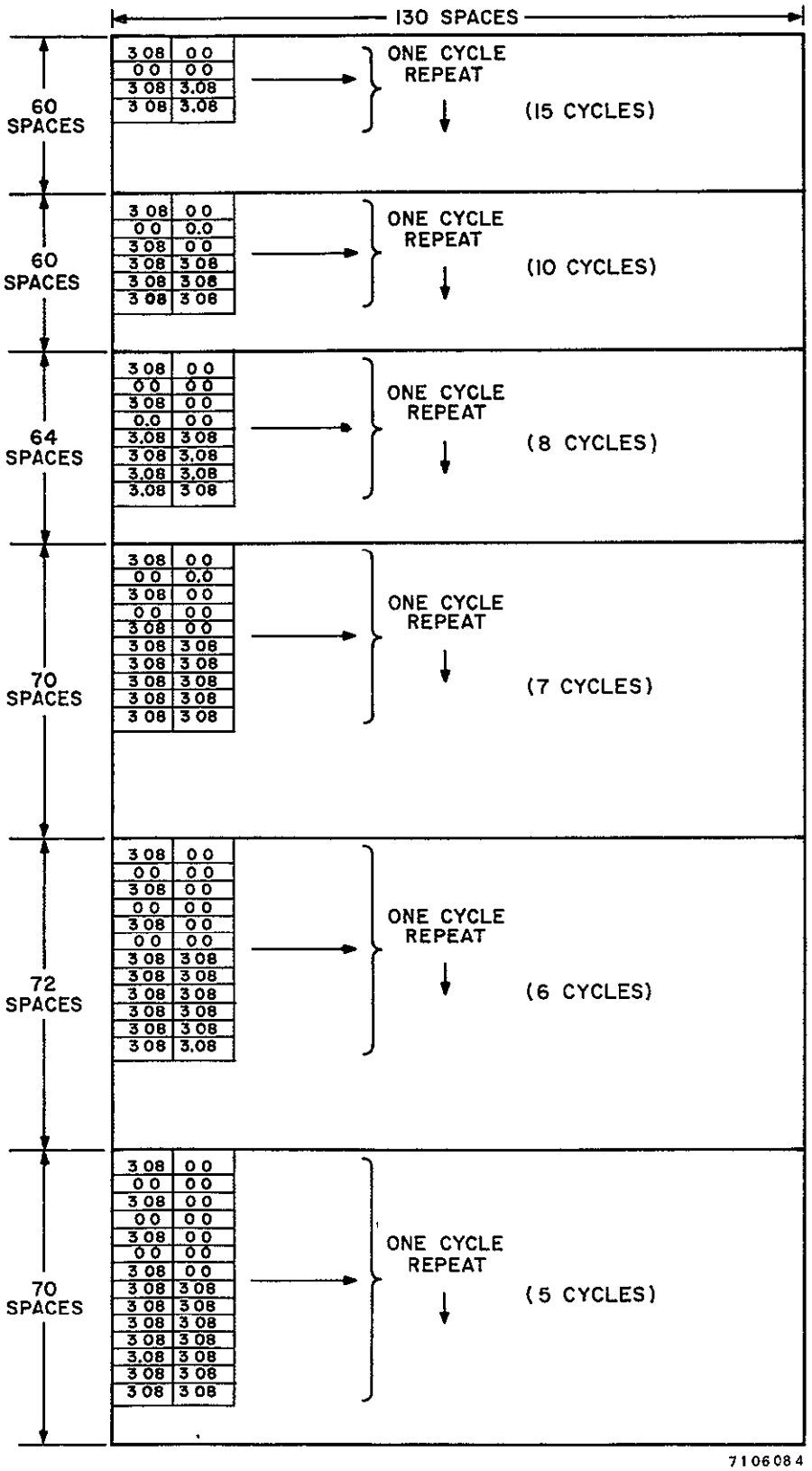

Figure 43. Resolution Bar Target Densities

PHOTOGRAPHIC FACSIMILE GENERATOR

The next step in this demonstration was to translate the density geometries of Figures 41, 42, and 43 into a set of commands in the form of paper tapes to drive the photographic facsimile generator. Normally this step-and-repeat device (Figure 44) makes precise exposures of preselected apertures on a photographic plate to generate a spatial filter in response to commands from a computer. These commands are generated by the computer software program from digital data supplied to the computer.

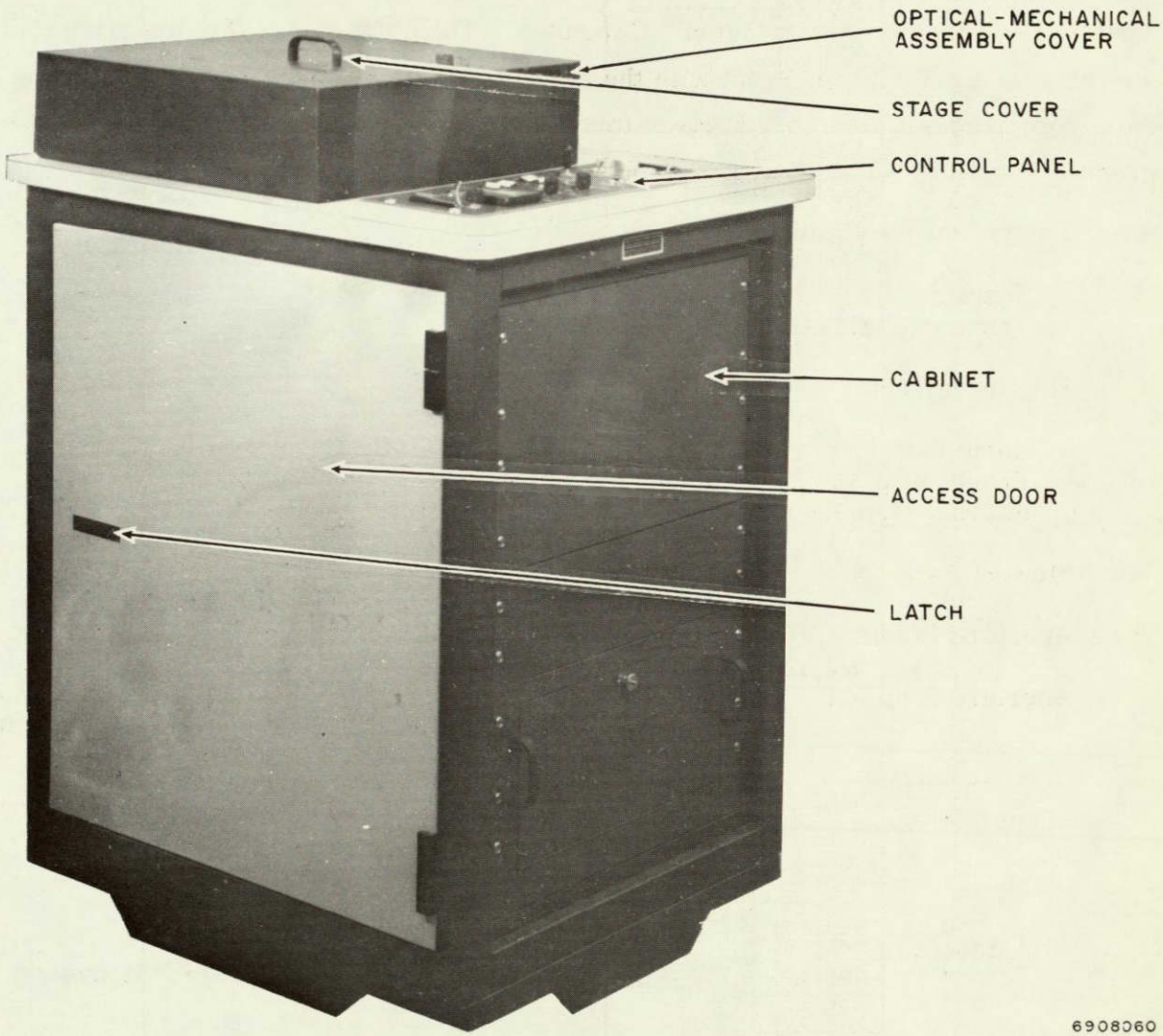

Figure 44. Photographic Facsimile Generator

In this study, however, the device was programmed to print out square array encoded color signals.

A paper tape reader interface unit and a computer buffer interface unit provide appropriate signal interfaces between the Photographic Facsimile Generator and the signal source. The paper tape reader interface permits the preparation of a complete program for reproducing a spatial filter with unique characteristics by separate peripheral equipment and then storing these data on paper tape for future or repeated use. Similarly, the computer buffer interface permits direct control of the Photographic Facsimile Generator with a Sigma 7 Computer. The computer buffer interface unit operates on a priority interrupt with the computer software arranged for accepting data from magnetic tape in a Fortran format. Typical specifications for the Photographic Facsimile Generator are given below.

Photosensitive Plate	
Size	4 by 5 in.
Thickness (glass)	1/8 to 1/4 in.
Step Increments	
Basic unit	0.00025 in.
Preset step	0.0025, 0.0050, 0.0100 in.
Internal step set range	Any multiple of 0.00025 times 1 through 127
Slewing Rate	0.1 in./sec
Aperture Holder	Accepts 1 in. square material up to 1/4 in. thick.
Aperture Supplied	0.002 in. copper-beryllium photoetched; hole corresponds to preset steps and to 0.020 for internal set.
Magnification	10.5X
Stage	
Type	x-y cross slide
Travel (nominal)	1 in. x and y directions; limit switches set at 1.1 in. travel
Image Location	Centrally located on the 4 by 5 in. glass plate

Exposure Duration	20 msec
Density	Two independent ten-position discs
Lamp	Quartz-halogen, 100 W
Lamp Current	7 to 8.5 A
Operational Modes	Manual-automatic
Repetition Cycle	Five to seven exposures per second
Exposure Repeatability	±2 percent
Exposure Uniformity	Less than 1 percent for a 0.0025 image
Position Accuracy	Better than 0.0004 in.
Power Requirements	
Voltage	117 Vac, single-phase, 60 Hz
Current	15 A

DRIVE TAPE PREPARATION

Before preparing the drive tapes the Photographic Facsimile Generator had to be calibrated in terms of output density versus the two density disc positions shown in Figure 45. Each disc has ten different levels and in their cascaded arrangement produce one hundred different exposure levels. For each element of the printout array, (400 by 400) elements, a uniform intensity square (0.0025 x 0.0025 in.) is exposed to one of the hundred different levels. The elements are displaced by (0.0025 in.) to form a continuous array.

Only seven density disc positions and one no exposure command were required in tape preparation; these are summarized in Table 10. Each target was abbreviated to about one-third of the format potential in an attempt to save printout time and increase realiability. Thus the targets were only 130 rather than 400 spaces wide. It was hoped that all three targets could be printed out side by side on a single photographic plate, but this task proved too time consuming and error prone.

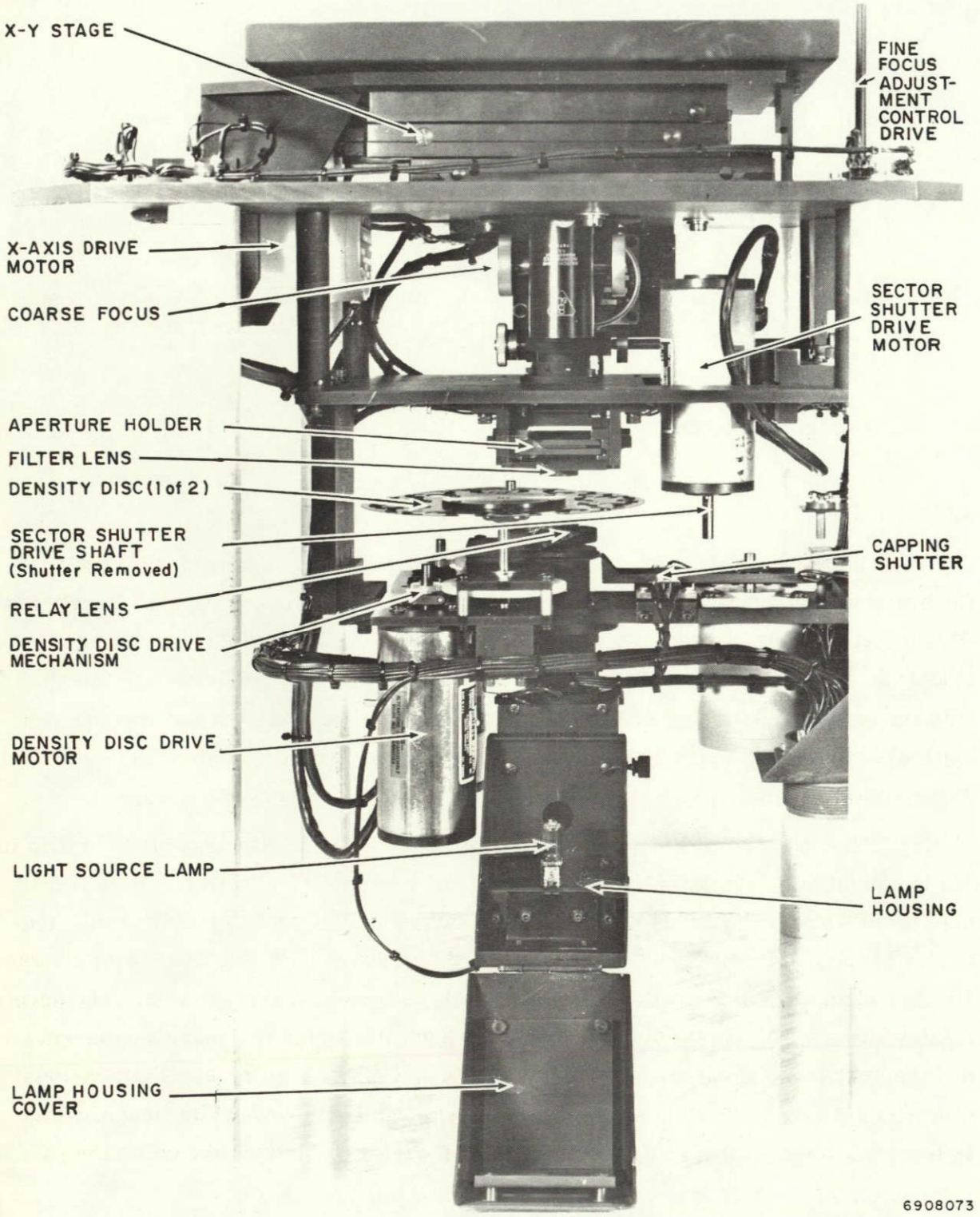

Figure 45. Optical-Mechanical Assembly of Photographic Facsimile Generator

Table 10. Density Disc Calibration

Output Density	Density Disc Position
3.08	50
0.79	57
0.62	65
0.58	72
0.42	89
0.27	74
0.12	64
0.00	Command C

TARGET PRINTOUT

The paper drive tapes were then used to command the Photographic Facsimile Generator which produced the printouts (Figures 46, 47 and, 48) on High Resolution Plates that were processed to a gamma of 2. Half a dozen printout errors are evident in Figure 46, but these were judged to be only minor and in no way interfered with the principle being demonstrated. A spatial phase error is also visible in just about the middle of Figure 47, whereas the resolution target of Figure 48 is virtually error free.

Recall that the primary objective has been to demonstrate the feasibility of printing out in completely automatic spatial registration on monochrome film, the three channels of information required for full color imagery. The input to the facsimile generator is the electronic signal from a punched tape taken as the equivalent to a signal from an electronic buffer with the three signals in temporal registration. The developed printout of the Photographic Facsimile Generator gives the resolution target and the gray scale immediately with results superficially similar to a halftone print. The printout for the three channel color appears in a black-and-white image, which is inserted into a Total Optical Color (TOC) projector to produce the color image.

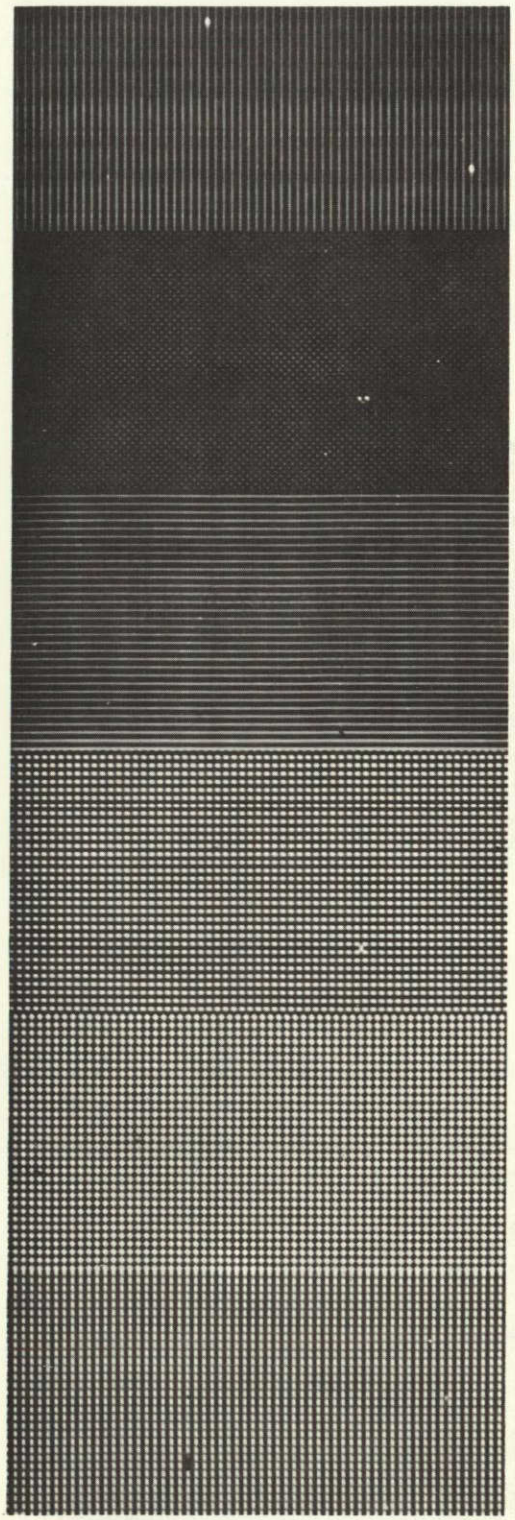

7106069

Figure 46. Printout of Color Bar Chart (at approx. 5.4X)

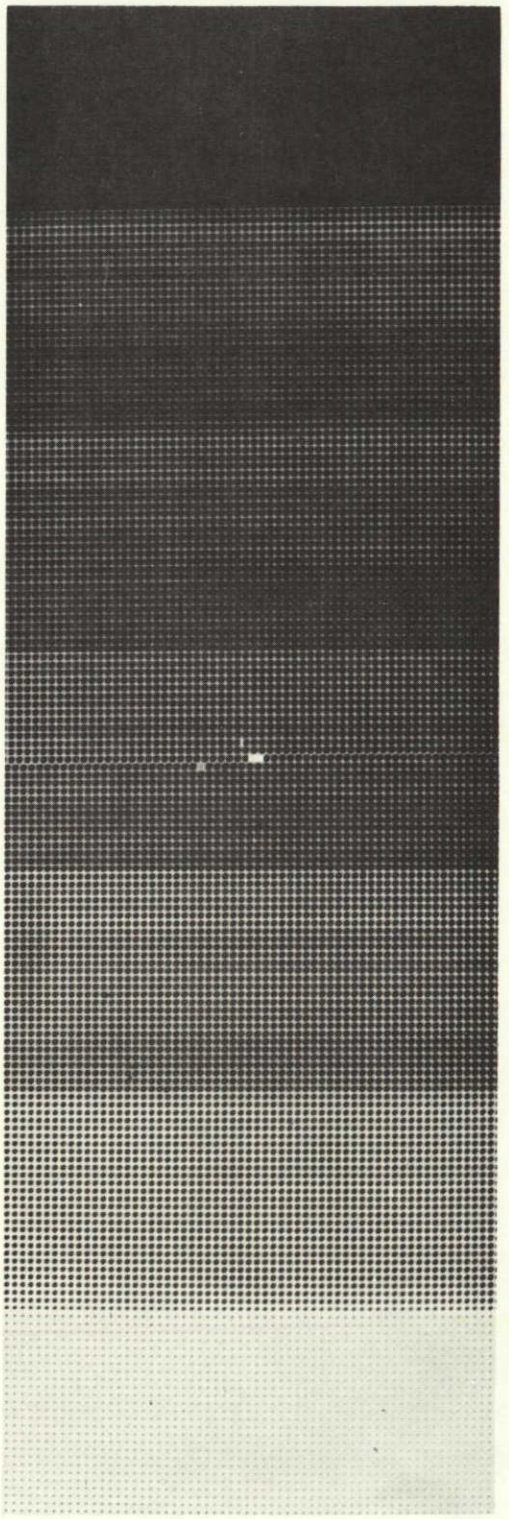

7106070

Figure 47. Printout of Gray Scale (at approx. 5.4X)

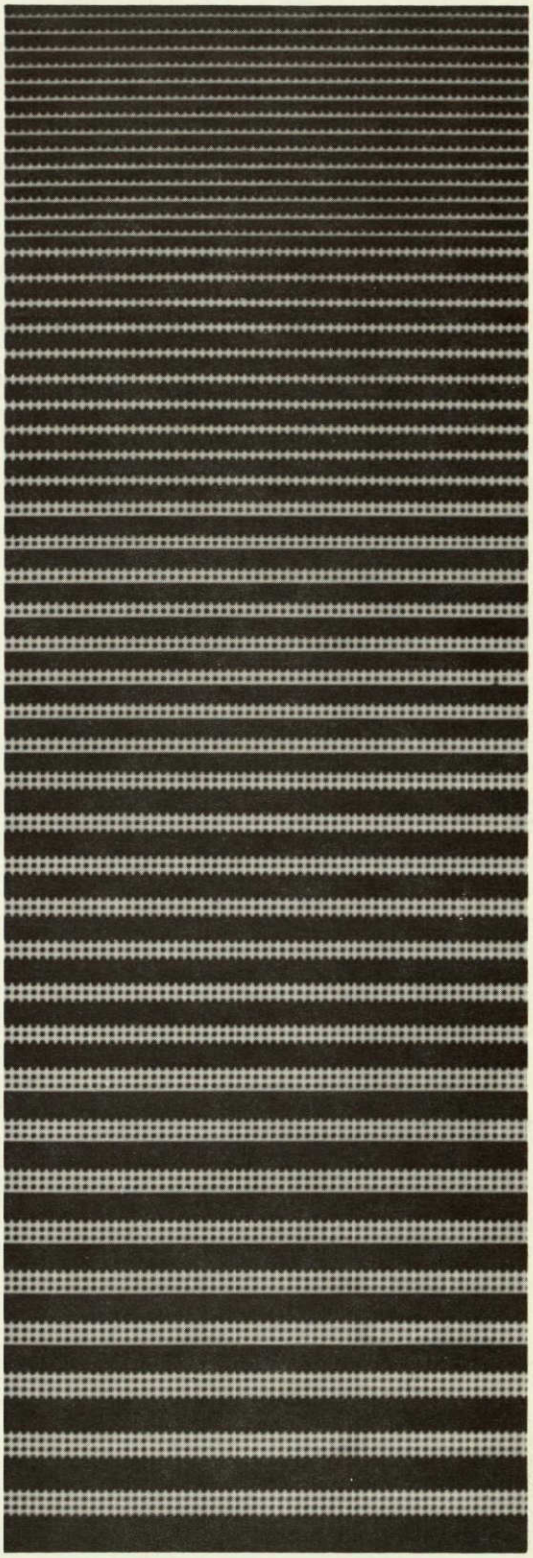

7106071

Figure 48. Printout of Resolution Target (at approx. 5.4X)

TARGET RETRIEVAL

The TOC projector used to retrieve the square array targets was similar in principle to the projector shown previously in Figures 22 and 23 except that longer focal length optics were required to separate the diffraction orders spatially. The optical arrangement is shown in Figure 49. Lenses L_1 and L_2 are both 495 mm focal length lenses used to image at 1:1. A 450 watt Xenon arc was used to provide white light illumination. A color retrieval filter of the geometry shown in Figure 50 was

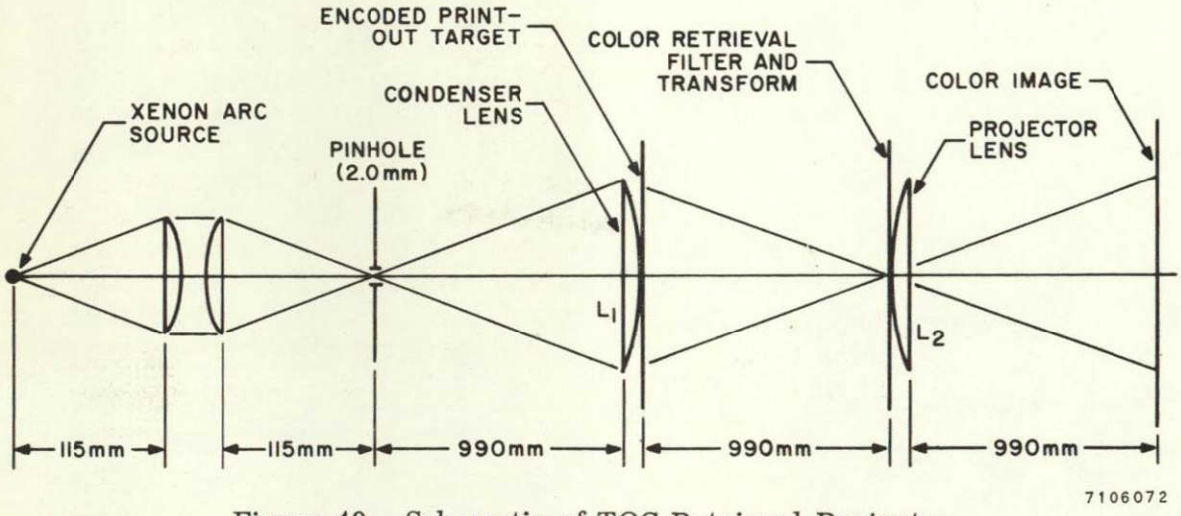

Figure 49. Schematic of TOC Retrieval Projector

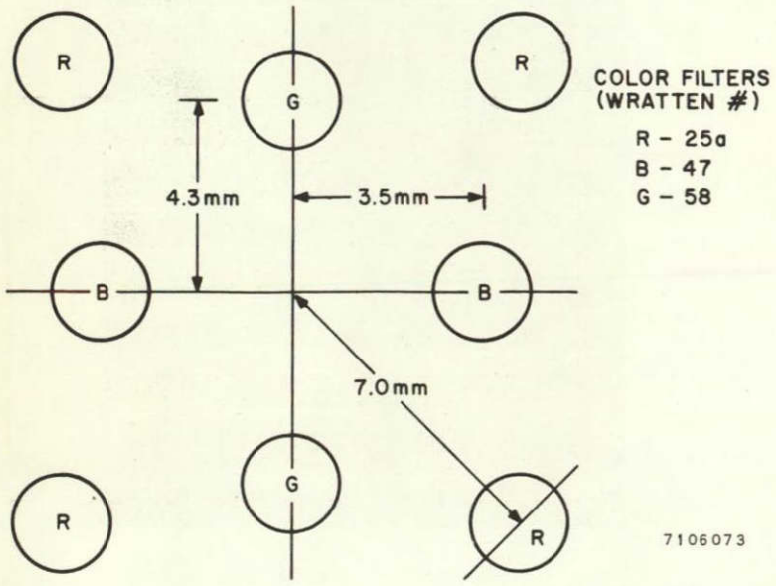

Figure 50. Color Retrieval Filter Geometry

aligned with the Fourier transform array shown in Figure 51 and placed directly in front of the projector lens L_2. The color bar chart was retrieved with the results shown in Figure 52, which is a Kodacolor print of a negative film exposed directly

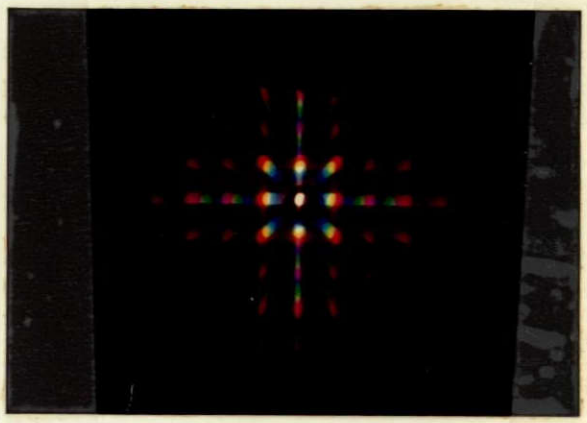

7106074

Figure 51. Fourier Transform Array

NOT REPRODUCIBLE

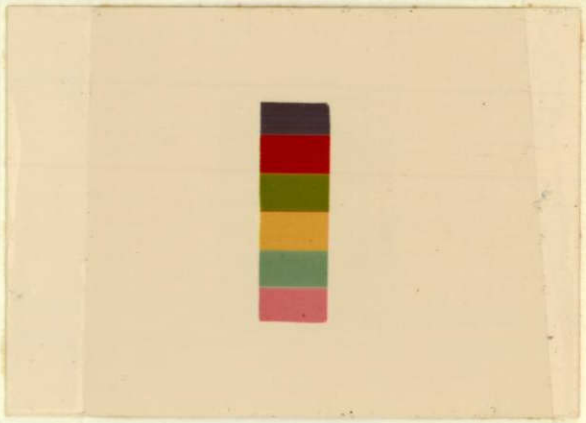

7106075

Figure 52. Retrieved Color Bar Chart

in the color image plane. The gray scale reconstruction is shown in Figure 53, and the equivalent retrieval densities are given in Table 11 with step 2 normalized to zero density.

7106076

Figure 53. Retrieved Gray Scale

Table 11. Equivalent Gray Scale Densities

Step	Density
1	0.0
2	.18
3	.28
4	.40
5	.52
6	.62
7	1.00 (or greater)

Finally the resolution target retrieval is shown in Figure 54, and the spatial frequency progression is given in Table 12.

7106077

Figure 54. Retrieved Resolution Target

Table 12. Resolution Target Spatial Frequencies

Group	Frequency (ℓp/mm)
1	4.0
2	2.67
3	2.0
4	1.6
5	1.33
6	1.14

IMPLEMENTATION

As emphasized earlier, this part of the program was to demonstrate the feasibility of making use of a high speed scanner-printer to print out monochrome information from which three-channel color could be retrieved. Since TOC systems for color encoding black-and-white films have generally been concerned with color filter gratings overlaying the film to be exposed, some conceptual changes are required in adapting to electronically recorded images. As it develops, the implementation for retrieval of images requires little or no modification to make use of the electronically recorded images. The Photographic Facsimile Generator is used to simulate the operation of what would generally be expected to be a higher speed device. In its implementation the square array method would either require a delay-storage device of sufficient storage time to hold one line of print and with a resolution time small enough to ensure registration as the stored information is printed out, or a dual writing beam device. A third approach described in the program proposal, but not demonstrated in this study, is to utilize a scanner with a "wobble" trace that prints out in a hexagonal as opposed to a square array. This approach eliminates the requirements of either a delay storage or dual beam printing device, but it introduces the somewhat unconventional "wobble" beam trace shown in Figure 55.

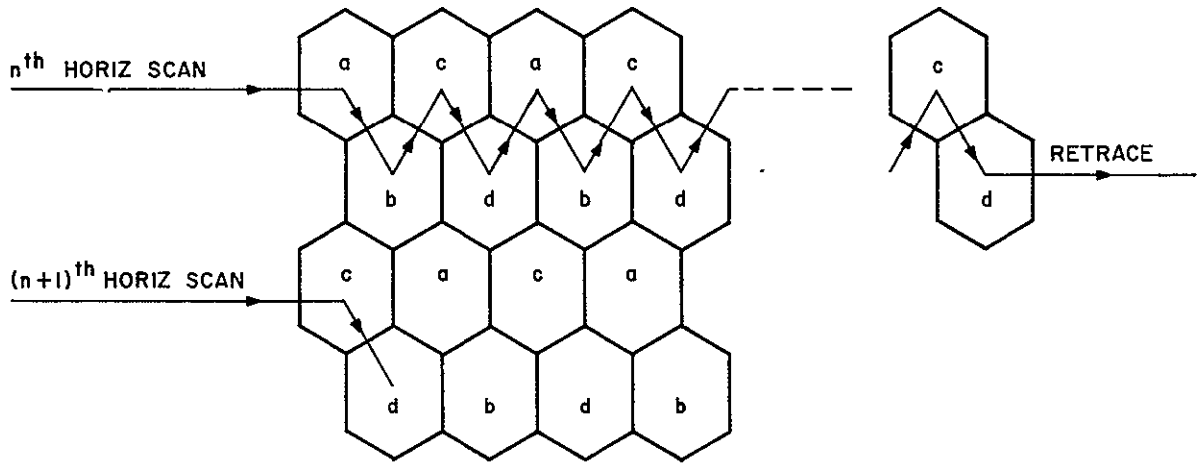

Figure 55. Hexagonal Array Modulation Geometry

SECTION 5

CONCLUSIONS

In this study we have demonstrated a multiplexing method capable of storing and retrieving twelve images at 10 ℓp/mm resolution with a brightness dynamic range of up to 100:1. Any dimensional distortions introduced by the method are inconsequential because they are small compared with the system spread function. To maintain completely linear tonal reproduction (i.e., gray scale) over the 100:1 output dynamic range, an intermediate square root storage step is required before exposing the composite recording. Crosstalk in the retrieval images was more difficult to suppress as the number of channels was increased from seven to twelve. For a seven-channel recording, crosstalk was undetectable subjectively, but it became noticeable for nine- and twelve-channel recordings.

The storage method demonstrated is practical in the sense that it was implemented with existing materials and state-of-the-art techniques. Exposure and processing controls required to minimize crosstalk are of a type that can be automated and do not inherently require the judgment of a trained technician. The question of whether this multiplexing method is acceptable must await an evaluation of this study since we are not in a position to determine whether the image quality is subjectively acceptable. Before the economics of this method can be realistically analyzed, a specific system must be defined.

In addition, we have demonstrated a step-and-repeat method for printing out and reconstructing three-zone color imagery with monochrome film such that registration accuracy of the zones is not degraded. The results provide a positive confirmation of the square array modulation theory as well as the method's registration precision. The resolution and dynamic range demonstrated were determined chiefly by the Photographic Facsimile Generator characteristics, which were incidental rather than fundamental to this simulation experiment.

All of the work statement objectives of this study were accomplished, and for the most part the results were those generally anticipated at the outset. One unexpected results was the superior performance of Recordak AHU Type 5460 processed in a direct reversal mode. The moderately wide output dynamic range and the hightened crosstalk sensitivity in regions of low average exposure were other interesting results that would have been difficult to predict from the theoretical system model.

Finally, the results of this study indicate that the primary objective is best achieved by limiting the number of input channels to seven.

SECTION 6

RECOMMENDATIONS

Assuming that the image quality of this storage and retrieval method is acceptable, we recommend two areas for future work:

1. Using seven actual ERTS spectral zonal separation negatives (7-1/2 inch square format) with registration marks as furnished by ground reconstruction printers, prepare overlay multiplex recordings with all channels in mutual registration.

2. Design and fabricate a prototype retrieval projector that has the potential for relatively low production cost and can be used to demonstrate retrieval image quality.

To pursue high speed scanner-modulator systems for printing out three-zone ERTS imagery would be redundant at the present time, first because the three color laser scanner currently under development for NASA will solve the same problem if successful, and second if registration can be adequately maintained in the seven-channel recording recommended above, the problem will once again be solved.

The two areas recommended for future action could be carried out either sequentially or concurrently since most of the projector design would be independent of recording preparation. Although projector design is vital in answering the question of system economics,it is not however essential in demonstrating large format retrieval and registration since that could be accomplished with a bench mock-up similar to the approach taken in this study.

21. C.B. Neblette, Photography, Its Materials and Processes (D. Van Nostrand Company, Inc., Princeton, N.J., 1962), p. 220.

22. The Focal Encyclopedia of Photography, ed. F. Purves (The Macmillan Company, New York, 1960), p. 629.

23. J.W. Goodman, Introduction to Fourier Optics (McGraw Hill Book Company, New York, 1968), p. 77.

24. Proposal to Study and Evaluate Multiple Image Overlay Storage Method for ERTS, Technical Operations, Inc. Proposal No. TO-B 34-70A (18 May 1970).

25. P. Mueller, Applied Optics 8, 2051 (1969).

REFERENCES

1. P. F. Mueller, Applied Optics 8, 267 (1969).
2. P. F. Mueller, U.S. Patent 3,425,770 (1969).
3. C. E. Shannon and W. Weaver, The Mathematical Theory of Communication (University of Illinois Press, 1949).
4. E. L. O'Neill, Introduction to Statistical Optics (Addison-Wesley Publishing Co., Inc., Reading, Mass., 1963), p. 168.
5. R. Bracewell, The Fourier Transform and Its Applications (McGraw Hill Book Company, Inc., New York, 1965), p. 197.
6. R. W. Wood, British Journal of Photography 46, 420 (1899).
7. R. W. Wood, U.S. Patent 755,983 (1904).
8. A. E. Ives, Physical Review 22, 339 (1906).
9. F. E. Ives, U.S. Patent 839,853 (1907).
10. C. Bocca, U.S. Patent 2,050,417 (1936).
11. W. E. Glenn, J. Opt. Soc. Am. 48, 841 (1958).
12. W. E. Glenn, J. Appl. Phys. 30, 1870 (1959).
13. E. Baumann, J. Soc. Motion Pict. Telev. Engrs. 60, 344 (1953).
14. A. Lohmann and J. Armitage, IBM Tech. Rep. 02.229, 09-10-62 (1962).
15. J. Armitage and A. Lohmann, Appl. Opt. 4, 399 (1965).
16. R. L. Lamberts and G. C. Higgins, Phot. Sci. Eng. 10, 209 (1966).
17. F. Bestenreiner, Optik 28, 263 (1968).
18. P. F. Mueller, J. Opt. Soc. Am. 58, 1557A (1968).
19. K. Biedermann, Optica Acta 17, 631 (1970).
20. G. C. Higgins, Phot. Sci. Engr. 15, 106 (1971).

APPENDIX A

DESIGN REQUIREMENTS TO EXTEND OVERLAY MULTIPLE IMAGE METHOD TO FULL FORMAT RECORDINGS

In this discussion we will restrict our considerations to a seven-channel system utilizing Recordak AHU Type 5460 Microfile film because that combination appeared most promising in this study. However, most of the design considerations could be extended to higher channel capacity if desired.

COPY CAMERA

Three major design elements must be addressed in the copy camera: first, the ruling must be capable of encoding 7-1/2 x 7-1/2 inch images; second, the copy lens must be essentially distortionless and free of vignetting; and third, a suitable pressure platen must be used to ensure uniform and controlled ruling contact. Typical ruling specifications are given in Table A-1. Other than a general scaling of size, the ruling specifications differ from the ruling used in this study only by the antireflection coating requirement.

According to the manufacturer's specifications, the 160 mm f/5.6 Fax-Nikkor lens used for this study can accommodate an 11 x 11 in. format (see Figure A-1). To minimize the effect of lens aberrations and the possibility of distortions and vignetting, however specifying a lens with greater format capability would be advisable. The 300 mm f/7 Fax-Nikkor lens (Figure A-2) can accommodate a 50 percent larger format or about 17 by 17 in., and therefore we recommend that lens or one equivalent to it for the 7-1/2 inch format application.

The pressure platen can be one of many various designs, but the pneumatic bag approach sketched in Figure A-3 seems well adapted to this relatively large format application. The platen consists of a smooth rubber membrane of fairly high density and thickness, which is sealed by means of a frame or vulcanized to a metal back plate. A port is provided in the back plate so that a pressurized gas can be alternately used to inflate the "bag" and then evacuate it. When inflated the

Table A-1. Encoder Ruling Specification for Imagery 7-1/2 Inches Square

Substrate	Optical quality waterwhite glass of nominal 0.250 in. thickness with a flatness tolerances of no more than 10 fringes/in. Diameter should be 12 in. ± 1/64 with chamfered edges.
Ruling Frequency	100 ℓp/mm (±2 percent).
Duty Cycle	50 percent square wave (i.e., bars and spaces equal to 0.0005 ± 5 percent).
Transmittance (micro)	Bar transmittance should be 1 percent or less. Space transmittance should be 94 percent or greater.
Transmittance (macro)	For sample patches greater than 50 periods (i.e., 5 mm width or diameter) average transmittance should be 47.5 percent ± 2.5 percent, but variations over the ruling format should not exceed ± 1.0 percent transmittance.
Ruling Format	Minimum of 11 in. diameter concentric with substrate.
Ruling Material	Metallic (equivalent to chromium or Inconel).
Antireflection Coating	On the ruling side, reflection must be less than 0.4 percent over the wavelength range of 400 to 650 nm and not exceed 0.7 percent from 360 to 700 nm. No anti-reflection coat is required on the substrate surface opposite the ruling surface. The antireflection coating must be extremely durable and scratch resistant, as would be achieved with titanium dioxide, sapphire, and fused silica dielectrics applied to hot substrates with an electron beam evaporator. No spit or spatter can be tolerated, and the surface must be as smooth as the original substrate polish with the exception of the ruling bars.

160mm f/5.6 Fax-Nikkor

Focal length	160mm
Max. aperture	f/5.6
Construction	6 elements 4 groups
Standard magnification	1 X
Range of magnification	1/3 X – 3 X
Image area	420mm at f/5.6
Picture angle	72°
Overall working distance	640mm
Correction wavelength range	350mμ–700mμ
Vignetting	0% at f/8
Aperture scale	5.6, 8, 11, 16, 22
Mounts	Screw (d=62mm p=0.75mm) & Adapter plate (o.d.=77.5mm)
Dimensions: max. diameter	70mm
max. length	53mm
Weight	320g
Shutter	B

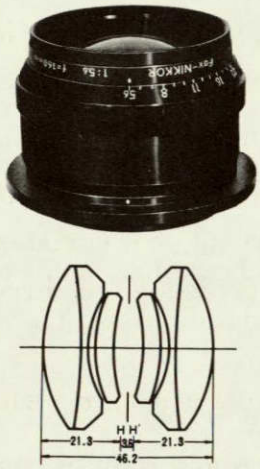

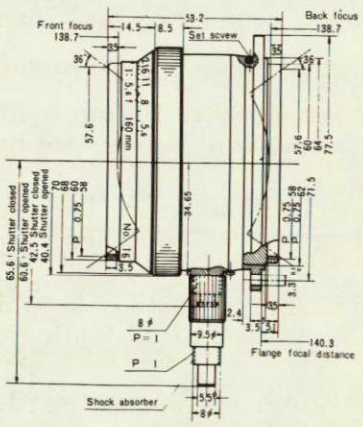

7106079

Figure A-1. Copy Lens Specifications Used for 35 mm Format Study

300mm f/7 Fax-Nikkor

Focal length	300mm
Max. aperture	f/7
Construction	6 elements 4 groups
Standard magnification	1X
Range of magnification	1/3X – 3X
Image area	630mm
Picture angle	52°
Overall working distance	1,200mm
Correction wavelength range	350mμ–700mμ
Vignetting	0% at f/7
Aperture scale	Slit for slip-in aperture control plate provided
Mounts	Screw (d=95mm p=1mm) & Adapter plate (o.d.=120mm)
Dimensions: max. diameter	103.5mm
max. length	96.5mm
Weight	1,700g
Shutter	B

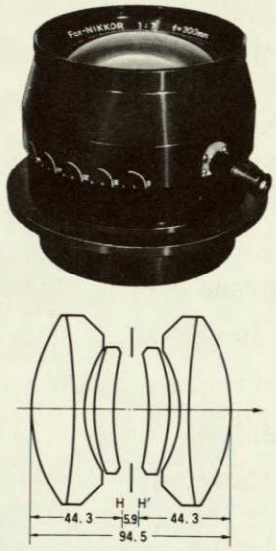

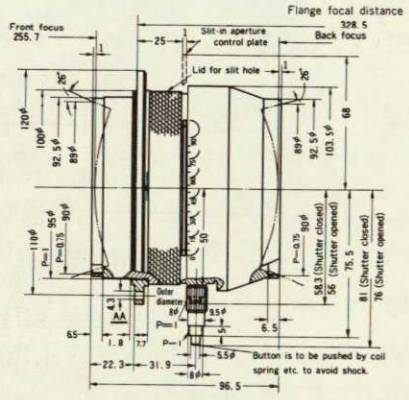

7106080

Figure A-2. Copy Lens Specifications Recommended for 7-1/2 in. Square Format

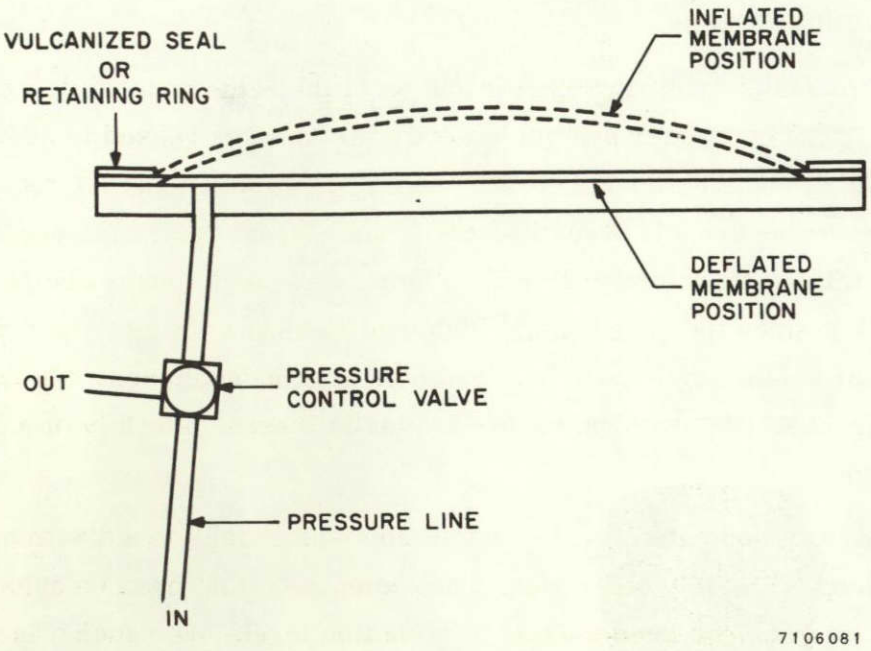

Figure A-3. Cross Section of Pneumatic Pressure Platen

rubber membrane presses the film into contact with the ruling, and when evacuated the pressure is released. The thickness, density, and texture of the rubber membrane, as well as the pressure differentials to be used, would have to be verified experimentally. This approach has the advantage of providing a pressure pad that conforms to any film base irregularities, which would tend to present a more serious problem for long width films than for the relatively narrow 35 mm chips used for this study.

FILM AND PROCESSING

Although 9 in. wide Type 5460 microfilm is a special-order item, we have confirmed that Eastman Kodak will supply it in minimum order quantities (20 rolls of 100 ft lengths). For a small number of duplicate recordings, say five or less, we recommend the same basic reversal chemistry used in this study except that it should be adapted to automatic machine processing. For a large number of duplicate copies, we recommend that the original multiplexed recording be processed as a relatively low gamma ($\gamma \leq 1$) negative on either Minicard film, Scientia 10E50 (by Agfa-Gaevert), or Type 5460. Release positives would then be contact-printed onto Minicard film processed to a $\gamma' \leq 2$ such that $\gamma\gamma' = 2$.

RETRIEVAL PROJECTOR

The large format retrieval projector can be of the same general design as shown in Figure 23. The condenser system however has to be increased to about 10.6 in. diameter. Using the 300 mm Fax-Nikkor as a projection lens at 1·1 requires that the condenser lenses be about 11.3 in. in focal length, which makes the condensers just greater than f/1 and therefore practical to fabricate. Such lenses are not off-the-shelf items, but since they need not be high quality lenses (in fact, they do not even have to be achromats), they could be fabricated at reasonable cost. In large quantities it would probably be economical to use plastic lenses. possibly of a light-weight Fresnel design.

We have already indicated that the projection lens should be a 300 mm Fax-Nikkor or an equivalent. The only other significant component that need be considered is the light source. To achieve even modest illumination levels over such a large format would require a source in the 500 watt class. A compact xenon or mercury arc would be preferable. A small filament tungsten halogen lamp would provide a more economical source if the projector were not used for extended periods; however, retrieval brightness would be lower than that achieved with an arc source.

The subtractive modulation approach requires that black (blank) be printed in the fourth zone. The subtractive approach simplifies not only the film problem, but also the scanner since three channels rather than four are printed.

Since the additive and subtractive colors are related linearly, a taking system utilizing either approach can be accommodated. The conversion merely represents another digital processing step prior to generating the film recording tapes.

It should be pointed out that if all the color information is present, the TOC approach permits complete flexibility in color balancing in the viewing device.

The specified format for the final imagery is a 7.5 in. square frame at a resolution of 10 ℓp/mm. Since the imagery is sampled, the sampling frequency must be at least twice, and preferably as much as three times, the maximum bandwidth of the imagery. The sampling frequency, then, must be at least 20 ℓp/mm and preferably as high as 30 ℓp/mm. As shown in Figure 8, each sample consists of 4 subsamples. At the resolution discussed, each subsample will have a maximum size of 25 x 25 microns and preferably will be as small as 16 x 16 microns.

In a step-and-repeat printer such as the Photographic Facsimile Generator, each printed spot is equivalent in size and shape to the image of an aperture. The image of the aperture is positioned at each point to be printed and the shutter opened long enough to yield the desired exposure.

In the ideal case, the aperture image will have sharp edges, and the positional accuracy will be such that there is no overlap or underlap between adjacent exposures. More realistically, neither situation will be entirely true and there will be some overlap between adjacent color samples. If the film recording is linear, this overlap has no effect except to desaturate the color information. Therefore, if the overlap is kept small, the effects will be negligible.

In a continuous scanner, the exposure is the convolution of the writing spot and a rectangle with width corresponding to writing time. Thus we have

$$E(x) = \int_0^x R(t)\, S(x - vt)\, dt \quad ,$$

APPENDIX B

DESIGN REQUIREMENTS FOR A HIGH SPEED SCANNER-MODULATOR TO IMPLEMENT THREE-CHANNEL INTERLACE STORAGE

The major considerations in the design of a printer to generate three-color TOC (Total Optical Color) are the required resolution, the format size, the dynamic range of the recorded image, and the required printout speed. These parameters in turn determine the required spot size and shape, the scanning speed and signal bandwidth, and the characteristics of the recording medium.

Since the TOC imagery is to be recovered in a spatial filtering system, careful consideration must be given to gamma control to ensure faithful reproduction with minimal crosstalk.

We assume that prior to recording on film, the data will be stored digitally on a mass storage medium such as magnetic tape. We further assume that nothing precludes the storage of the various color channels on the same tape or on two or three separate tapes. Any operations such as changing from additive to subtractive modulation can be performed prior to generating the film recording tapes.

Since the spatial filtering operation associated with recovering the color imagery requires a transparency that is linear in amplitude, the intensity transmission must be a square function. Therefore, to ensure linear filtering, the film must be developed to a gamma of -2. The further the deviation from a gamma of -2, the more nonlinear will be the filtering operation and the more crosstalk that will ensue.

To compensate for this data expansion, precompressing the data with a square root function might be desirable. It is anticipated that this operation would be done prior to exposure.

As pointed out earlier, the colors can be encoded with either subtractive or additive modulation, and theoretically these two approaches are equivalent. The additive approach, however, requires that the white information, which is the sum of the three colors, be printed in the fourth zone. Since the white channel has a wider dynamic range than any of the color channels, the constraints on the film would be quite severe.

where E(x) is the exposure on film, R(t) is 1 during the writing time and 0 elsewhere, and S(x) is the function describing the writing spot.

Even if S(x) is rectangular, the exposure will be trapezoidal with tails equal to one half the spot width. Therefore, either overlap or gaps between adjacent samples must be tolerated. Roughly speaking, if the overlap is to be less than 20 percent, the half spot width must be less than 20 percent of the equivalent writing time. Since, by previous calculations, the subsample spot size is between 16 and 25 microns, the writing spot must be on the order of 7 to 10 microns.

The effects of spot size versus color quality are not readily determined theoretically. Although the figure given may be conservative, it should represent a lower limit on spot size.

Based on the restriction on spot size, consideration can be given to the printing concept. With a format of 7-1/2 inches and a subsample size of 16 to 25 microns, the resolution elements per line are on the order of 10^4. This figure precludes a CRT printer.

The two most likely approaches, depending on speed requirements, are a step-and-repeat printer similar to the Tech/Ops Photographic Facsimile Generator or a rotating mirror laser scanner.

The Tech/Ops Photographic Facsimile Generator operates at up to 20 exposures per second, but this type of device could be made to operate at up to 100 exposures per second. Even at 100 exposures per second, a 7-1/2 in. square format consists of more than 5×10^7 exposures and would therefore take longer than 150 hours (5×10^5 sec) to print.

A laser printer operating at an average data rate of 1 MHz would require about 1 minute to print the same format. With a duty cycle of less than 100 percent, the peak data rate would have to be correspondingly higher or the printing time longer.

The last item to be considered is the dynamic range of the recorded image. A nominal requirement of 16 density levels over a range of 0.0 to 2.0 is well within the capabilities of film, lasers, and laser modulators. The density range requires an extinction ratio of the modulator of 100:1, which is well within the state of the art. Sixteen

equal levels correspond to density increments of 0.125, which in turn correspond to changes in transmission of about 5.5 percent. The two most serious problems in attaining this figure are modulator drift and laser noise. The mode switching noise in HeNe lasers can be limited to 1 percent or less. By using feedback techniques, both modulator and laser drift can be held to well within 1 percent.

A printing system that will yield TOC coded color imagery at the rate of about one frame per minute is apparently well within the state of the art. We assume that pre-processing can be done digitally and the three-color information stored on magnetic tape or a similar medium. The most likely printing technique uses a rotating mirror laser printer with a spot size of about 10 microns. A medium performance modulator in conjunction with a HeNe laser provides sufficient dynamic range for good quality color retrieval.